INL/MIS-23-71173-Revision-0

Slides on AFC-4C-R5 (MNT20E) destructive PIE :SEM, Micro-tensile testing, Post-test TEM Characterization

March 2024

Yachun Wang, Luca Capriotti

Changing the World's Energy Future

Idaho National Laboratory

INL/MIS-23-71173-Revision-0

Slides on AFC-4C-R5 (MNT20E) destructive PIE :SEM, Micro-tensile testing, Post-test TEM Characterization

Yachun Wang, Luca Capriotti

March 2024

Idaho National Laboratory
Idaho Falls, Idaho 83415

http://www.inl.gov

Prepared for the
U.S. Department of Energy
Under DOE Idaho Operations Office
Contract DE-AC07-05ID14517

Slides for AFC-4C-R5 (MNT20E) destructive PIE : SEM, Micro-tensile testing, Post-test TEM Characterization

Yachun Wang
Luca Capriotti

Updated to 1/23/2023

20E PIE data

Data		Credit
Metallurgy	Cross-section OM images clearly revealed the Cr linear	Scott
SEM-EBSD (PFIB)	Cross-section high resolution EBSD images (stitched images)	Danielle
SEM-EDS for cladding LALO (G4, sample ID MNT20E-Cladding-LALO)	EDS mapping revealing composition near matrix-linear interface Local Ln-attack Cr-linear observed	Ya
Fuel lift out for TEM characterization (2 extracted, sample ID: MNT20E-Fuel-LALO (G4& IMCL-FIB)	Thinning	Fei Teng
Micro-tensile testing (7 bars, Sample ID: MNT20E-Cladding-LALO), PI88, RT testing		Cameron & David
TEM characterization on Fuel and post-tested cladding tensile bars		TK / Ya
Data analysis, report, publication		Lead by Ya

1. Luca, Scott, Daivid, Cameron, Fei, Daniel, TK, IMCL facility
2.

Why Cr-liner

FCCI plays major role in weakening cladding integrity and against reaching to ultra high burnup
In order to optimize the fuel performance, the concept of using liner/interdiffusion barrier to mitigate FCCI has been raised and investigated.

One strategy to mitigate or prevent FCCI that has been under active exploration is to introduce a barrier layer between the fuel and clad material. Chromium (Cr) is a good candidate for its low neutron cross section, high thermal conductivity, chemical stability, and high melting point (~2200 °C) [32]. Some exciting progress has been made in recent years.

Yeo et al. (2020) [32] have successfully coated a ~27 μm thick, crack-free Cr barrier on the inner surface of HT9 cladding tube using a developed electrodeposition system. The diffusion couple test at 580 °C revealed that the Cr barrier can hinder the diffusion of fuel constituents under steady state conditions in reactor. However, the Cr barrier cannot suppress fuel constituent diffusion when temperature increases to 650 °C, revealing the limit of Cr barrier under transient conditions.

More recently, Yeo et al. (2022) [33] reported the study to fabricate Cr and chromium nitride multi-coating barrier on HT9 by combing the conventional electroplating and plasma-nitriding. The latter technique not only provides the crack-closure effect of microcracks in the electroplated Cr coating but also allows the formation of an additional chromium nitride layer on the outer surface of the Cr coating. Diffusion couple study at 650 °C for 25 h found that the 72-h-nitrided Cr barrier exhibited significantly enhanced barrier property without any visible inter-diffusion, when comparing with the untreated Cr barrier. The plasma nitriding technique seems to be a positive solution to enhance the Cr barrier property to prevent FCCI.

Although such encouraging progress has been made through out-of-pile diffusion couple studies, *the in-pile performance of Cr barrier*, including *the micromorphology and microstructure evolution*, needs to be investigated in detail to evaluate the feasibility of Cr barrier against FCCI in reactors.

Optical Microscopy Characterization of Cross Section

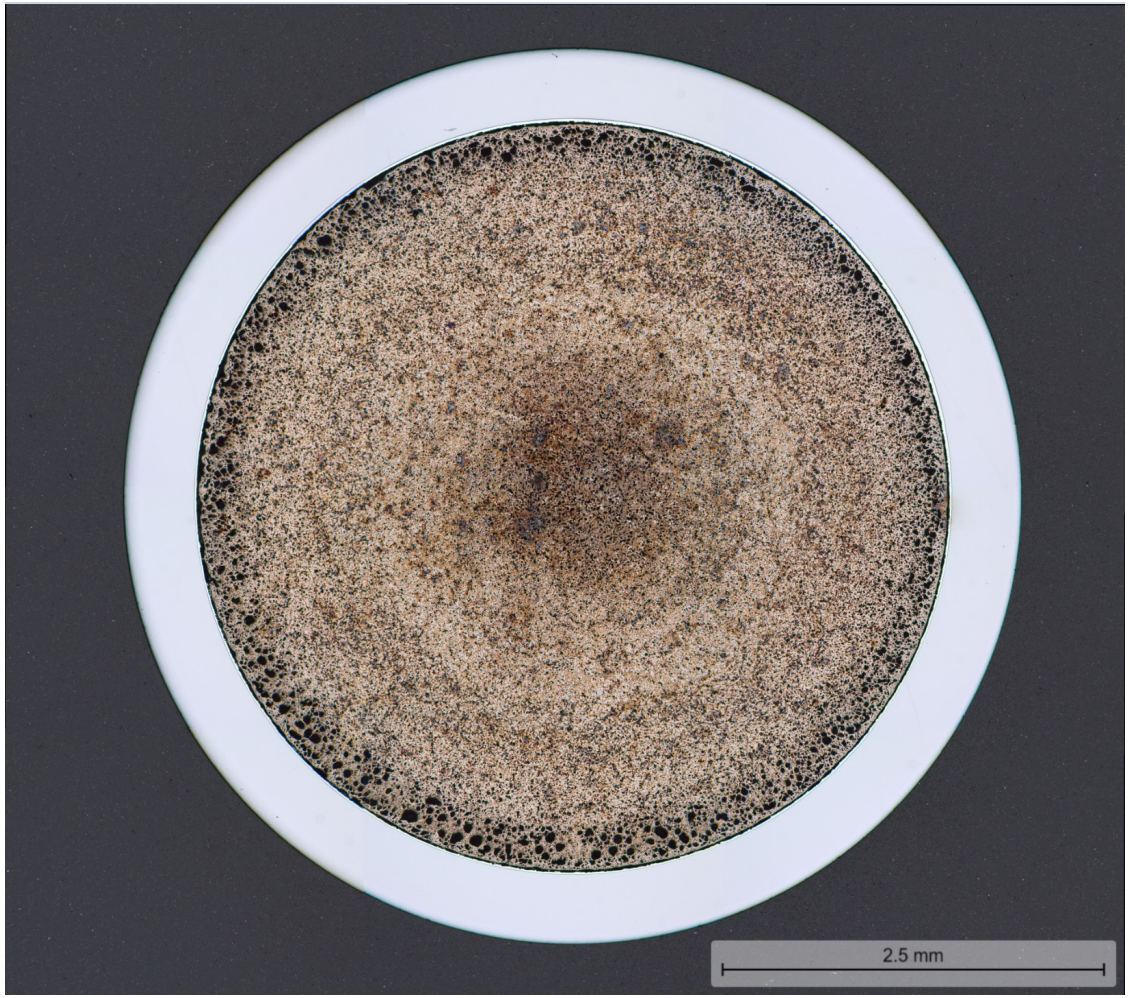

- OM image clearly revealed the cladding-Cr interface

High magnification BSE Cross-sectional image

A stitched BSE mage:

- SEM examination showed **no observable crack in the Cr-liner circumference, suggesting a high barrier integrity under the achieved irradiation condition**
- There is still some space in between the fuel and cladding (possibly due to its low burnup)
- More irradiation tests, like higher burnup and higher operation temperature, are needed to testify the applicability of Cr-liner as a high-burnup barrier at wider operation temperature range in metallic fuel.

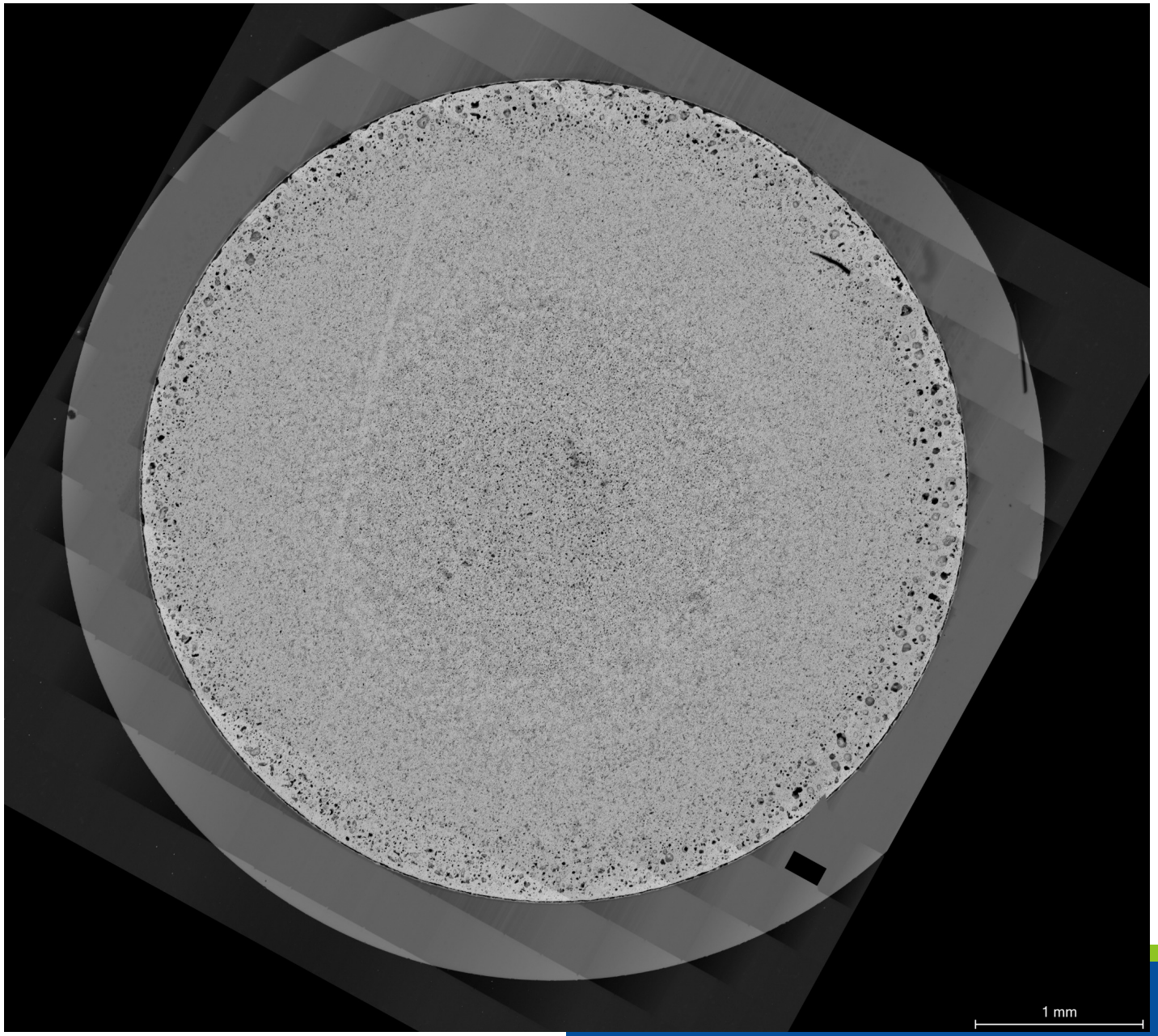

BSE images of Cr-liner

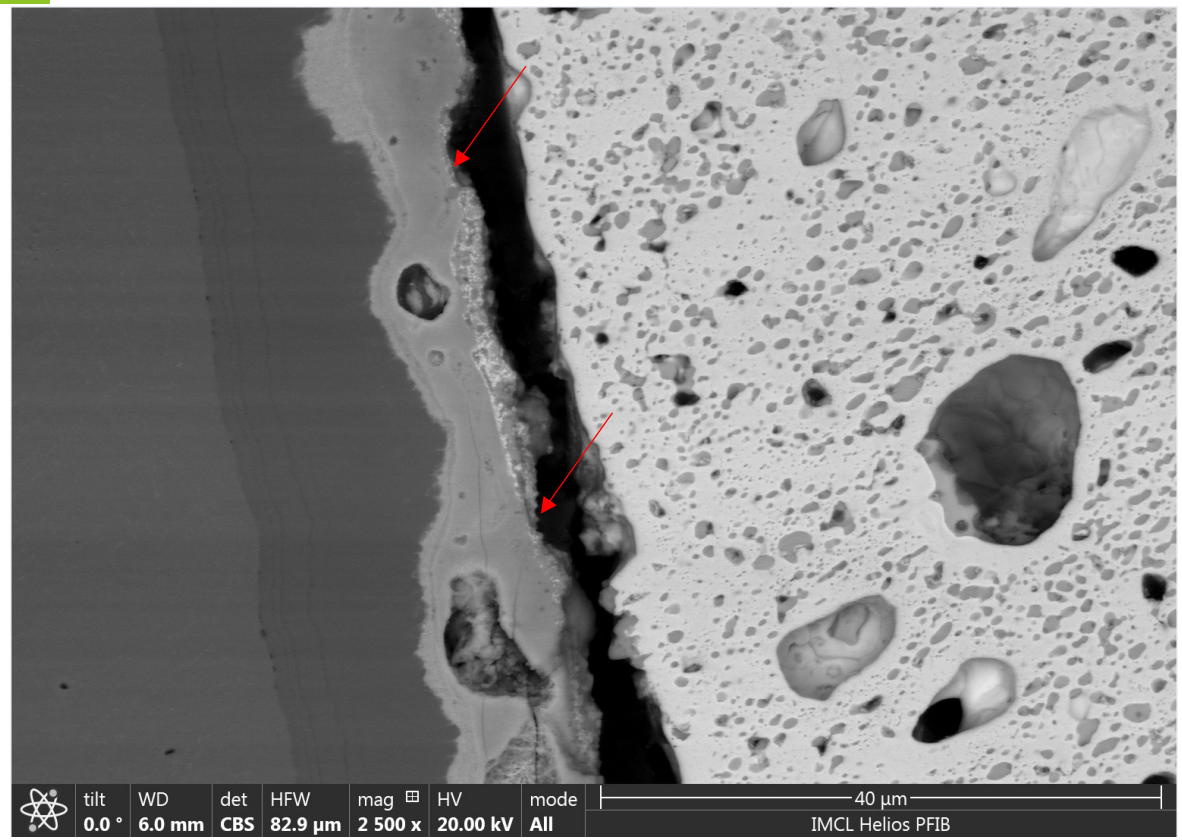

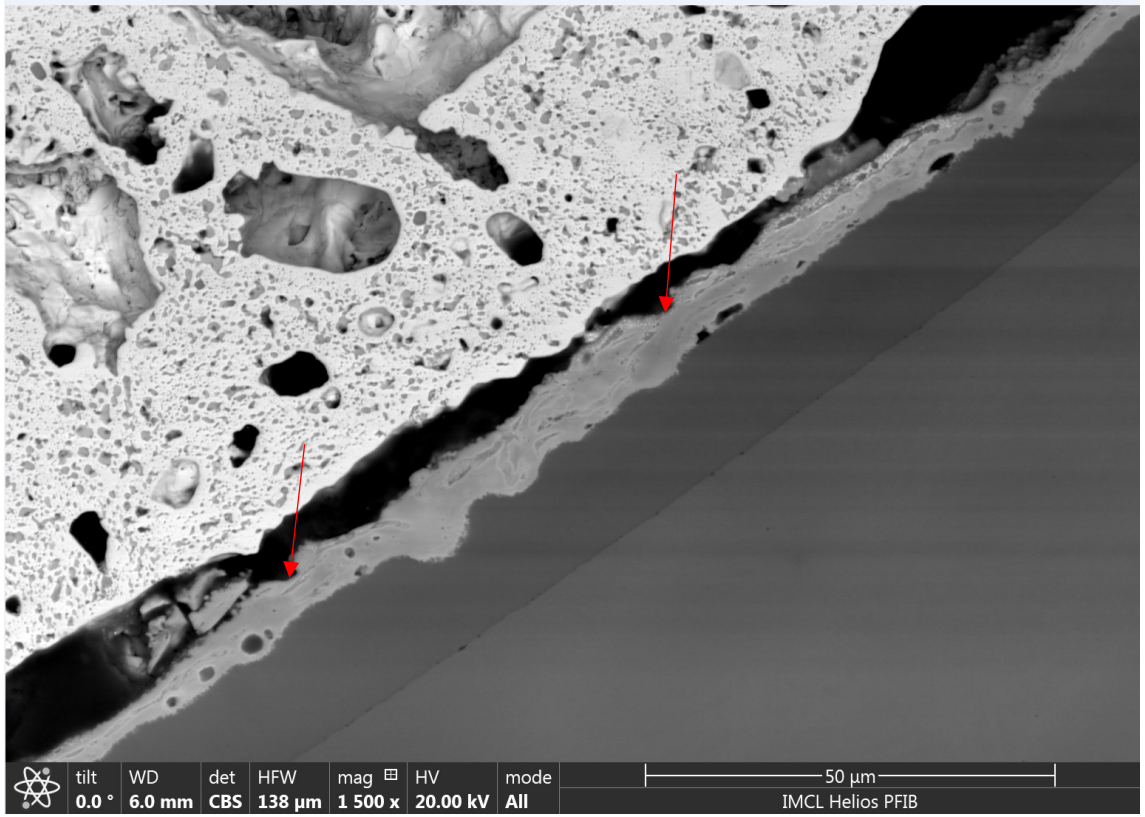

- Observable (narrow) reaction layer revealed in high magnification backscattered electron images

BSE images of Cr-liner (cont.)

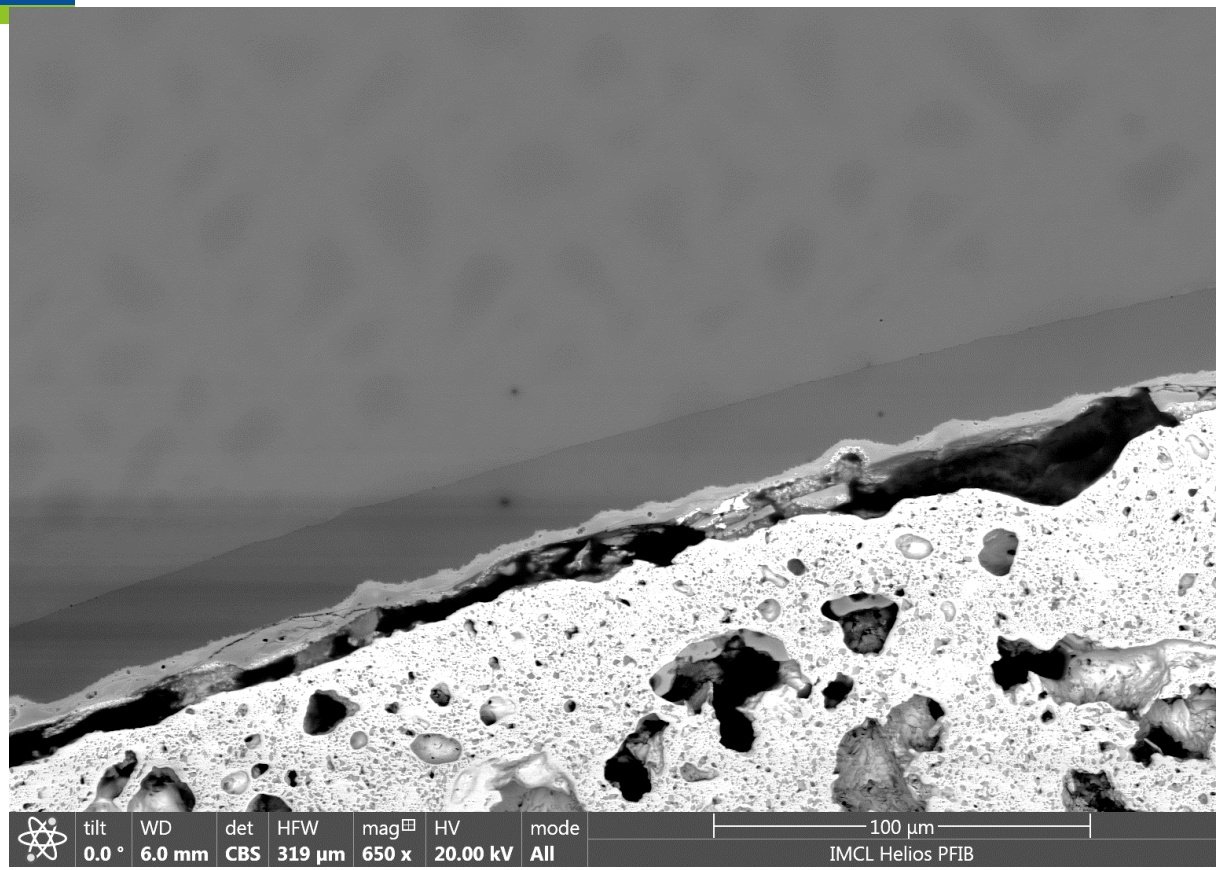

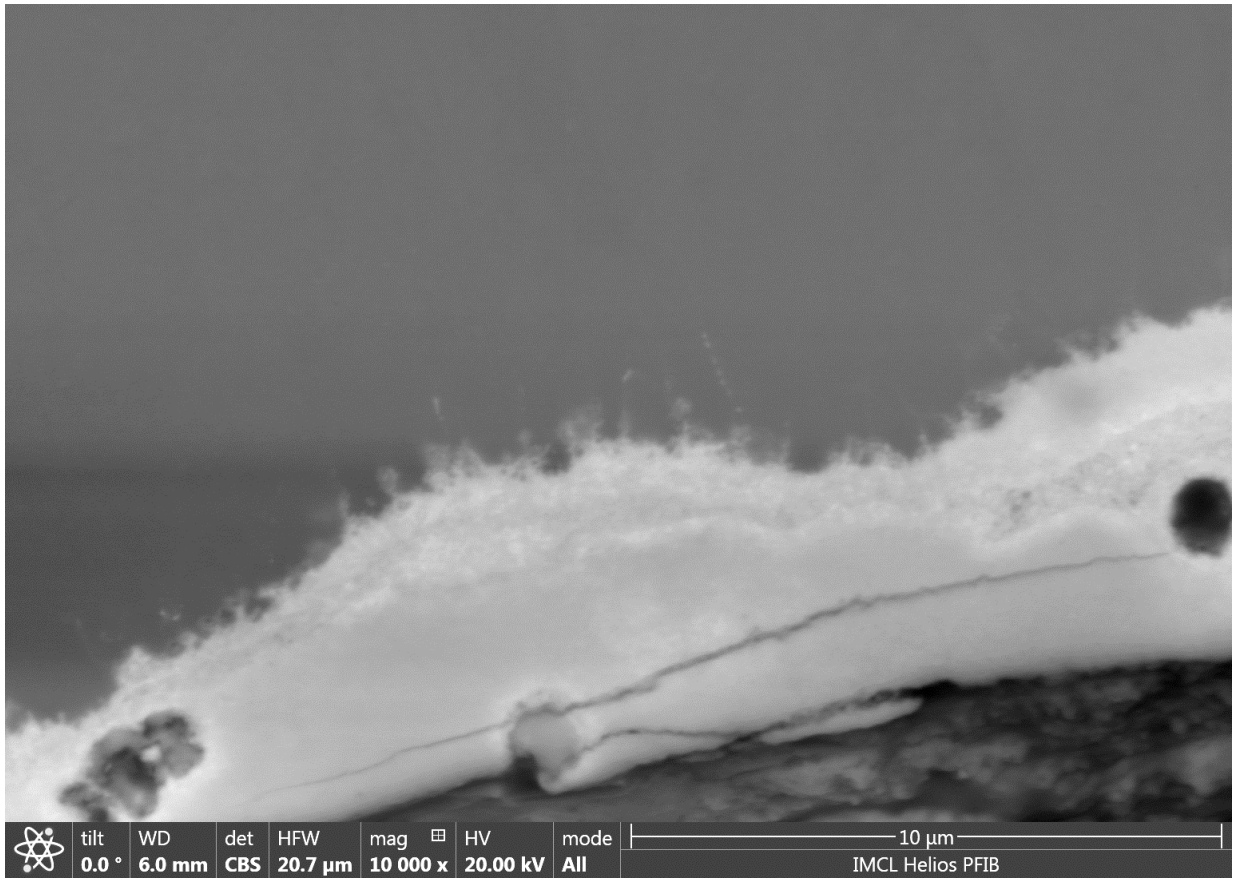

- Reaction layer becomes brittle as indicated by the longitudinal microcracks
- The reaction layer is uneven with furry boundary in between reacted and unreacted region.

Residual Cr-liner thickness measurement

	Length (μm)
#1	11.9
#2	12.4
#3	12.5
#4	12.3
#5	11.8
#6	8.8
#7	9.8
#8	9.7
#9	9.2
#10	8.6

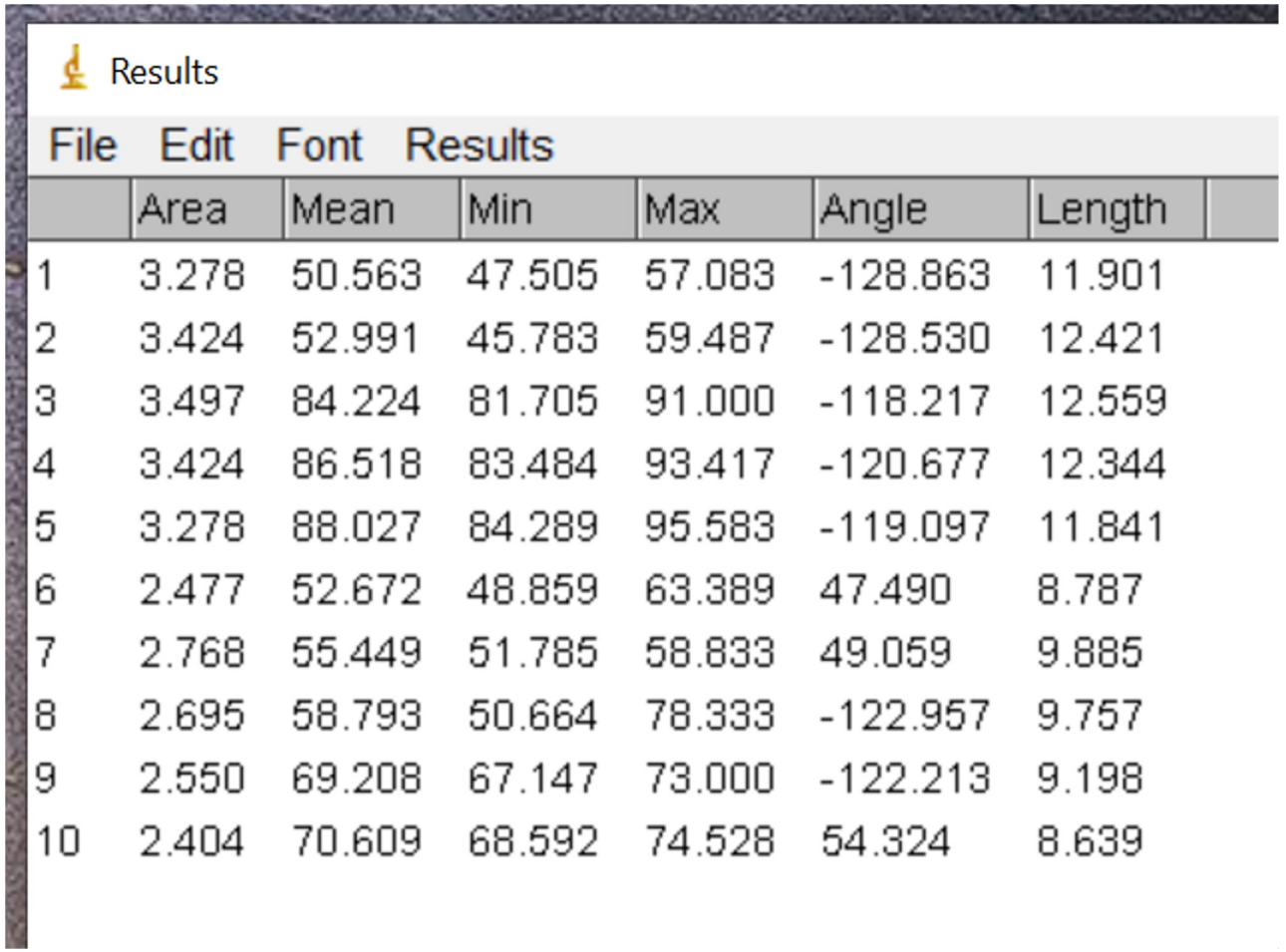

	Area	Mean	Min	Max	Angle	Length
1	3.278	50.563	47.505	57.083	-128.863	11.901
2	3.424	52.991	45.783	59.487	-128.530	12.421
3	3.497	84.224	81.705	91.000	-118.217	12.559
4	3.424	86.518	83.484	93.417	-120.677	12.344
5	3.278	88.027	84.289	95.583	-119.097	11.841
6	2.477	52.672	48.859	63.389	47.490	8.787
7	2.768	55.449	51.785	58.833	49.059	9.885
8	2.695	58.793	50.664	78.333	-122.957	9.757
9	2.550	69.208	67.147	73.000	-122.213	9.198
10	2.404	70.609	68.592	74.528	54.324	8.639

BEI image

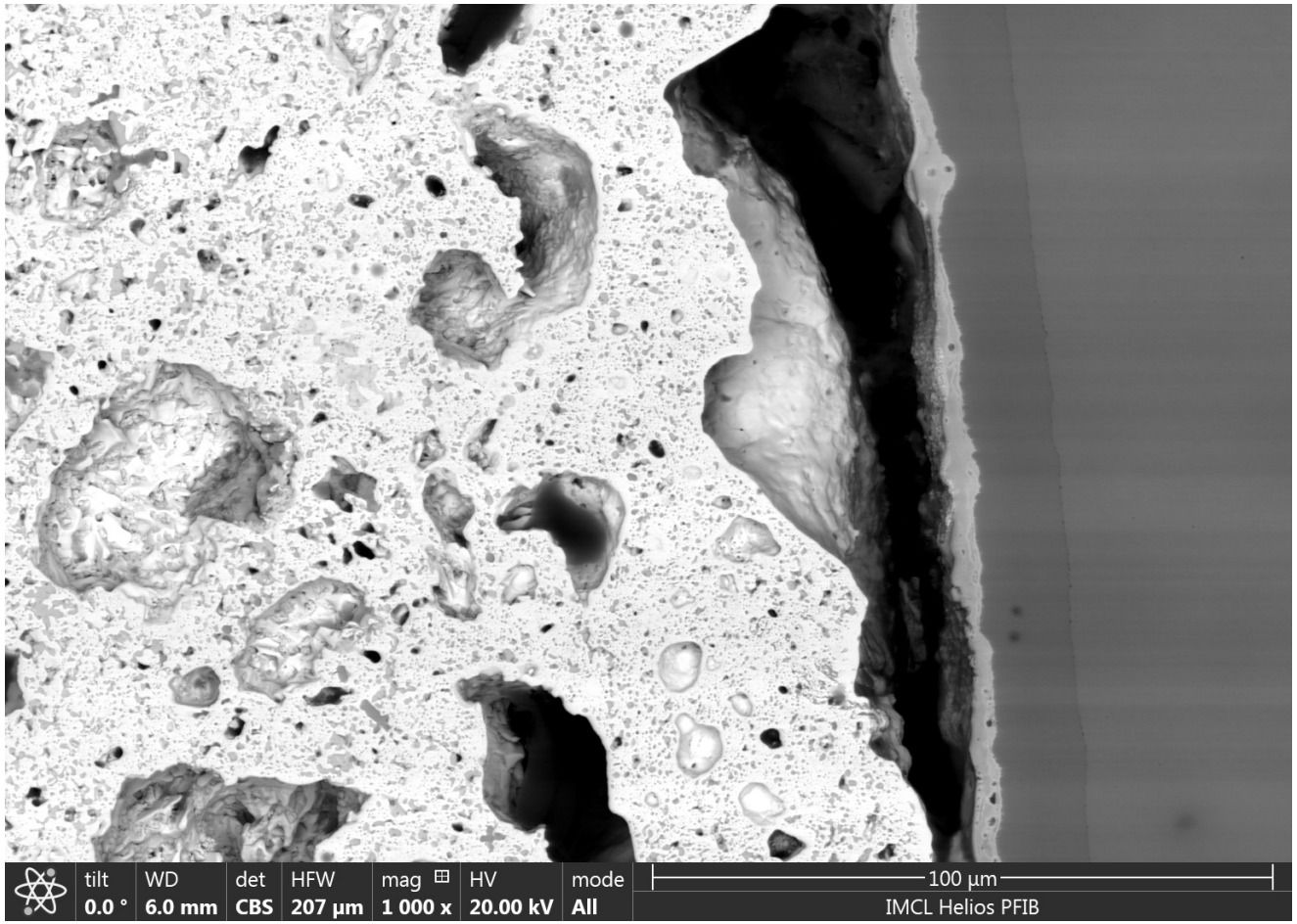

- Partial Cr-liner circumference hasn't touched with fuel yet.

SEM Characterization on Cladding

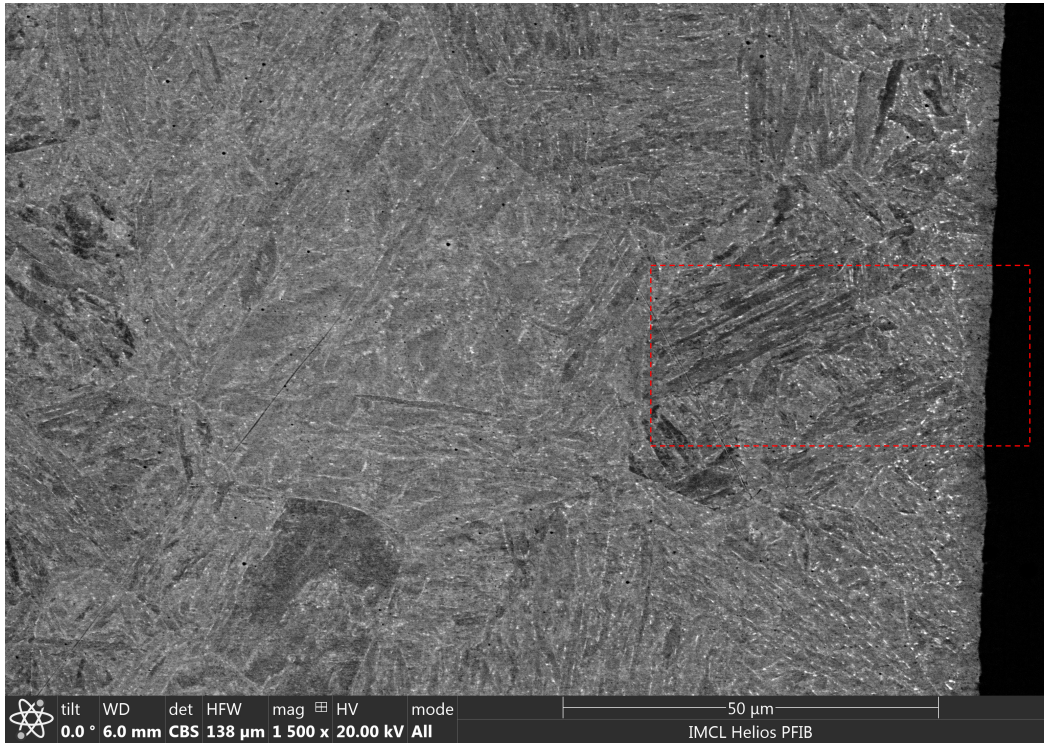

Cr-liner

A narrow layer where lath structure seems disappeared

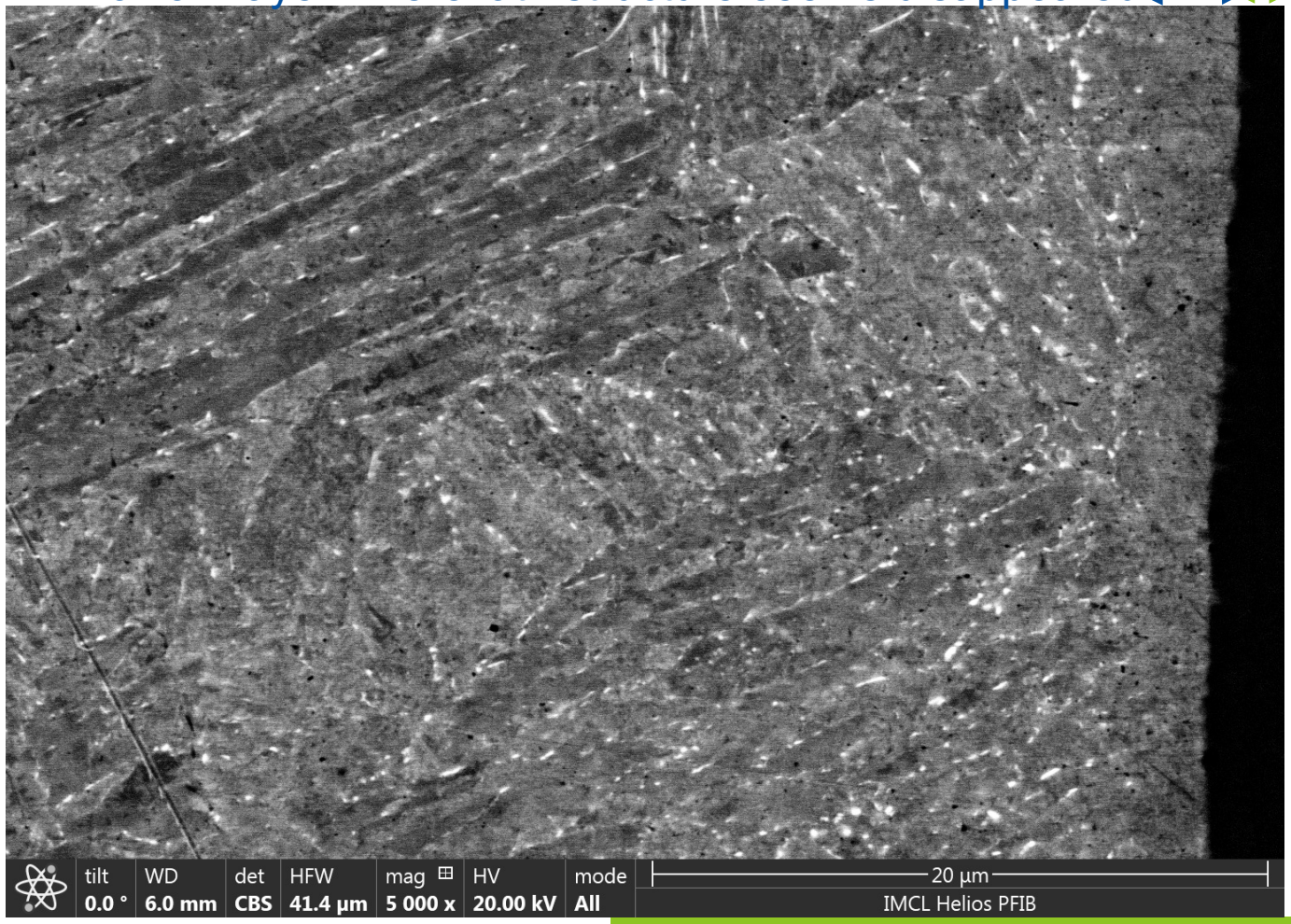

- The typical lath structure was clearly revealed cross the majority of cladding
- Nearby the Cr-liner, there seems a narrow layer where lath structure disappeared (blue double-arrowed line) . This could be induced during Cr-liner fabrication (temperature effect, or potential Fe-Cr reaction)
- TEM characterization will be conducted on this layer to understand the potential microstructure and composition changes nearby Cr-liner.

Large Lift-out cross Fuel, Cr-liner, and HT9 Cladding

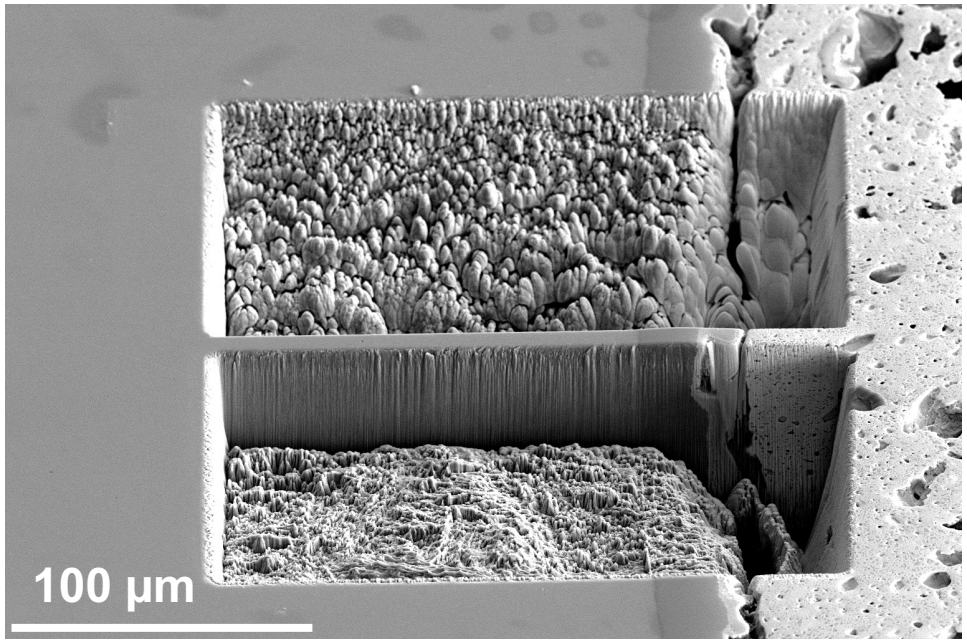

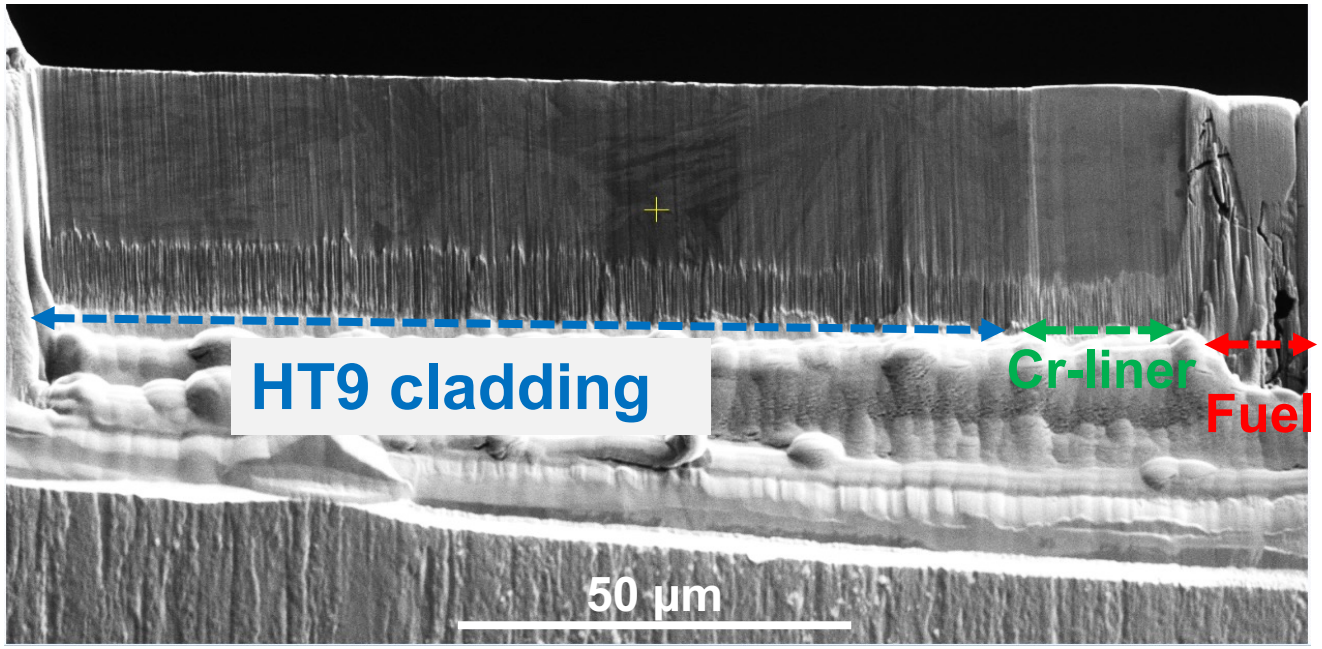

The plan is

1) to conduct SEM-EDS characterization because the parent sample is too hot for SEM-EDS characterization (Finished, results showing in next slide)
2) Then to conduct in-situ SEM micro-tensile testing (Finished)
3) Followed by thinning in FIB and perform post-test TEM characterization to facilitate understanding the micromechanical behavior. (Finished sample prep, Not TEM)

SEM-EDS on large liftout

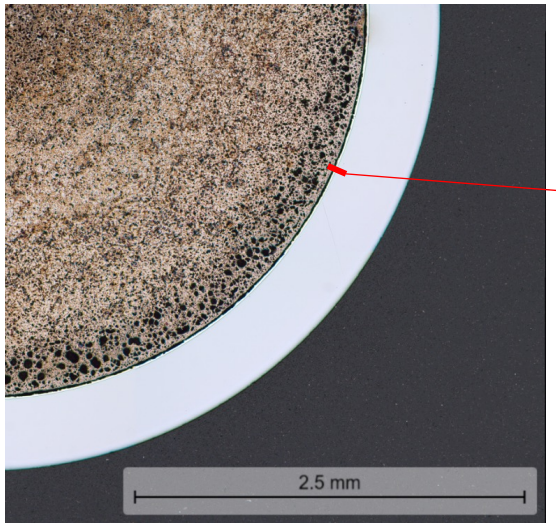

The parent sample is too hot to directly conduct SEM-EDS

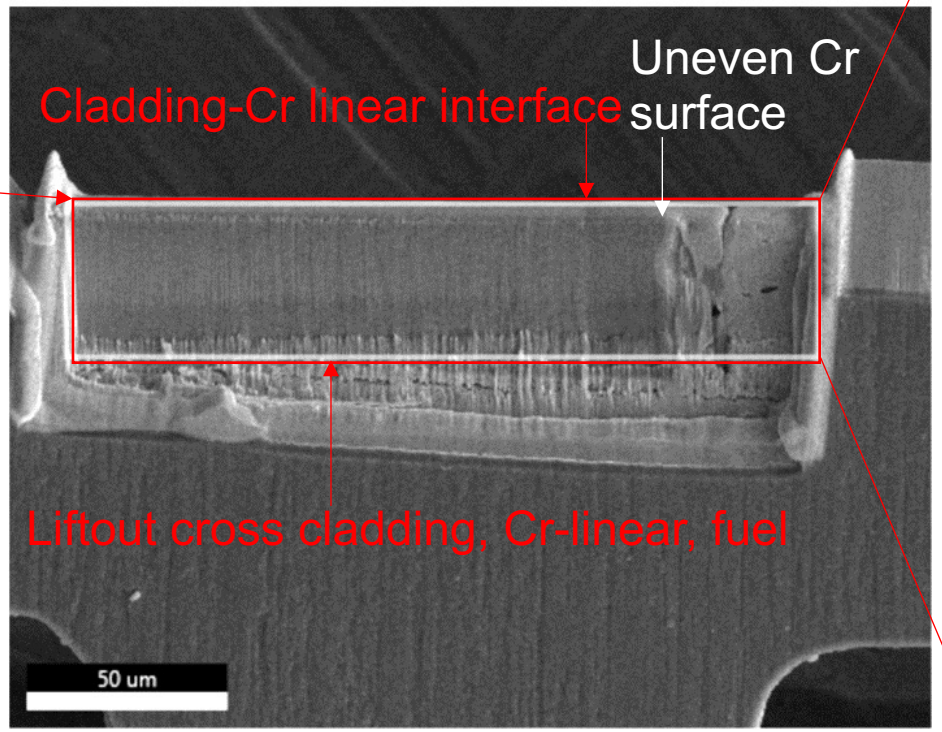

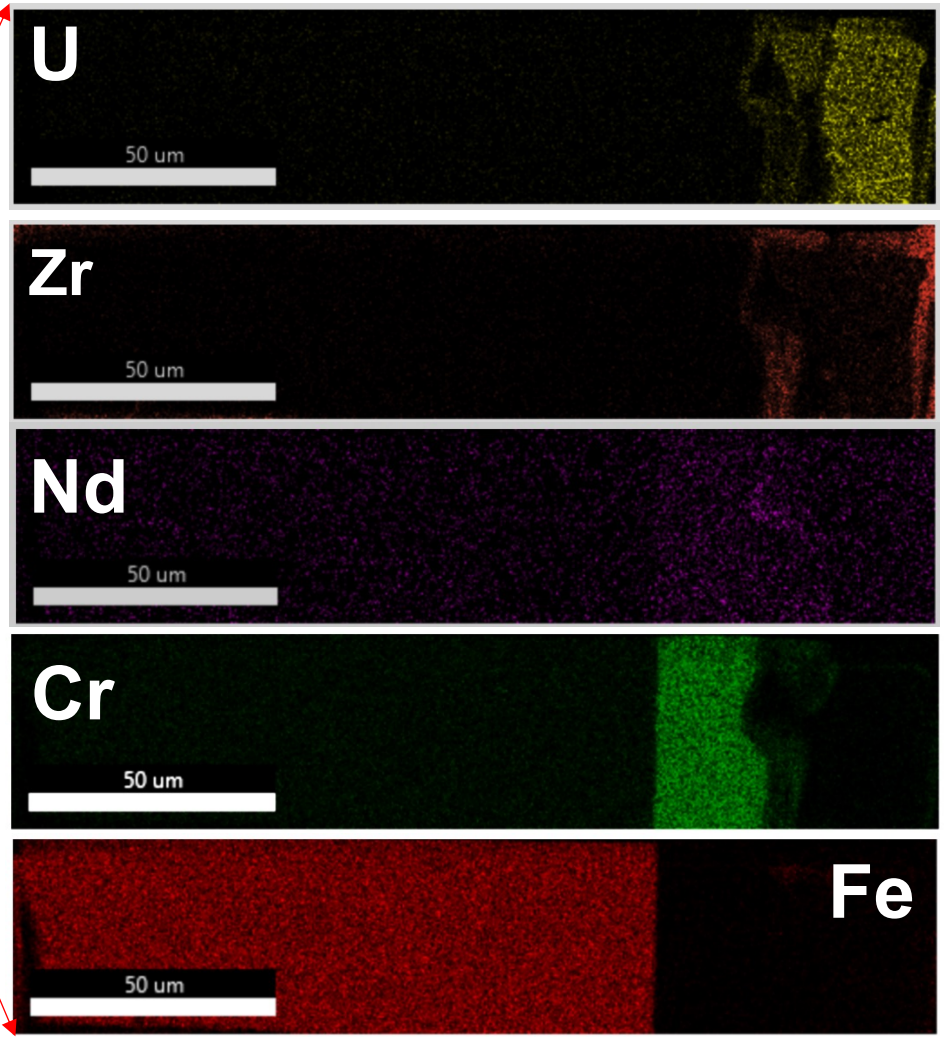

SEM-EDS on side cross section of liftout:

- Potential attack on Cr-linear due to diffusion of fuel constituents and local accumulation of Nd
- The majority of Cr-linear was retained after irradiation testing

Micro-tensile Testing

Summary of Micro-tensile Testing (RT)

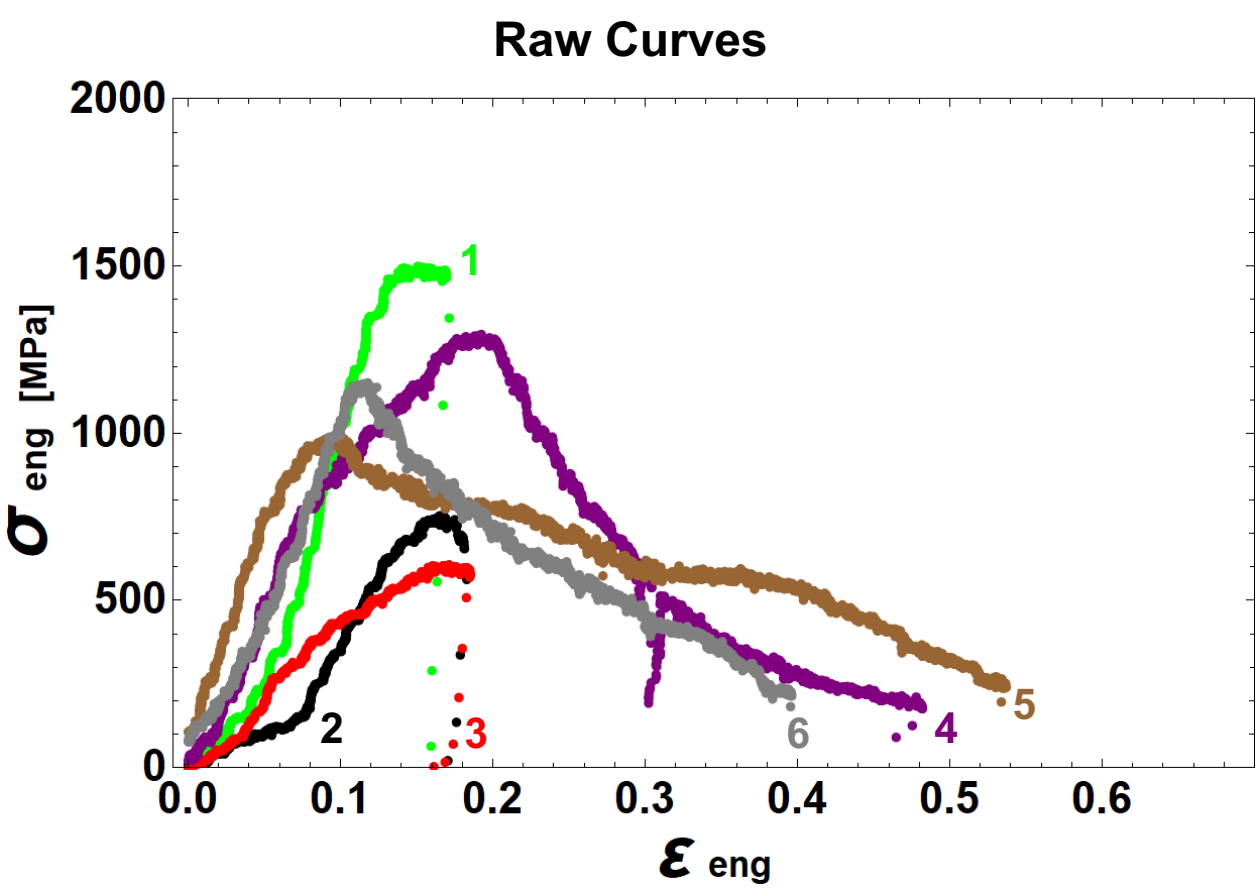

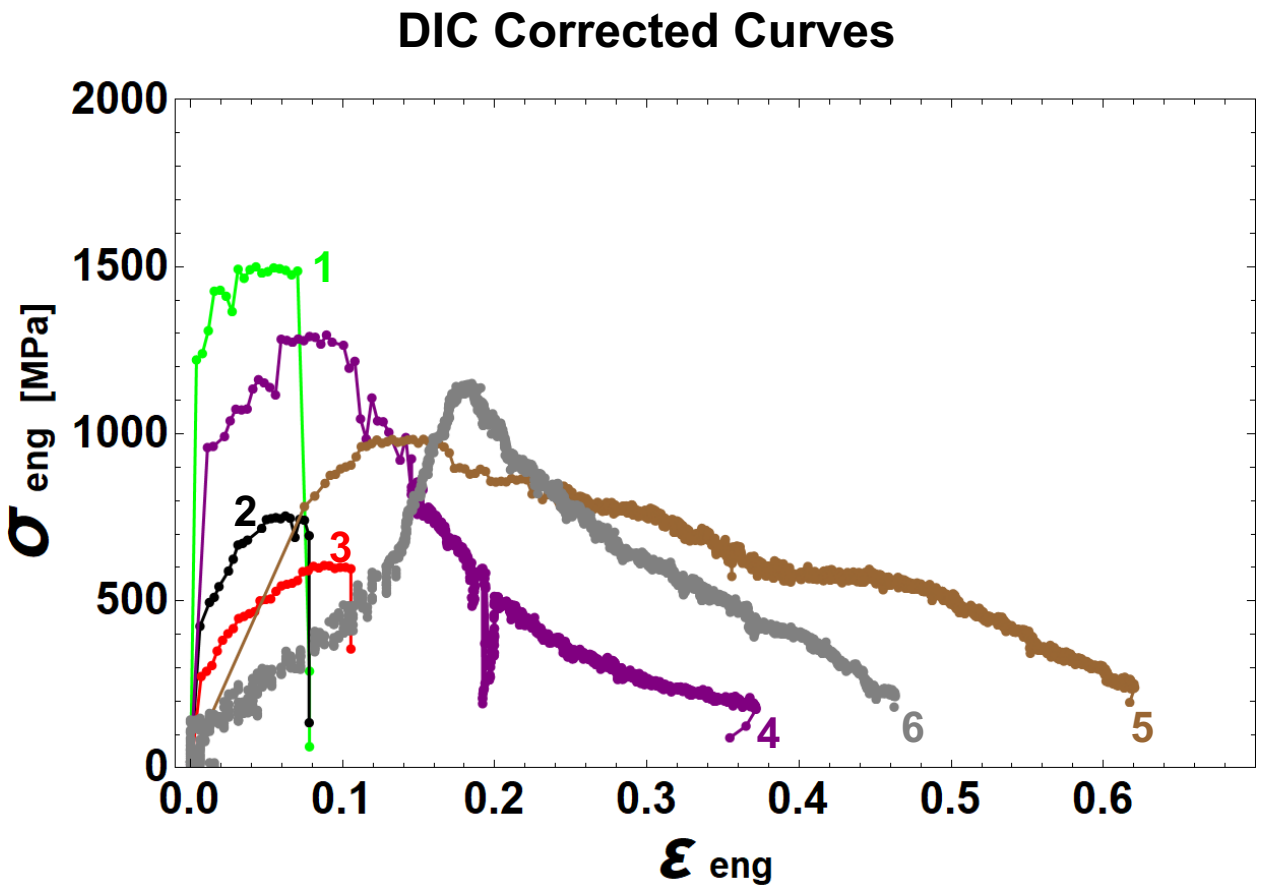

DIC corrected stress-strain curves (RT)

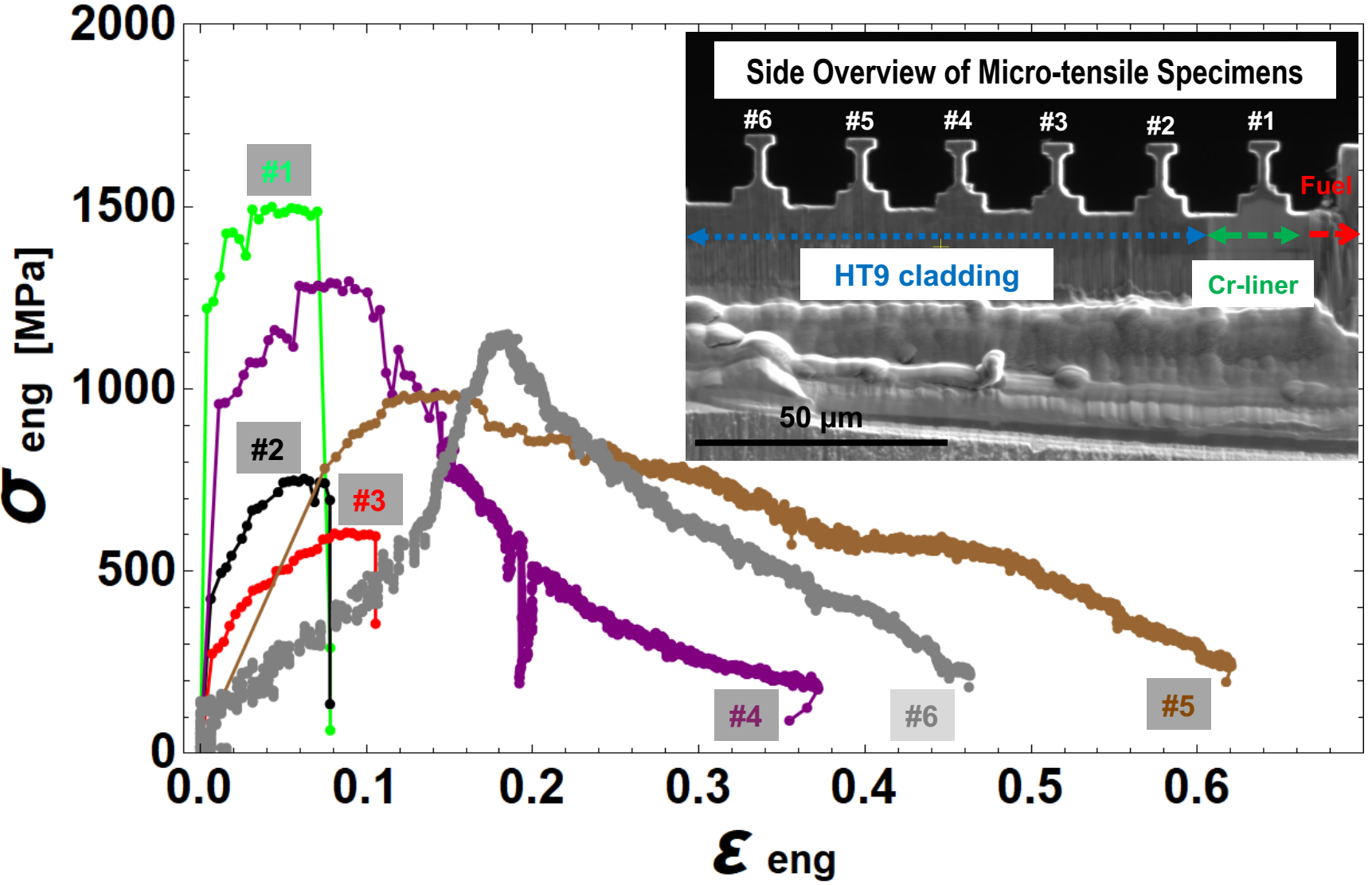

Micro-tensile specimens	Material	$\sigma_{y\text{-}DIC}$ [Mpa]	σ_{max} [Mpa]	$\varepsilon_{total\text{-}DIC}$ [%]
#1	Cr-liner	1231	1500	7.8*
#2	HT9	451	754	7.8*
#3	HT9	284	606	10.5*
#4	HT9	961	1296	37.2
#5	HT9	799	984	61.7
#6	HT9	957	1151	46.3
HT9 Average (#2-6)		690 ± 275	958 ± 252	
HT9 Average (#4-6)		906 ± 75	1144 ± 127	

Note: *Stopped after yielding plus first observable deformation in tensile gauge

Summary

Micro-tensile specimens	Material	$\sigma_{y\text{-}DIC}$ [Mpa]	σ_{max} [Mpa]	$\varepsilon_{total\text{-}DIC}$ [%]
#1	**Cr-barrier**	1231	1500	7.8*
#2	**HT9**	451	754	7.8*
#3	**HT9**	284	606	10.5*
#4	**HT9**	961	1296	37.2
#5	**HT9**	799	984	61.7
#6	**HT9**	957	1151	46.3
HT9 Average (#2-6)		690 ± 275	958 ± 252	
HT9 Average (#4-6)		906 ± 75	1144 ± 127	
Note: *Stopped after yielding plus first observable deformation in tensile gauge				

Tensile Bar	Material	$\sigma_{y\text{-}raw}$ [MPa]	$\sigma_{y\text{-}DIC}$ [MPa]	σ_{max} [MPa]	$\varepsilon_{total\text{-}raw}$ [%]	$\varepsilon_{total\text{-}DIC}$ [%]
1	CrN coating	1351	1231	1500	17.1*	7.8*
2	HT9	647	451	754	18.3*	7.8*
3	HT9	431	284	606	18.5*	10.5*
4	HT9	843	961	1296	48.2	37.2
5	HT9	762	799	984	53.7	61.7
6	HT9	1103	957	1151	39.6	46.3
HT9 Average	HT9	757 ± 248	690 ± 308	958 ± 282	47.2 ± 7.1	48.4 ± 12.4

*Stopped after yielding + first observable deformation on tensile gage.

High Resolution Figure for 1st paper

Figure 1&2 (Sample prep, SEM characterization

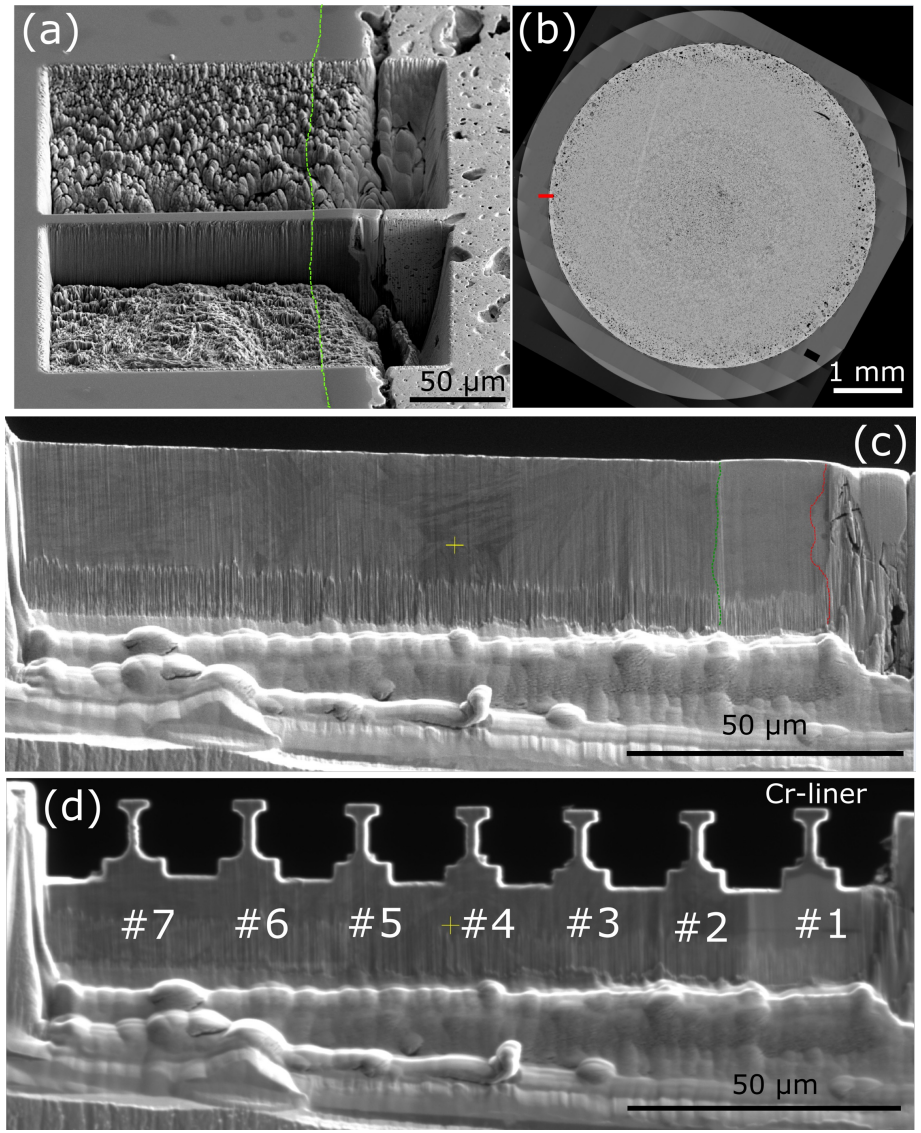

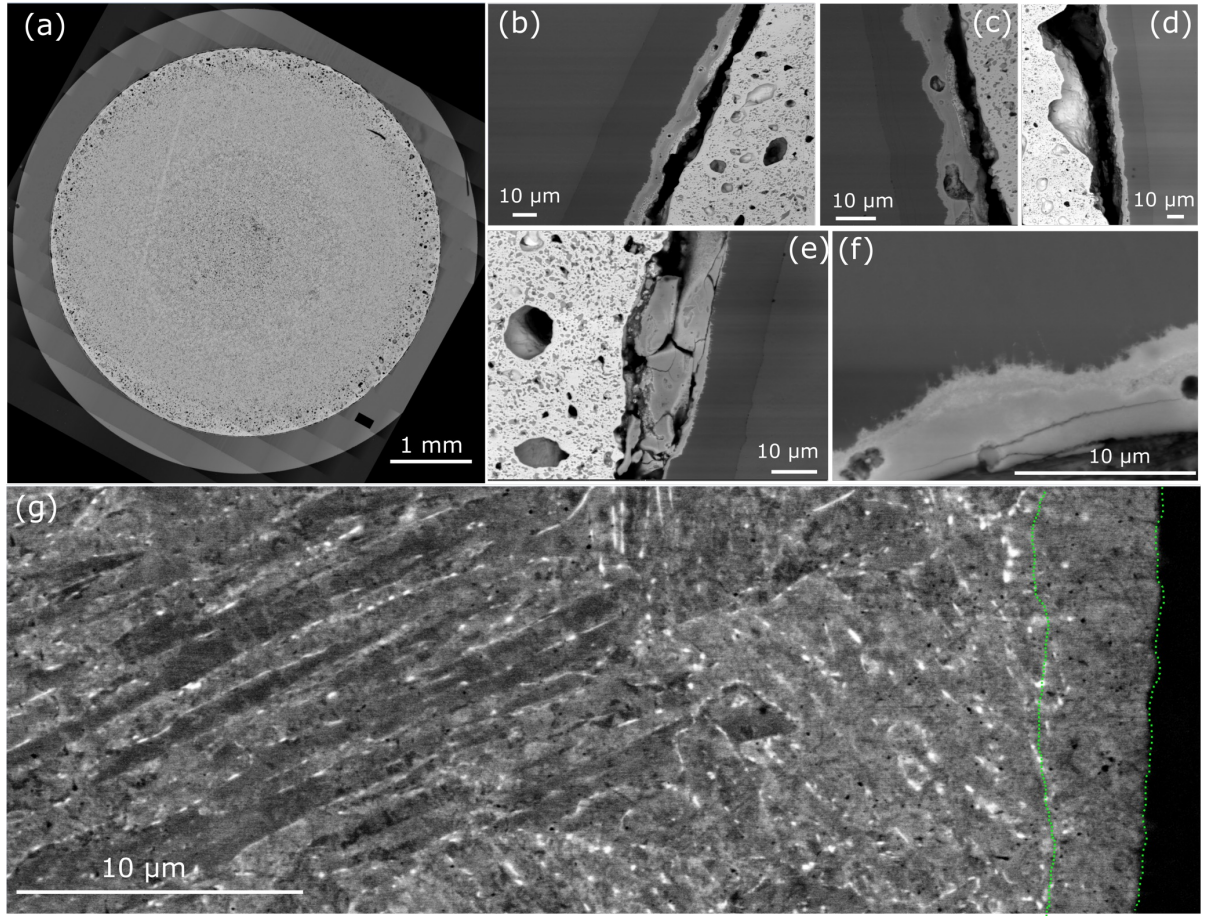

Left: green line highlights the HT9-Cr liner interface in (a); a SEM image showing the large liftout cross HT9 cladding (on the left of dashed green line), Cr-liner (in between dashed green and red lines), and the fuel periphery (on the right of dashed red line); a SEM image showing the fabricated micro-tensile specimens, #1 is Cr-liner.
Right: (a) A stitched backscattered electron image revealing the entire cross section the sample. There is no observable microcracks in the Cr-liner. (b)-(f) SEM images showing the localized interaction zones along Cr-liner circumference. (g) A SEM image of HT9 cladding revealed the disappearance of typical lath structure in proximity to Cr-liner.

Figure 3: SEM-EDS characterization of large liftout cross fuel periphery, Cr liner, and HT9 cladding

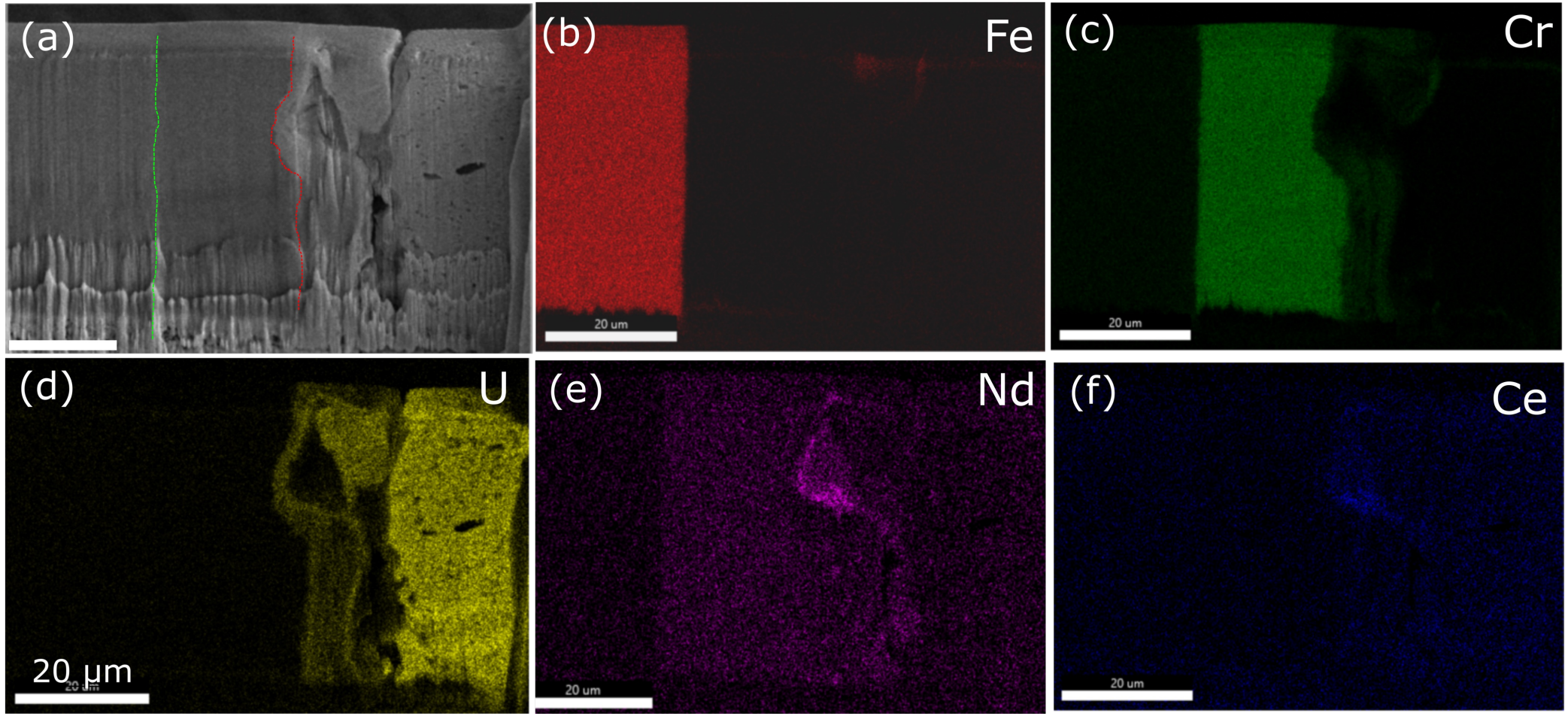

Figure 4: Stress-Strain curves for In-situ SEM micro-tensile testing

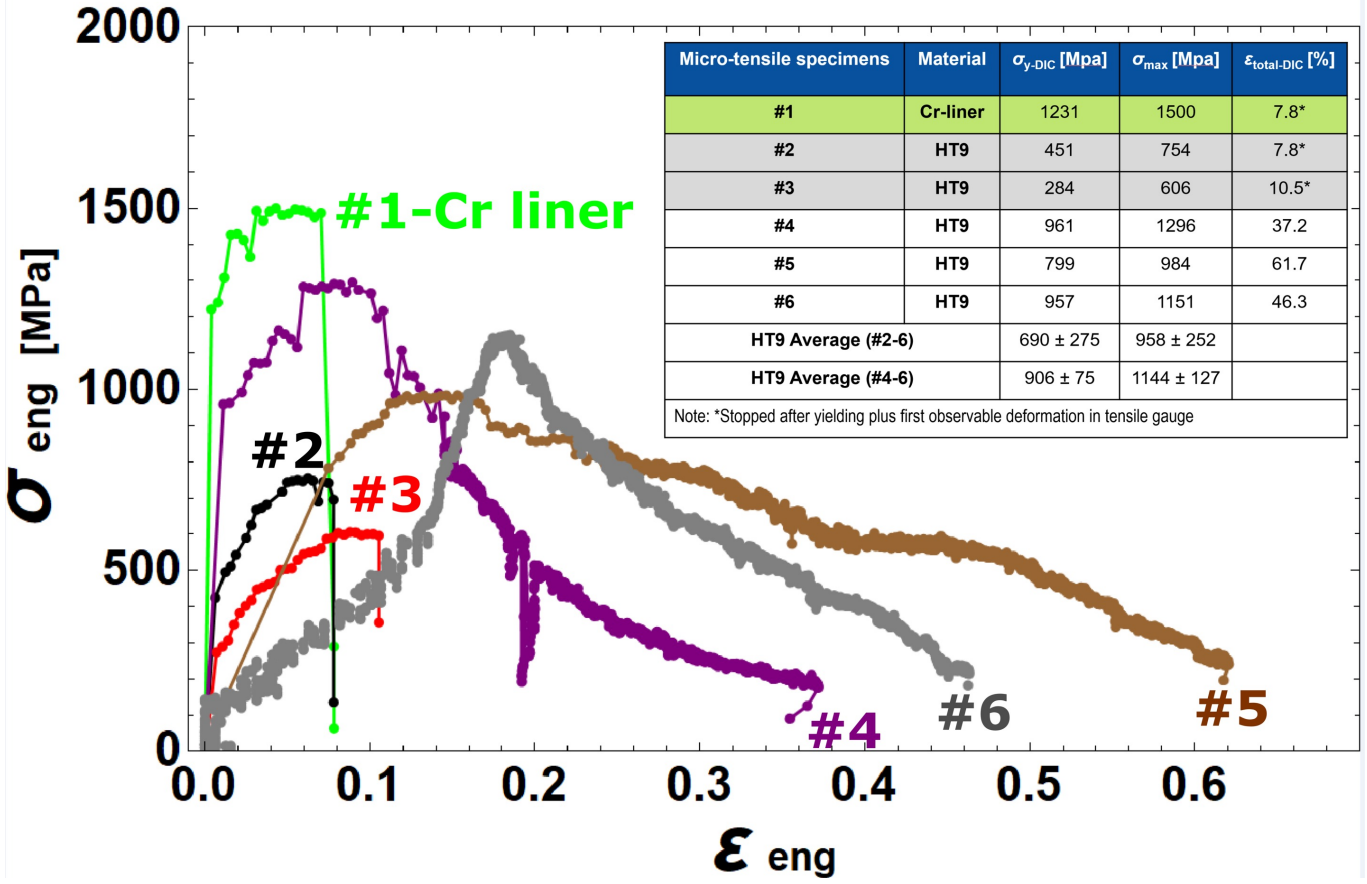

Micro-tensile specimens	Material	$\sigma_{y\text{-}DIC}$ [Mpa]	σ_{max} [Mpa]	$\varepsilon_{total\text{-}DIC}$ [%]
#1	Cr-liner	1231	1500	7.8*
#2	HT9	451	754	7.8*
#3	HT9	284	606	10.5*
#4	HT9	961	1296	37.2
#5	HT9	799	984	61.7
#6	HT9	957	1151	46.3
HT9 Average (#2-6)		690 ± 275	958 ± 252	
HT9 Average (#4-6)		906 ± 75	1144 ± 127	

Note: *Stopped after yielding plus first observable deformation in tensile gauge

In-situ SEM micro-tensile testing was conducted at RT:

1. One Cr-liner micro-tensile bar and five HT9 bars tested
2. Microtensile bar gauge geometry: 3 μm *3 μm *8 μm
3. The measured stress-strain results, together with yield strength and ultimate tensile strength results, were shown in the figure.
4. As expected, the Cr-liner bar exhibited much stronger strength than the HT9 ones
5. Among the five tested HT9 micro-tensile bars, the #2 and #3 showed remarkable mechanical softening as indicated by their much lower yield strength (284-451 Mpa) than that of the rest three HT9 tests (799-961 Mpa). Mechanical softening in reactor-irradiated HT9 cladding has been reported recently (33A work)
6. TEM characterization on tested bar3 and bar2 will add on insight into understanding the observed softening

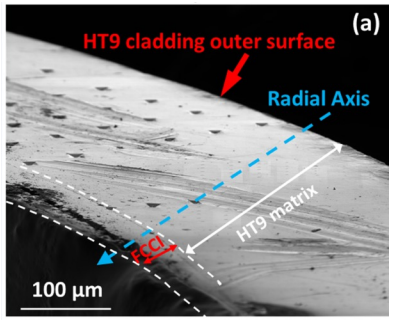

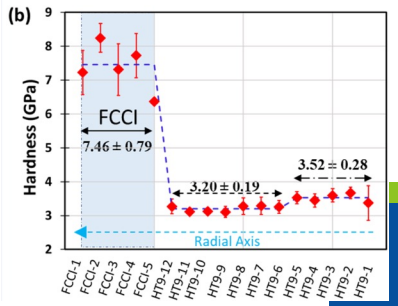

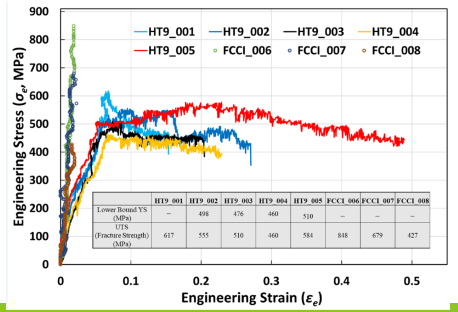

Figure 5: TEM/STEM Characterization of tested Bar3 which exhibited dramatic mechanical softening

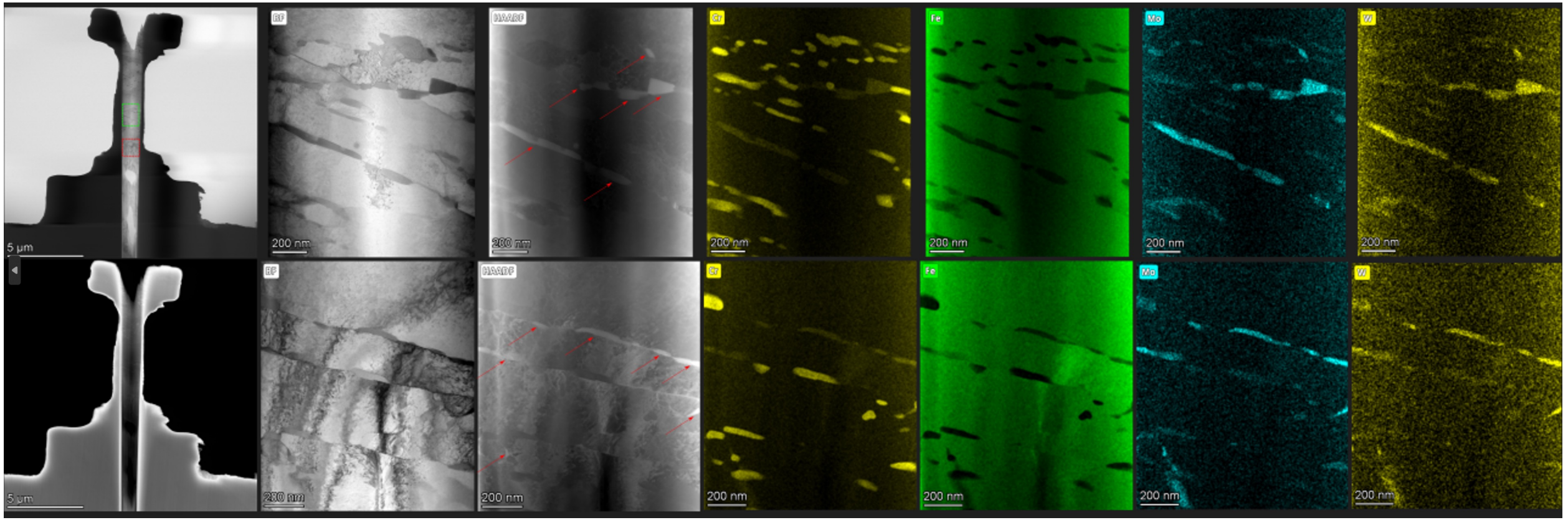

To better understand the observed mechanical softening in Bar 3 (and 2), post-test TEM/STEM characterization was conducted.

1. The typical lath structure was retained (BF images)
2. A high density of precipitates along lath boundary was observed
3. STEM characterization revealed two types of precipitates:
    - Typical $M_{23}C_6$ (M = Cr and Fe)
    - Mo and W-rich phases (red arrow highlighted), which could be intermetallic Fe_2(Mo, W) Laves phase (Refer to 33A paper in which detail discussion of its effect on mechanical property has been reported)

Figure 6 &7: TEM/STEM Characterization of tested Bar1-Cr liner

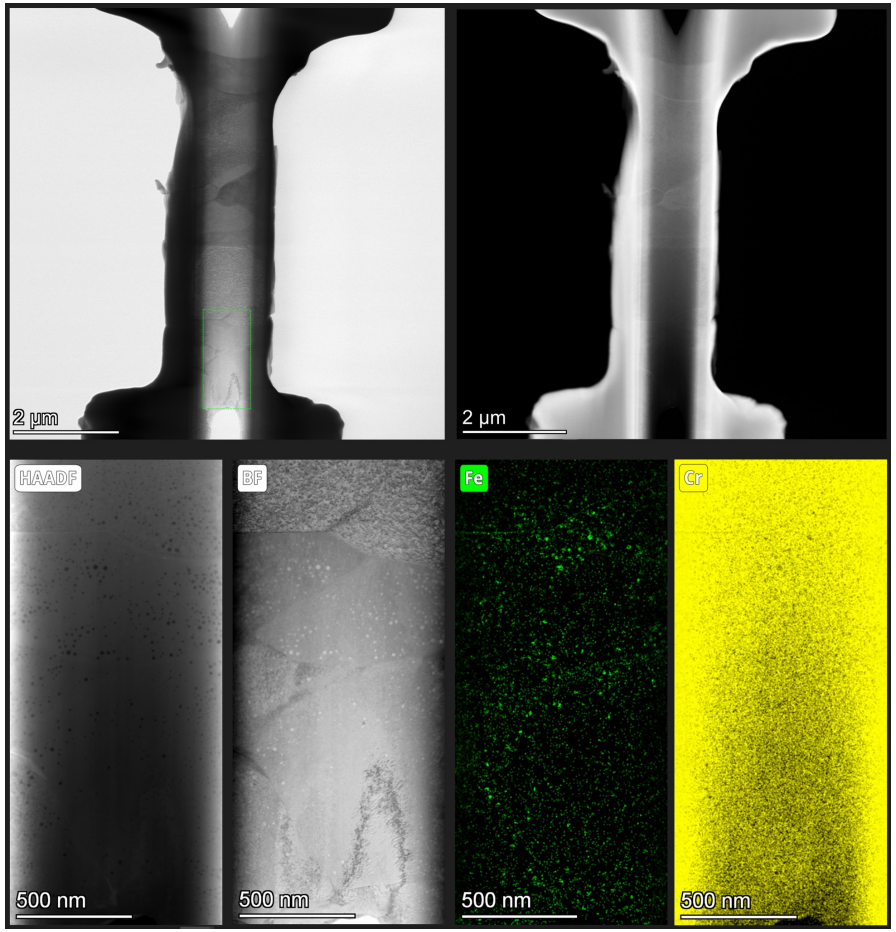

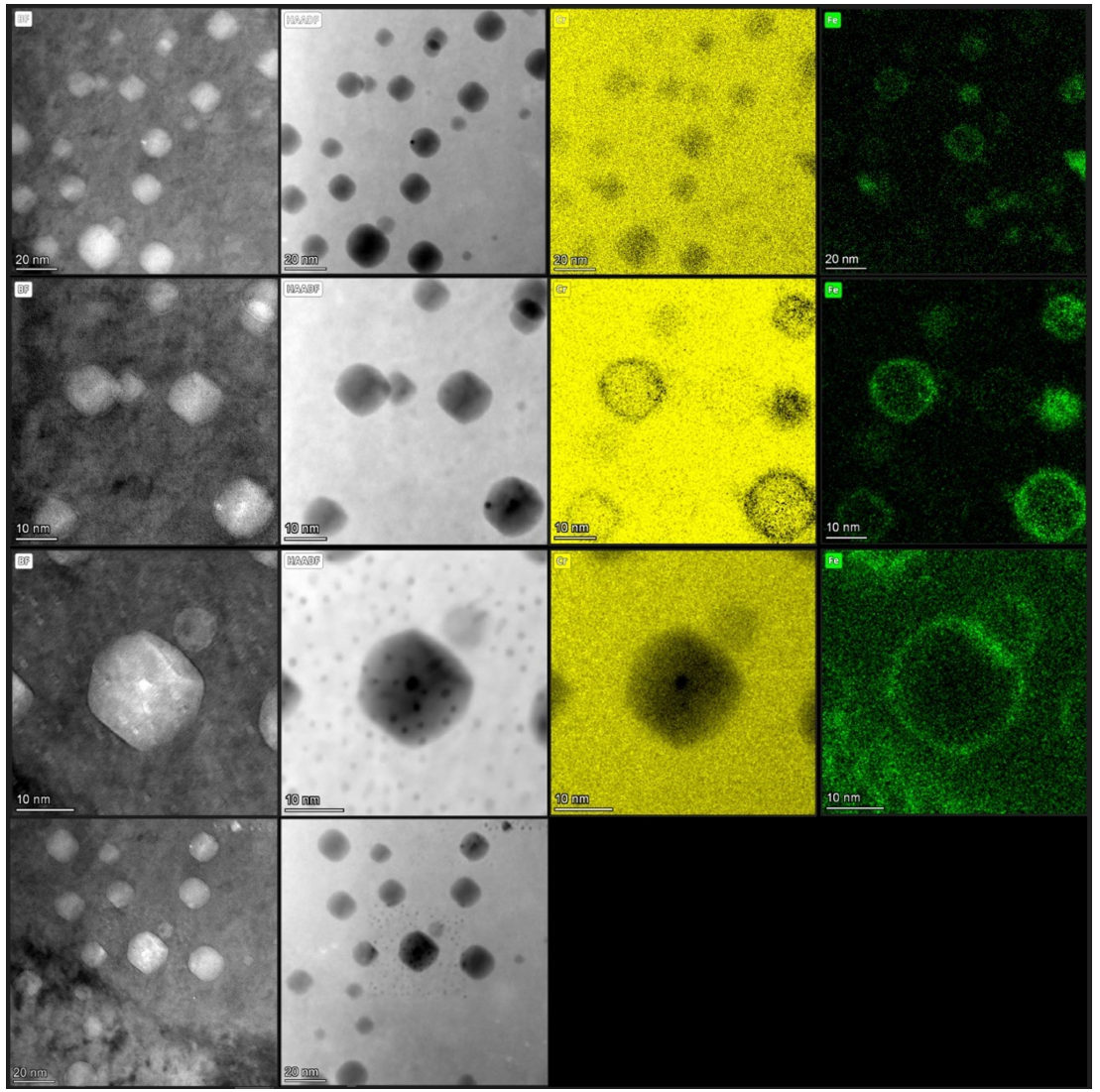

To better understand the micromechanical behavior of Cr-liner, TEM/STEM (and potentially EELS) was conducted:

1. TEM images revealed the nanoscale grains
2. A high density of voids formed. Void formation could cause embrittlement/hardening in Cr-liner and then affect Cr-liner integrity and diffusion barrier performance. There is no microcracks detected in the current sample.
3. High magnification STEM characterization found there is a Fe shell associated with those voids. It is likely that Fe diffused from HT9 during Cr-liner fabrication (temperature?)
4. The nanodots in (HAADF 3rd row) was electron beam damage caused during STEM mapping for no such dots exhibited outside of the scanned area (last row)

Figure 8: TEM/STEM Characterization of HT9- Cr liner interface

Will add on soon.

Figure 9: TEM/STEM Characterization of bar2 (nearby Cr-liner)

Will add on soon.

Abstract Figure

Will add on soon.

Tensile Specimen 1: Cr-liner

w_{min} = 1.953 µm
w_{avg} = 2.089 ± 0.084 µm

t = 1.579 ± 0.095 µm
ℓ = 4.735 ± 0.066 µm, $\dot{e} = 10^{-3}$ -> loading rate = 5 nm/s

Aspect Ratios $\ell : t$ = 3.00:1, $\ell : w_{avg}$ = 2.27:1, $\ell : w_{min}$ = 2.42:1

A_{min} = 3.084 ± 0.186 µm^2
A_{avg} = 3.299 ± 0.331 µm^2

Top

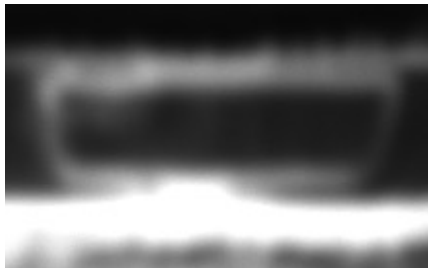

5 µm

Side

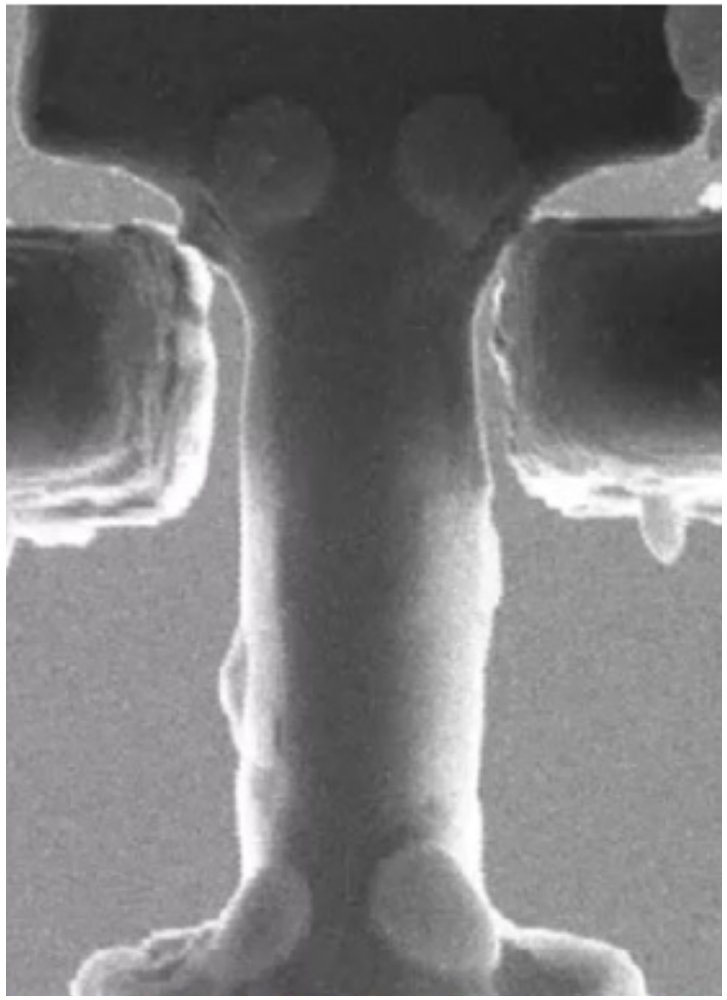

4 µm

Tensile Specimen 1 Test Video

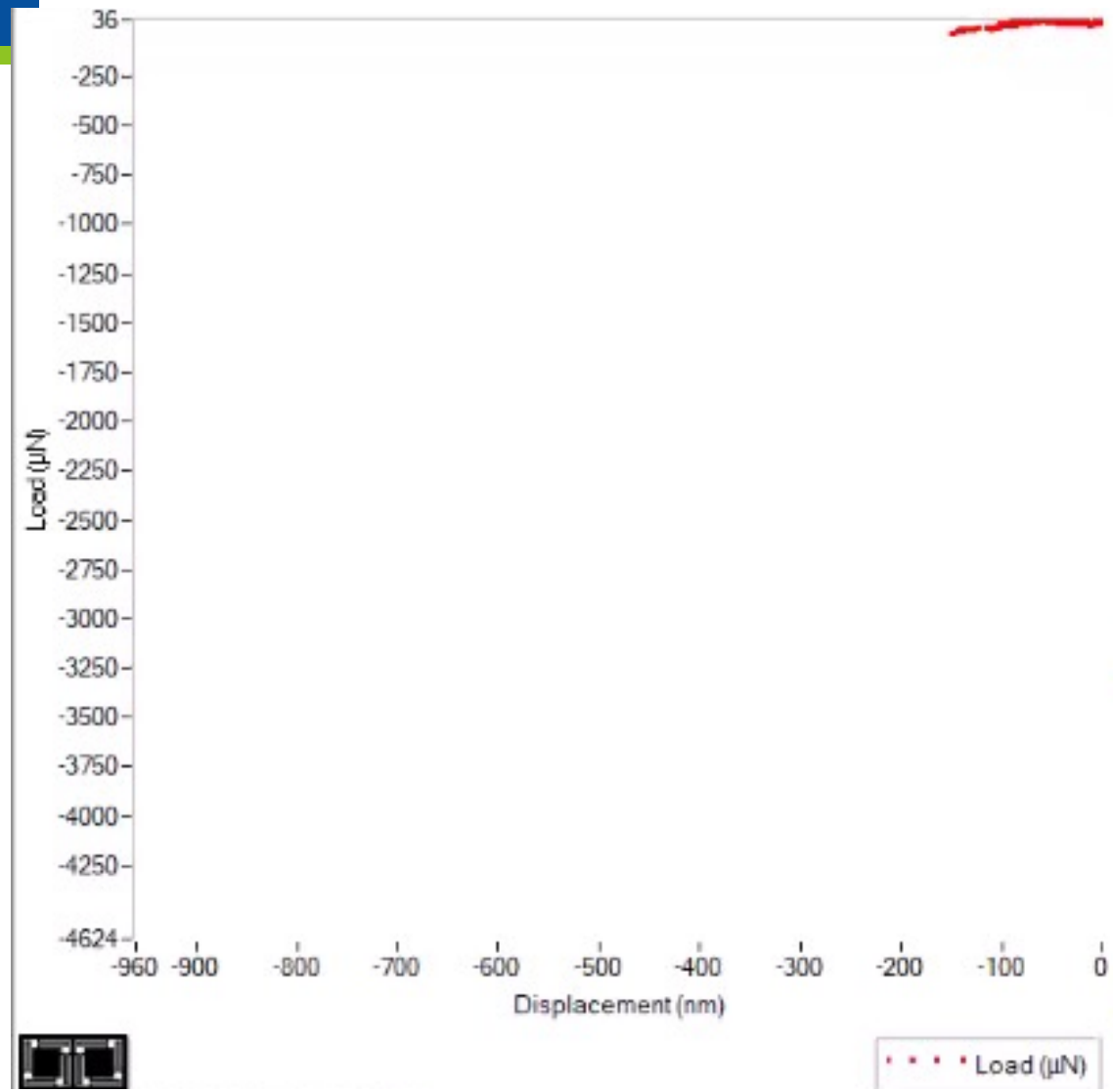

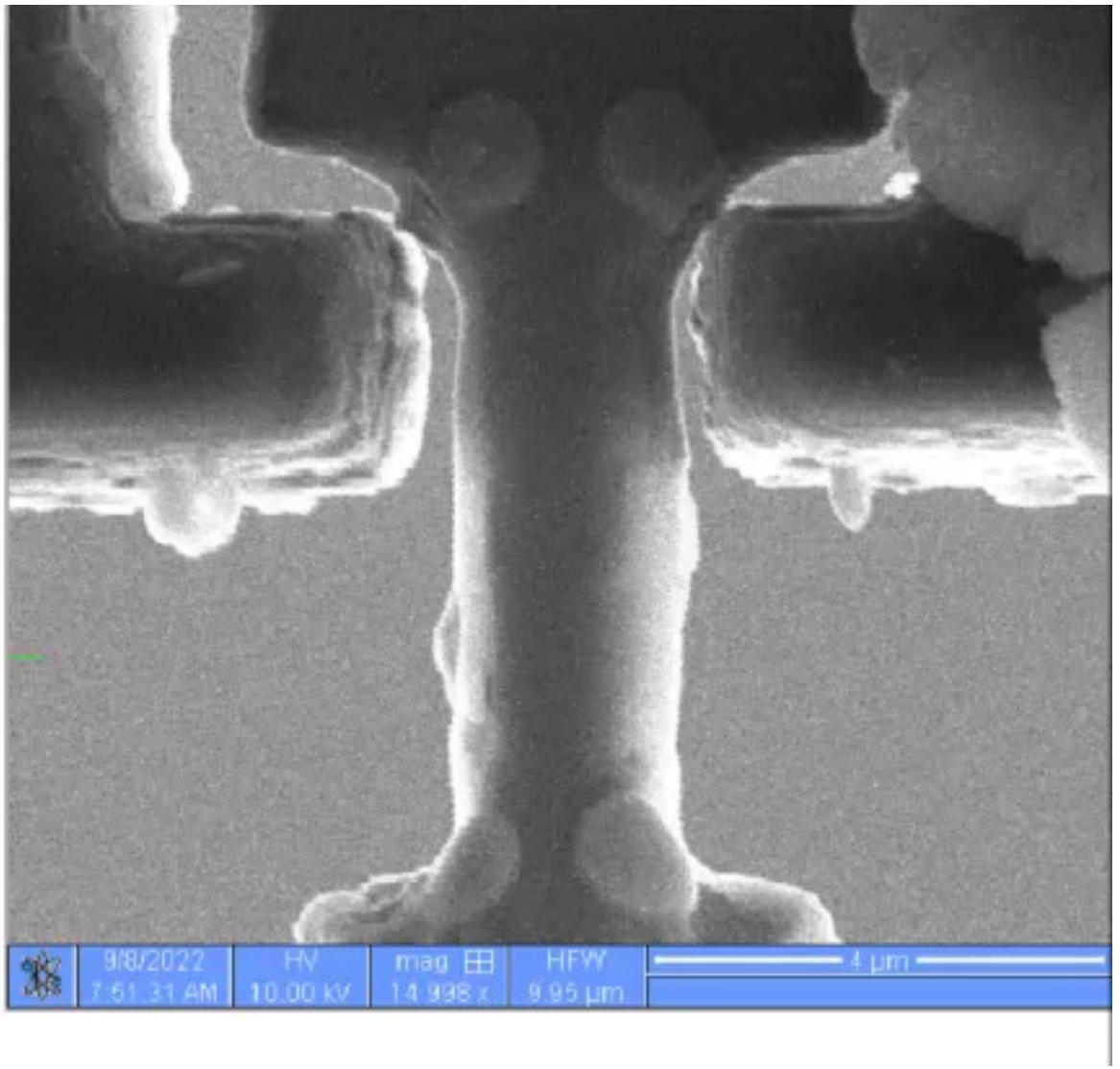

Tensile Specimen 1 Raw Engineering Stress-Strain

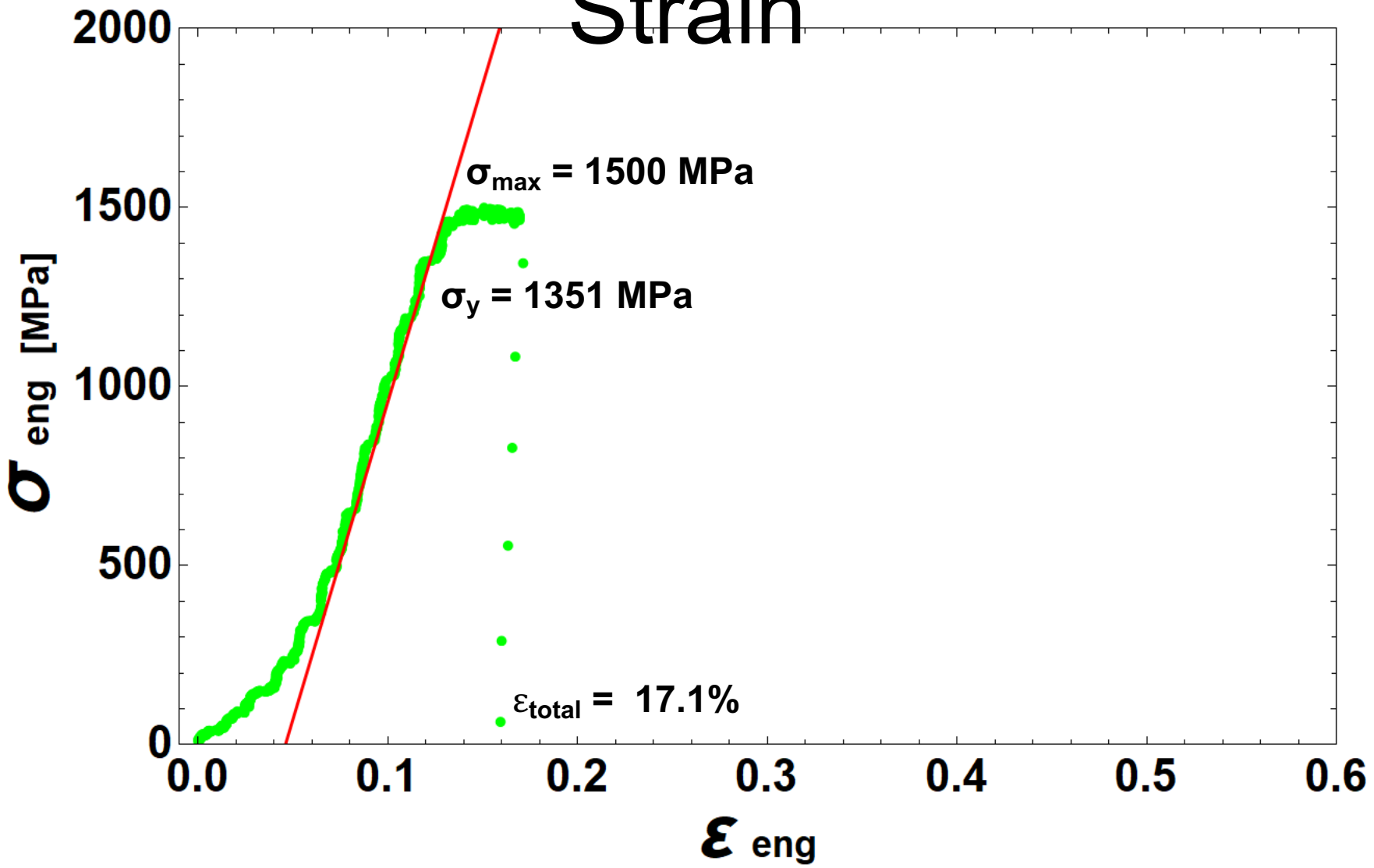

Tensile Specimen 1 DIC Corrected Engineering Stress-Strain

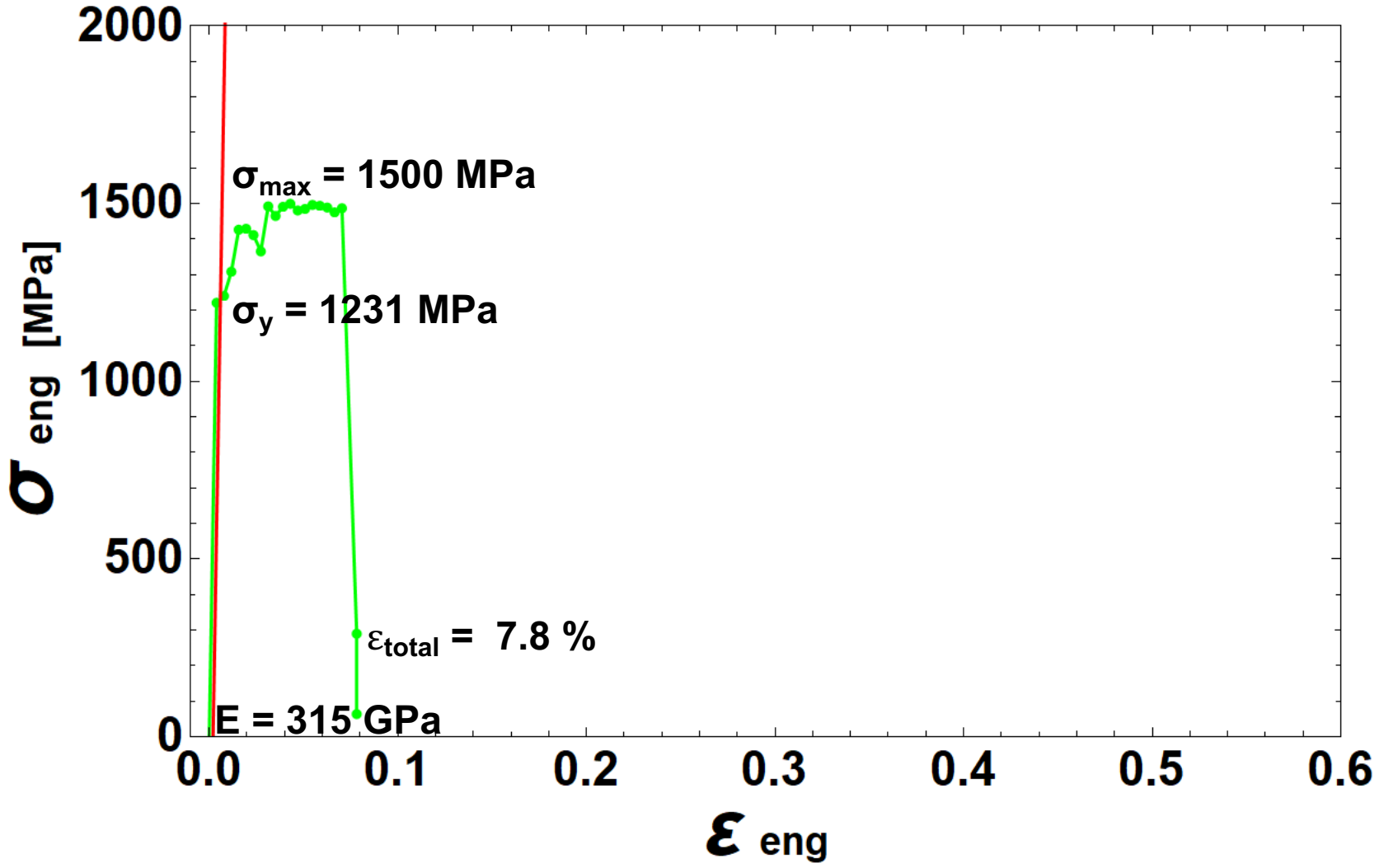

Tensile Specimen 1 Post Test Images

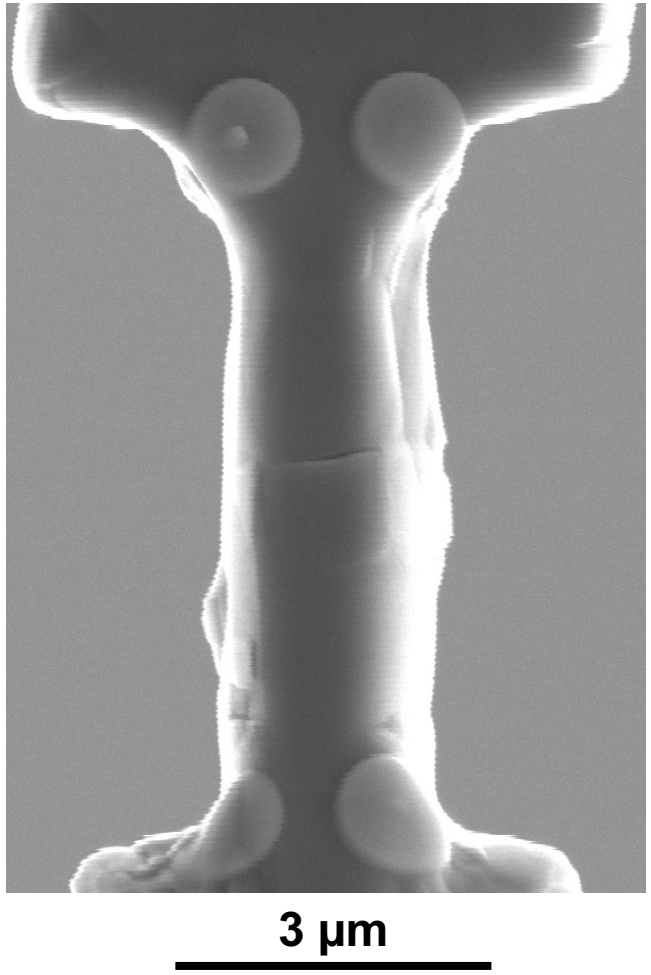

Tensile Specimen 2: HT9 Cladding

w_{min} = 2.073 µm
w_{avg} = 2.147 ± 0.050 µm

t = 1.672 ± 0.131 µm

ℓ = 4.825 ± 0.123 µm, $\dot{e} = 10^{-3}$ -> loading rate = 5 nm/s

Aspect Ratios $\ell : t$ = 2.89:1, $\ell : w_{avg}$ = 2.25:1, $\ell : w_{min}$ = 2.33:1

A_{min} = 3.466 ± 0.272 µm^2
A_{avg} = 3.590 ± 0.365 µm^2

Top

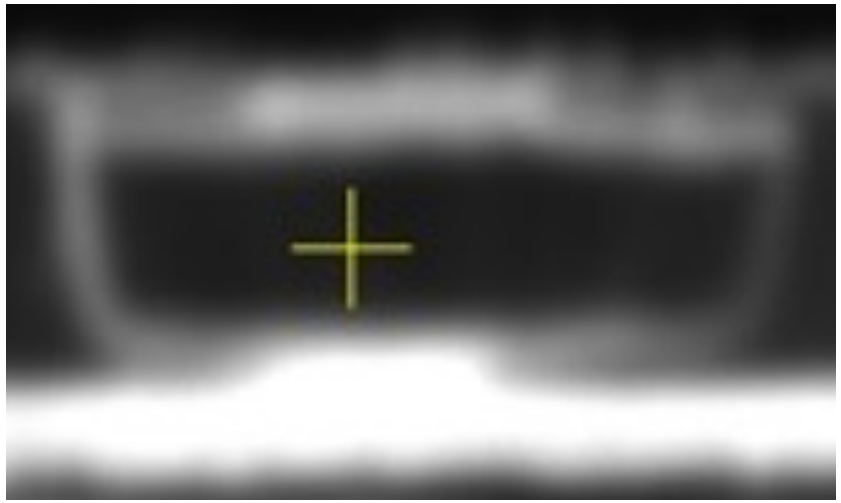

5 µm

Side

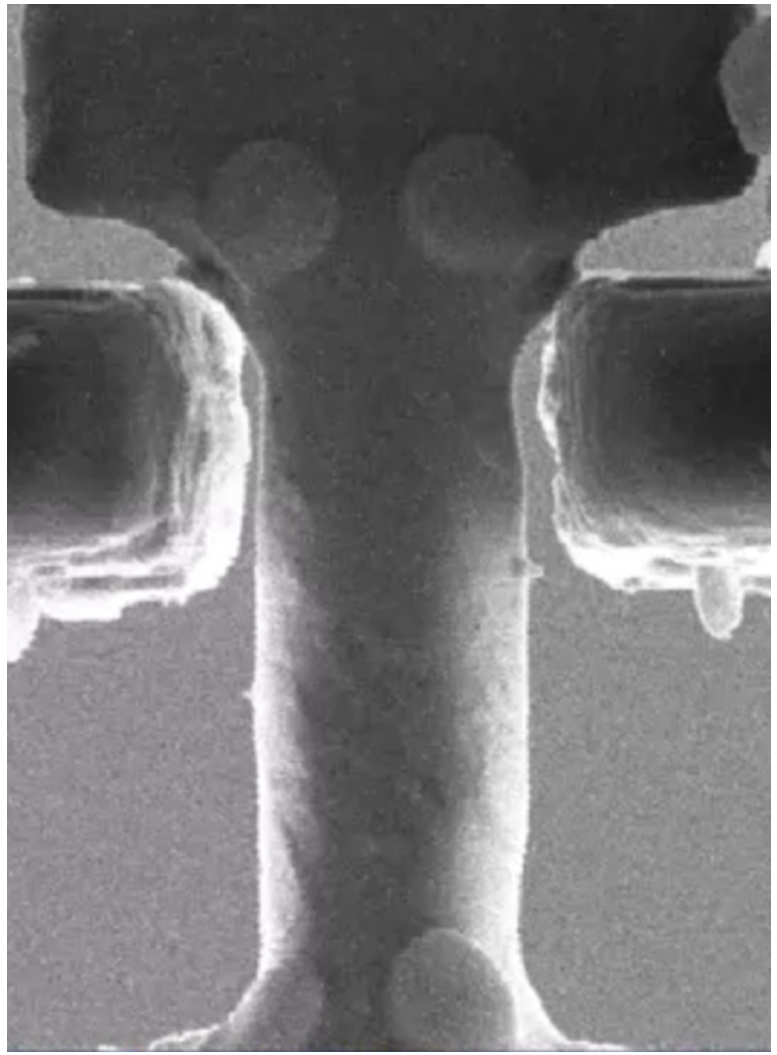

4 µm

Tensile Specimen 2 Test Video

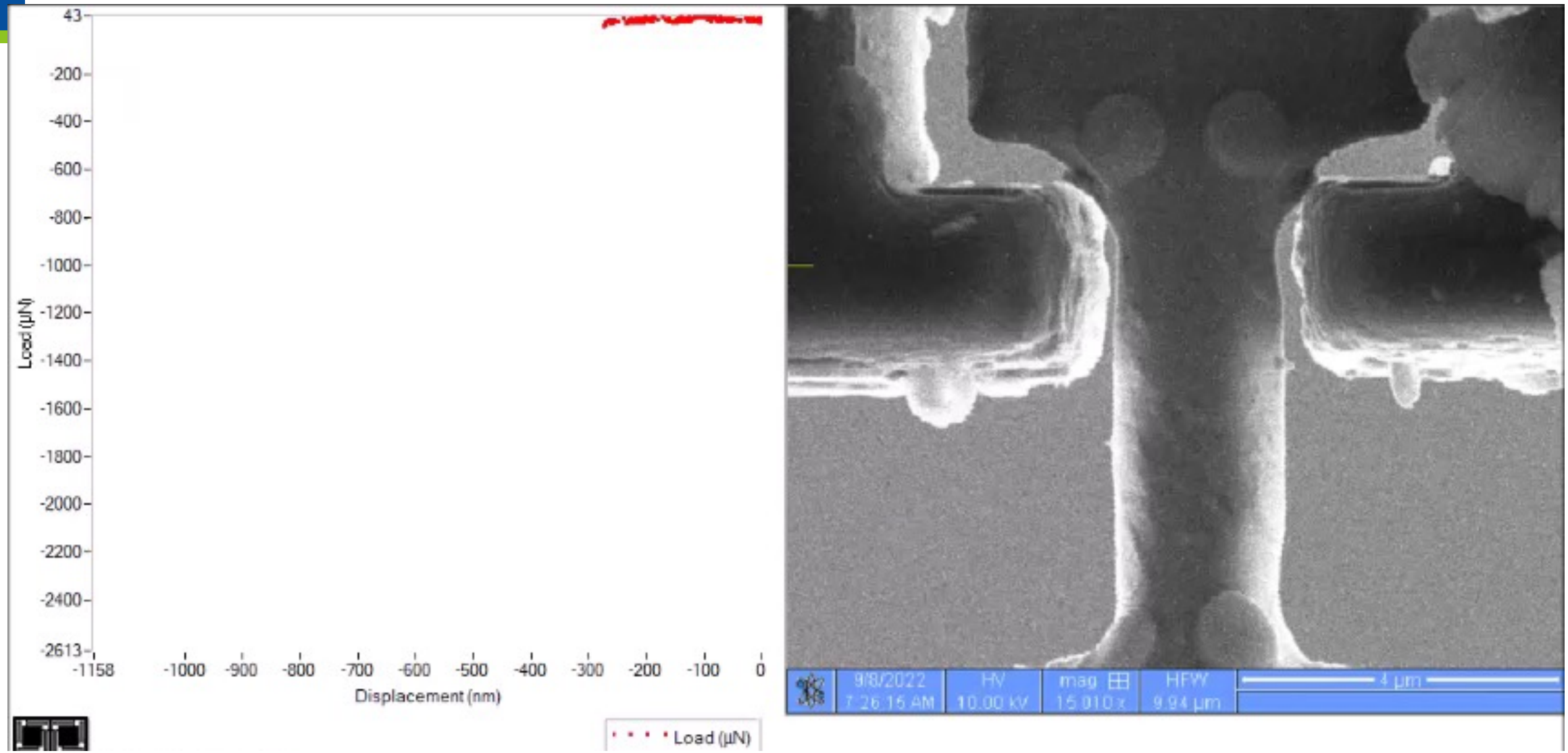

Tensile Specimen 2 Raw Engineering Stress-Strain

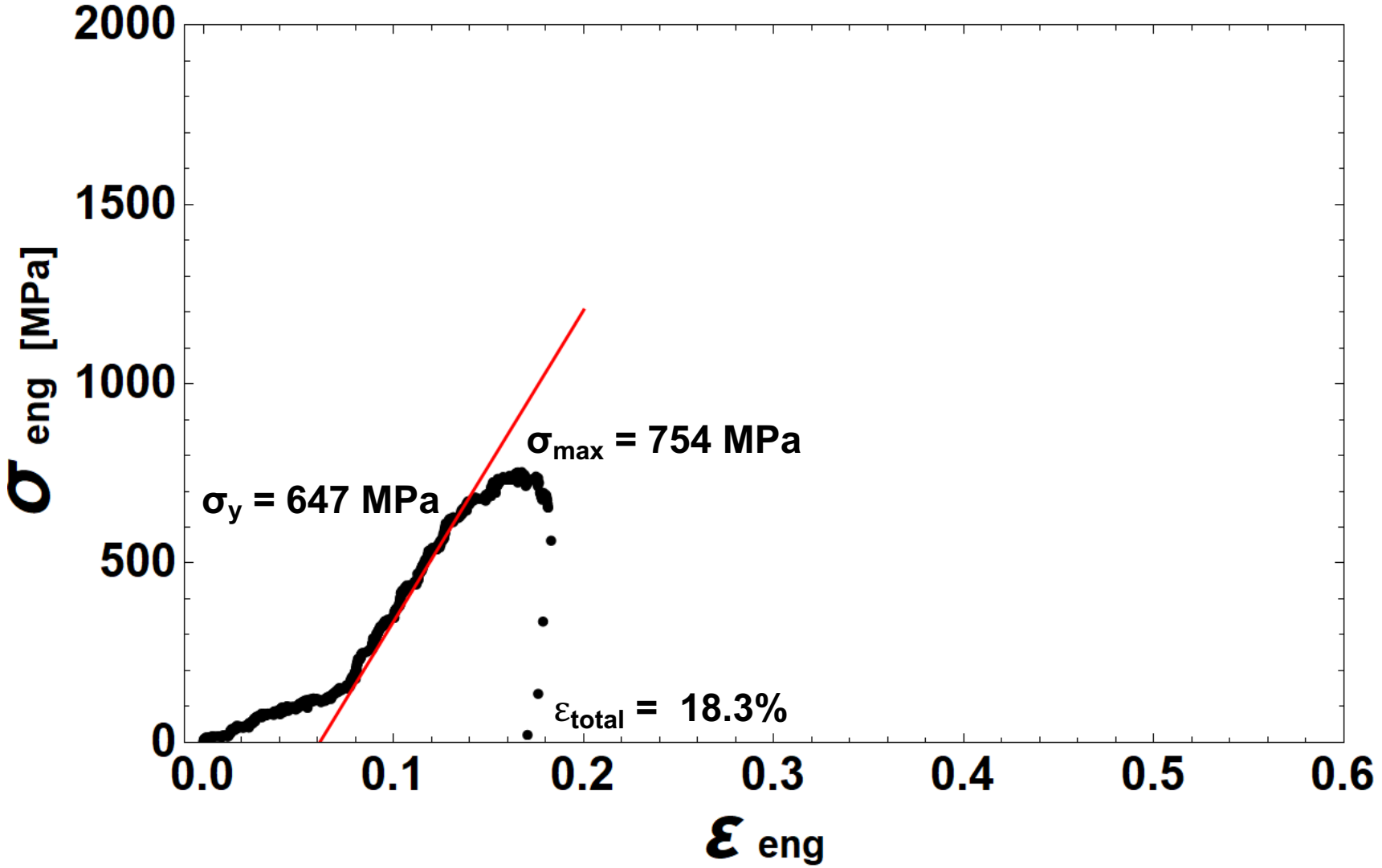

Tensile Specimen 2 DIC Corrected Engineering Stress-Strain

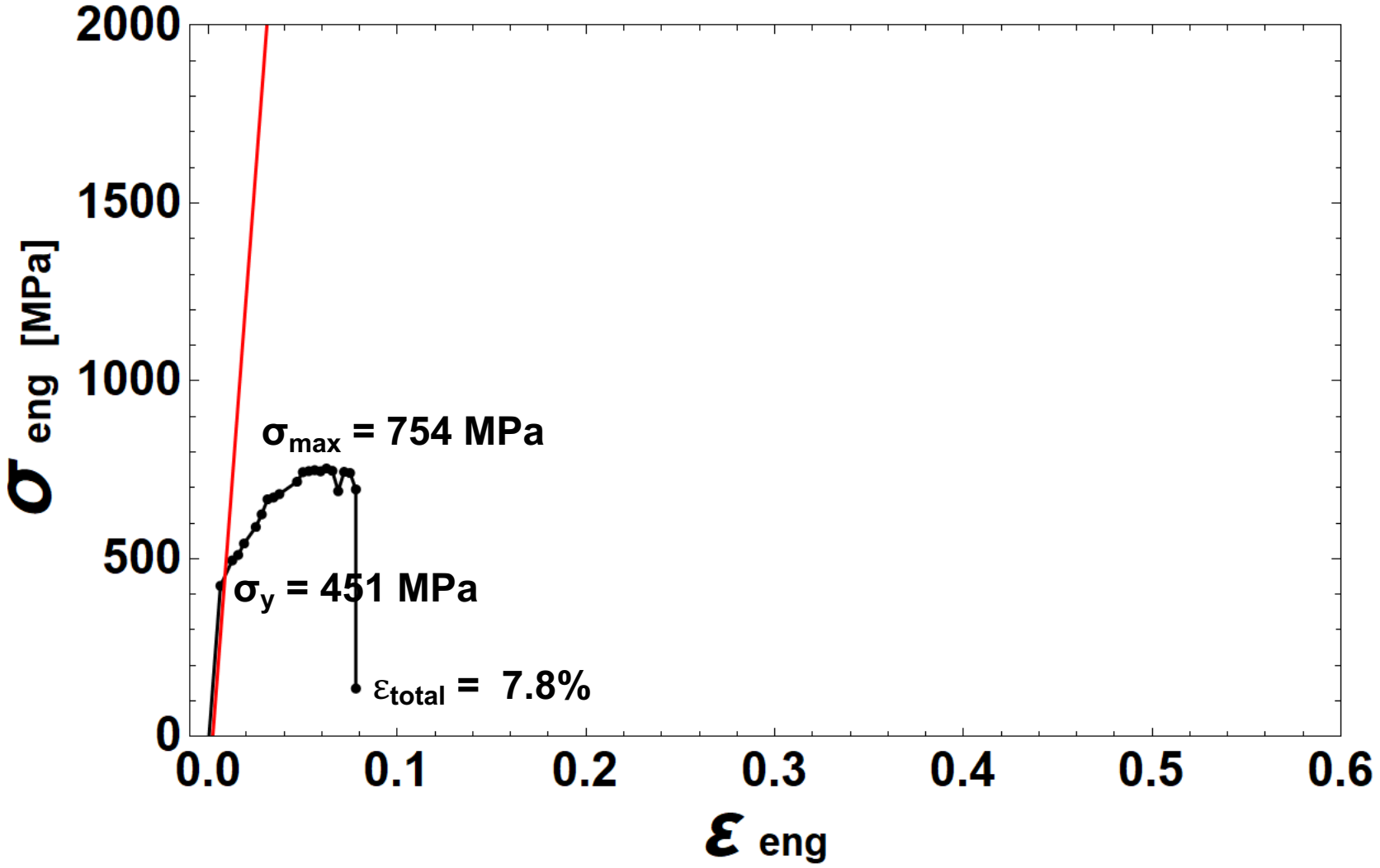

Tensile Specimen 2 Post Test Images

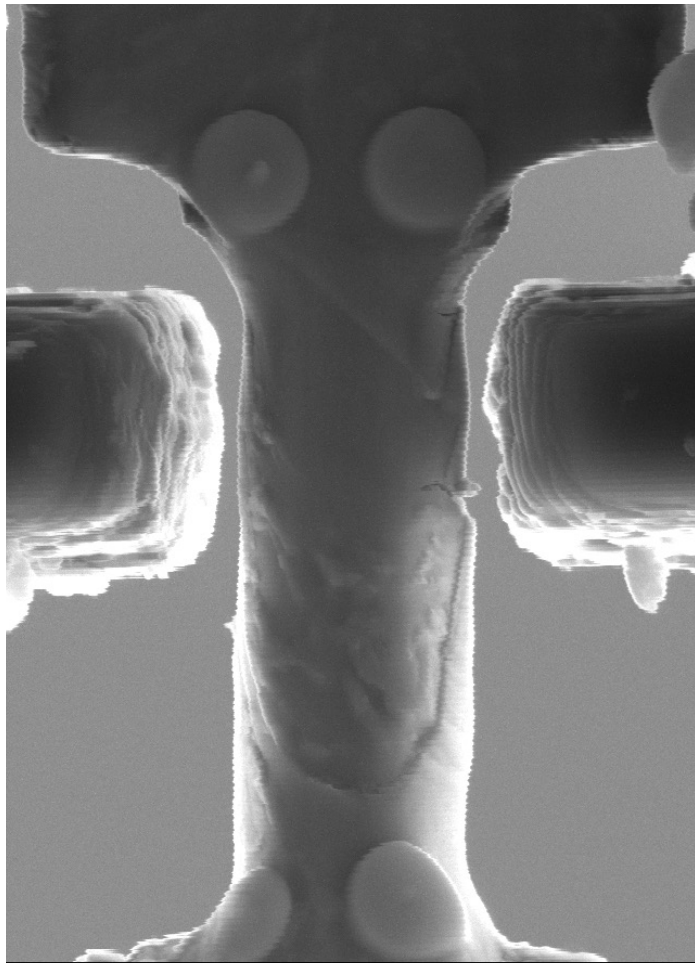

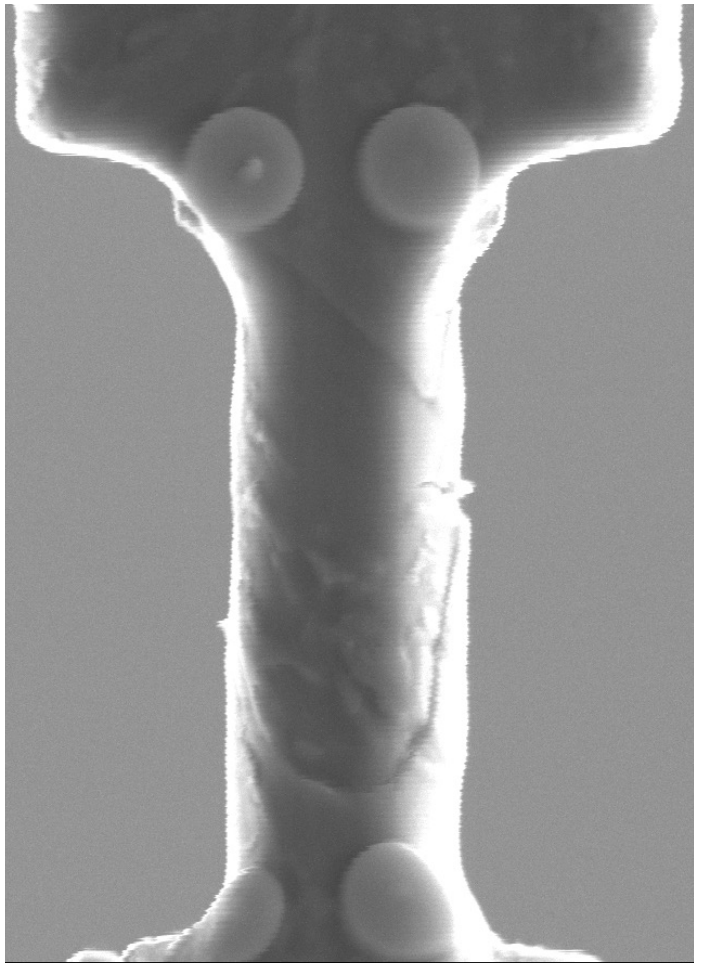

Tensile Specimen 3: HT9 Cladding

w_{min} = 1.962 µm
w_{avg} = 2.013 ± 0.034 µm

t = 1.944 ± 0.131 µm

ℓ = 4.714 ± 0.021 µm, $\dot{e}$ = 10^{-3} -> loading rate = 5 nm/s

Aspect Ratios ℓ : t = 2.42:1, ℓ : w_{avg} = 2.34:1, ℓ : w_{min} = 2.40:1

A_{min} = 3.814 ± 0.257 µm^2
A_{avg} = 3.913 ± 0.330 µm^2

Top

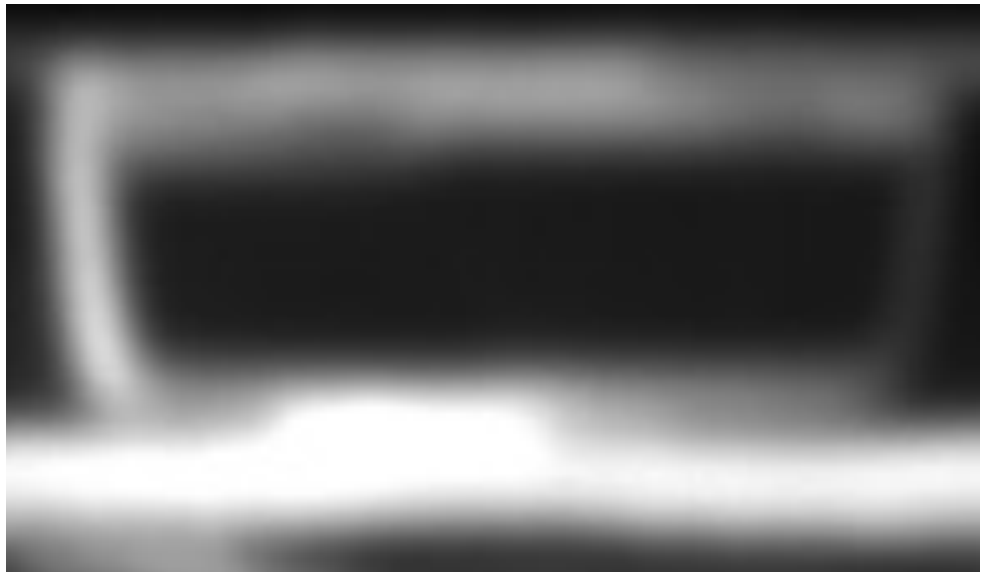

5 µm

Side

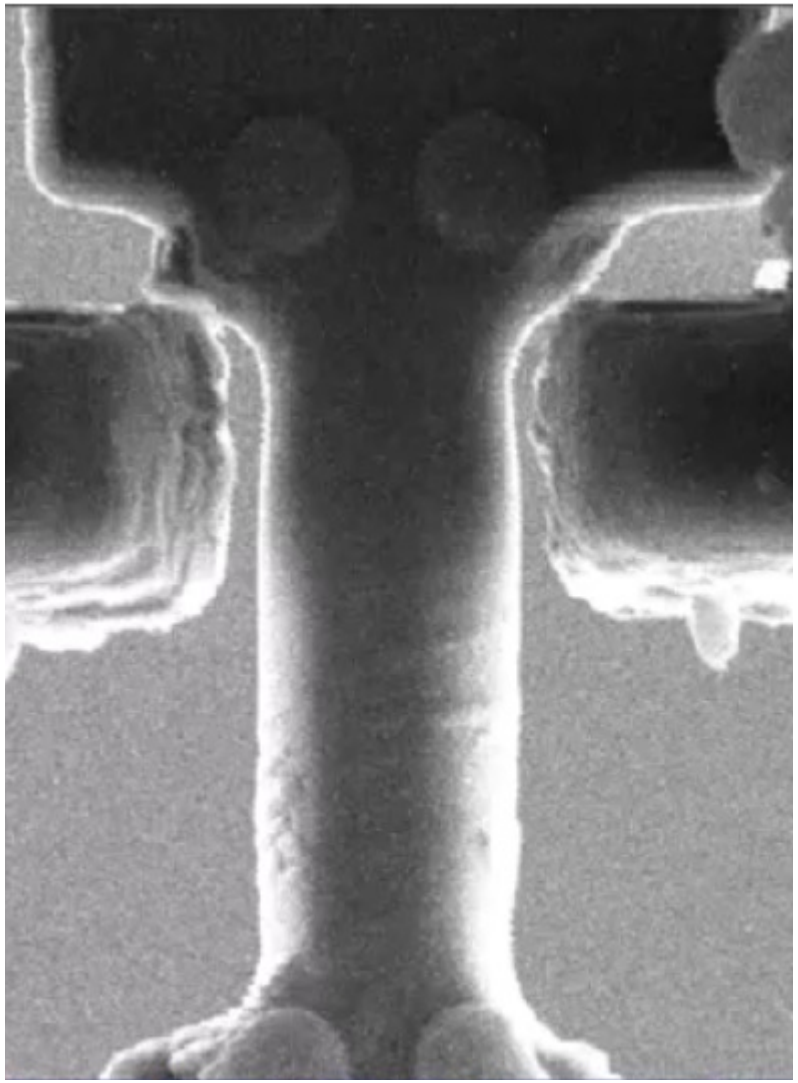

4 µm

Tensile Specimen 3 Test Video

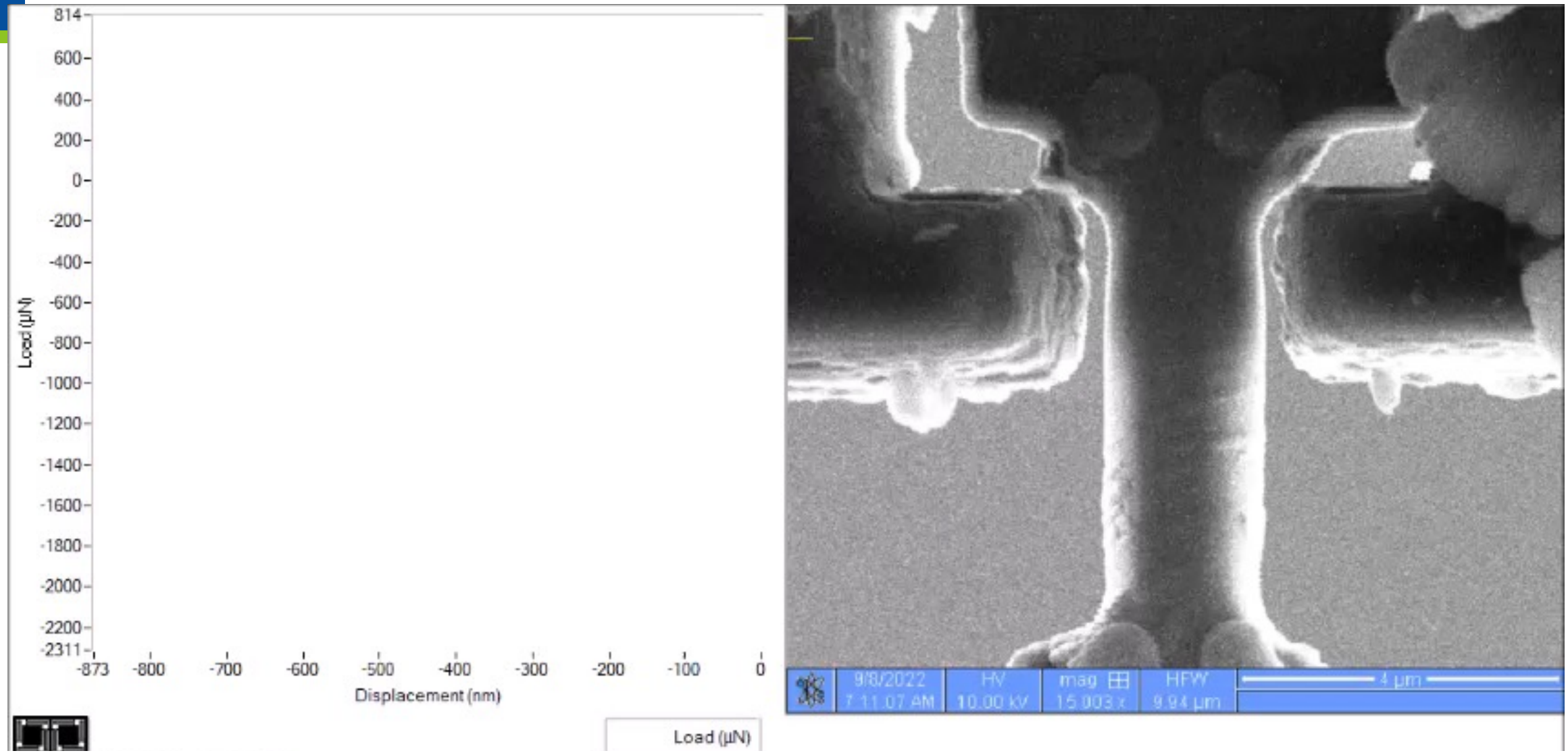

Tensile Specimen 3 Raw Engineering Stress-Strain

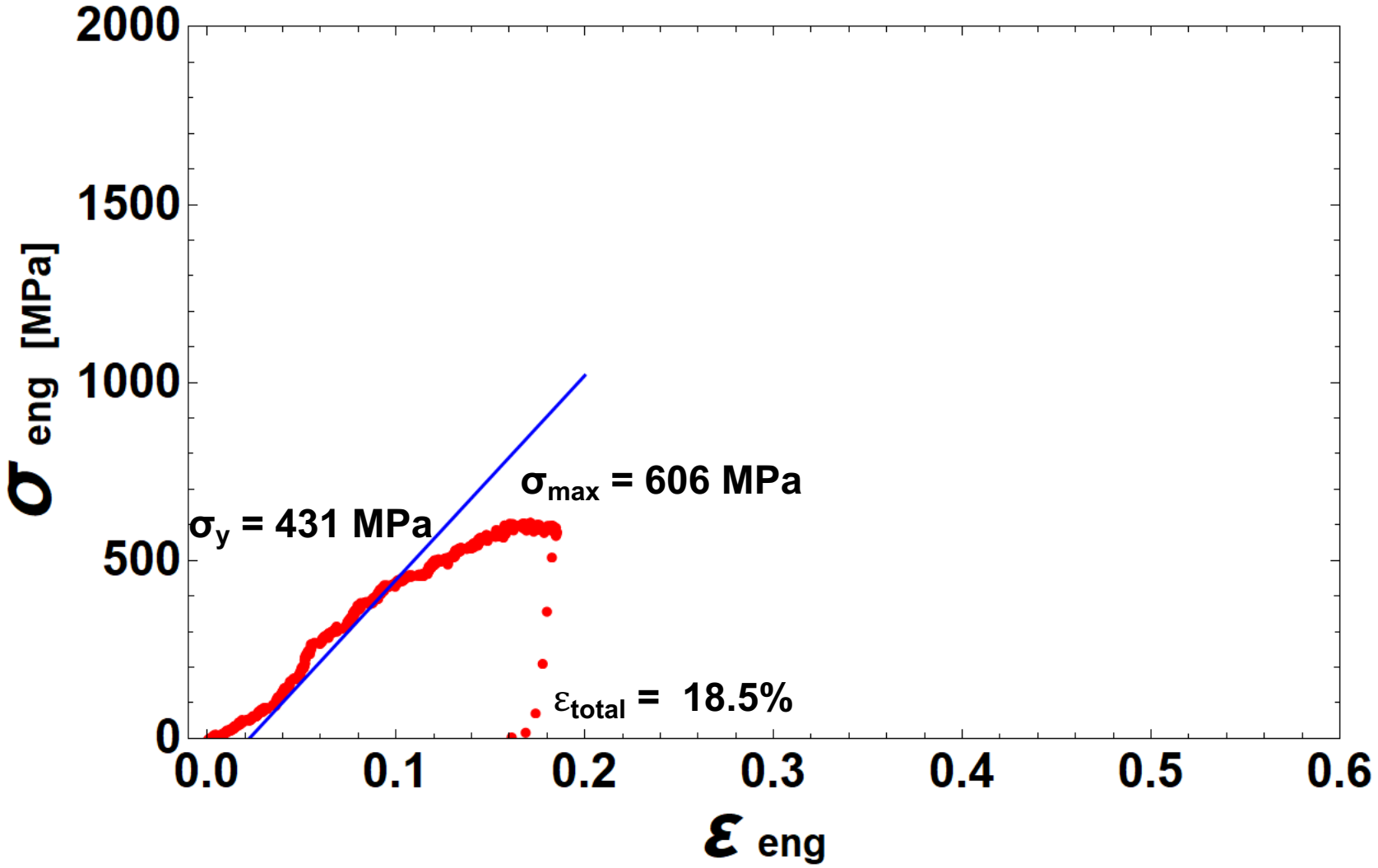

Tensile Specimen 3 DIC Corrected Engineering Stress-Strain

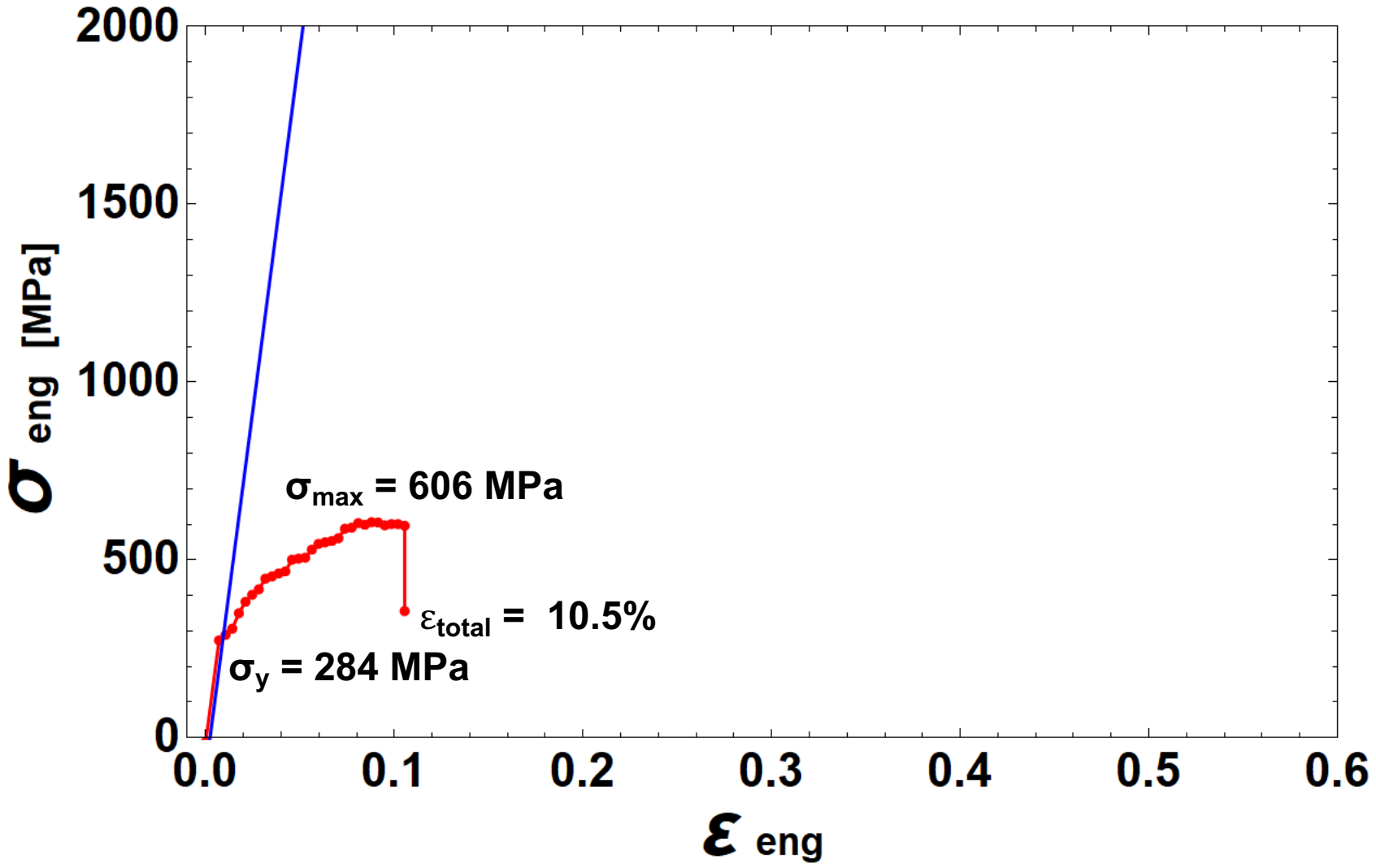

Tensile Specimen 3 Post Test Images

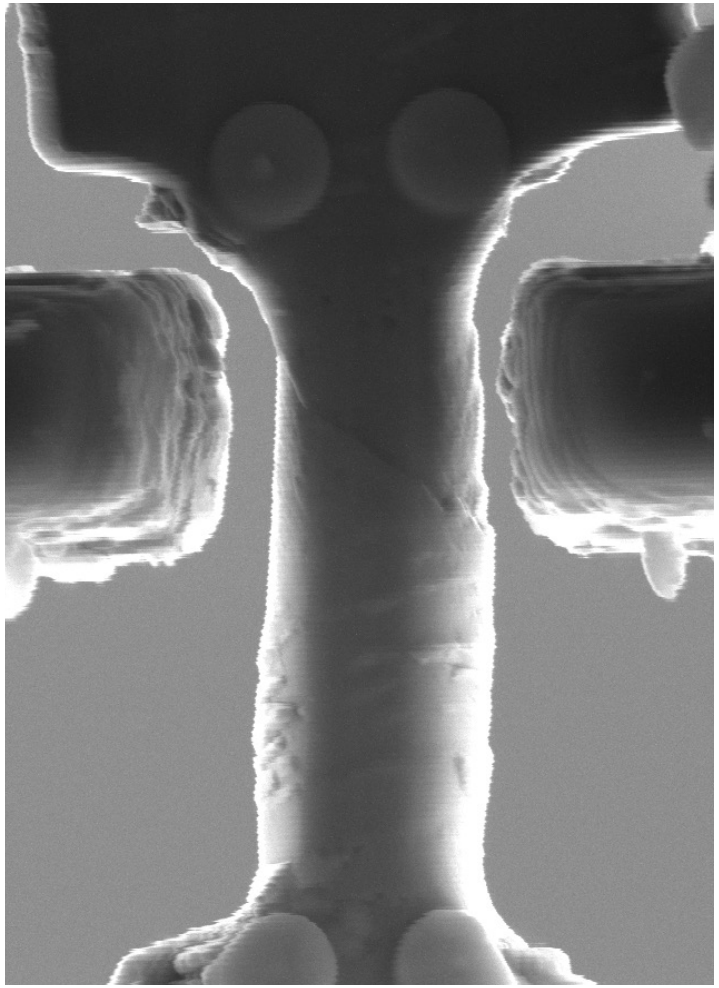

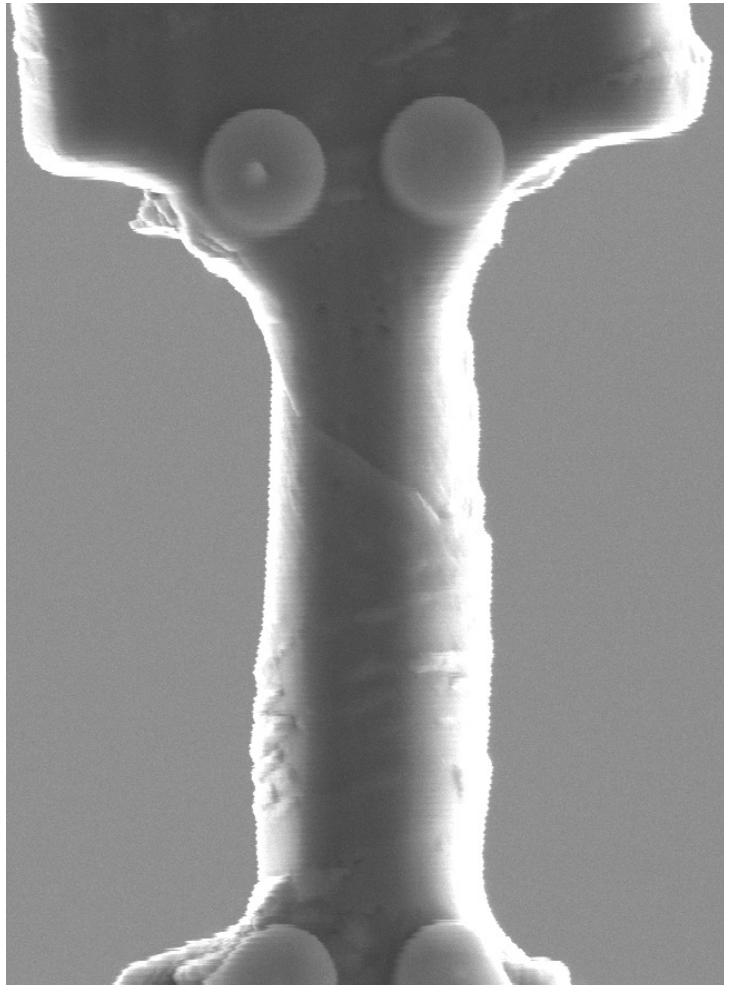

Tensile Specimen 4: HT9 Cladding

w_{min} = 1.873 µm
w_{avg} = 2.019 ± 0.075 µm

t = 1.281 ± 0.077 µm

ℓ = 5.027 ± 0.079 µm, $\dot{e}$ = 10^{-3} -> loading rate = 5 nm/s

Aspect Ratios ℓ : t = 3.92:1, ℓ : w_{avg} = 2.49:1, ℓ : w_{min} = 2.68:1

A_{min} = 2.399 ± 0.144 µm^2
A_{avg} = 2.586 ± 0.252 µm^2

Top

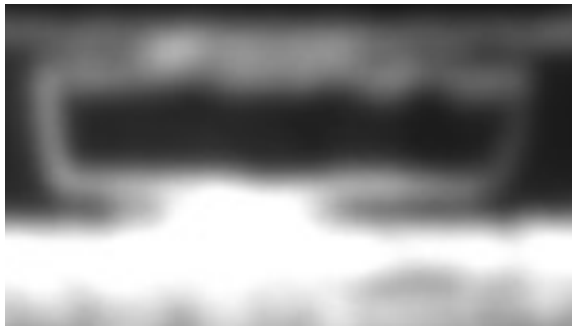

5 µm

Side

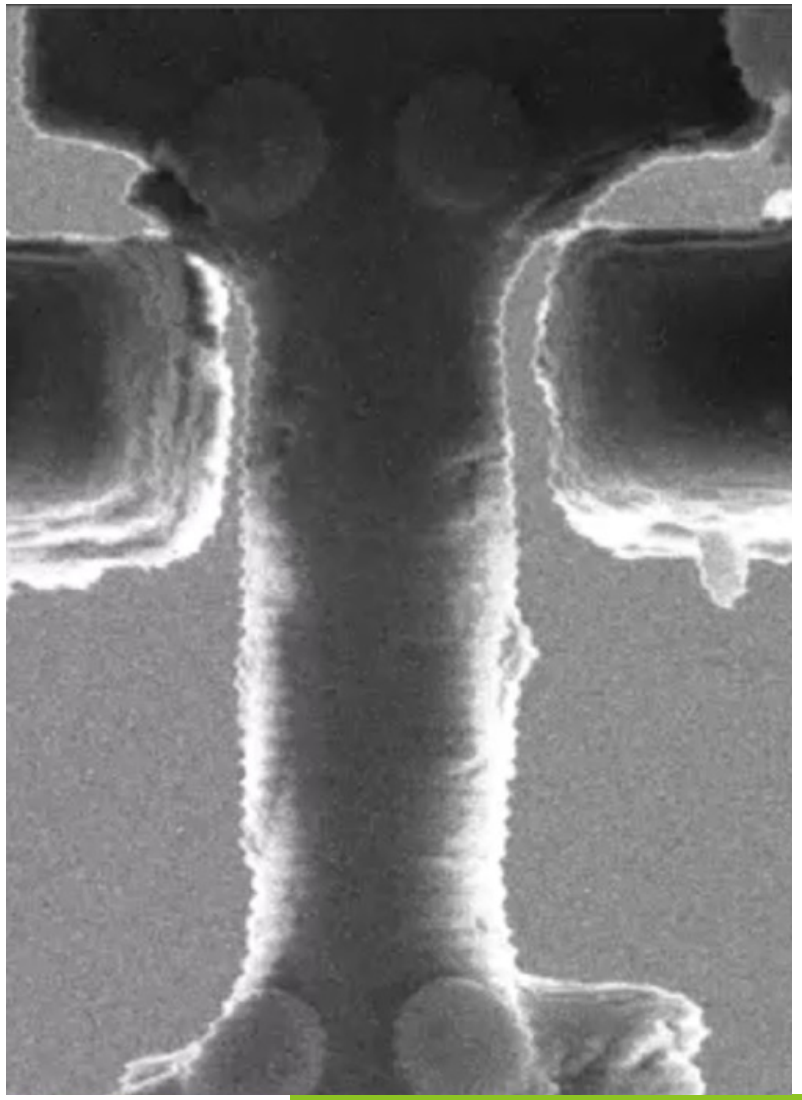

3 µm

Tensile Specimen 4 Test Video

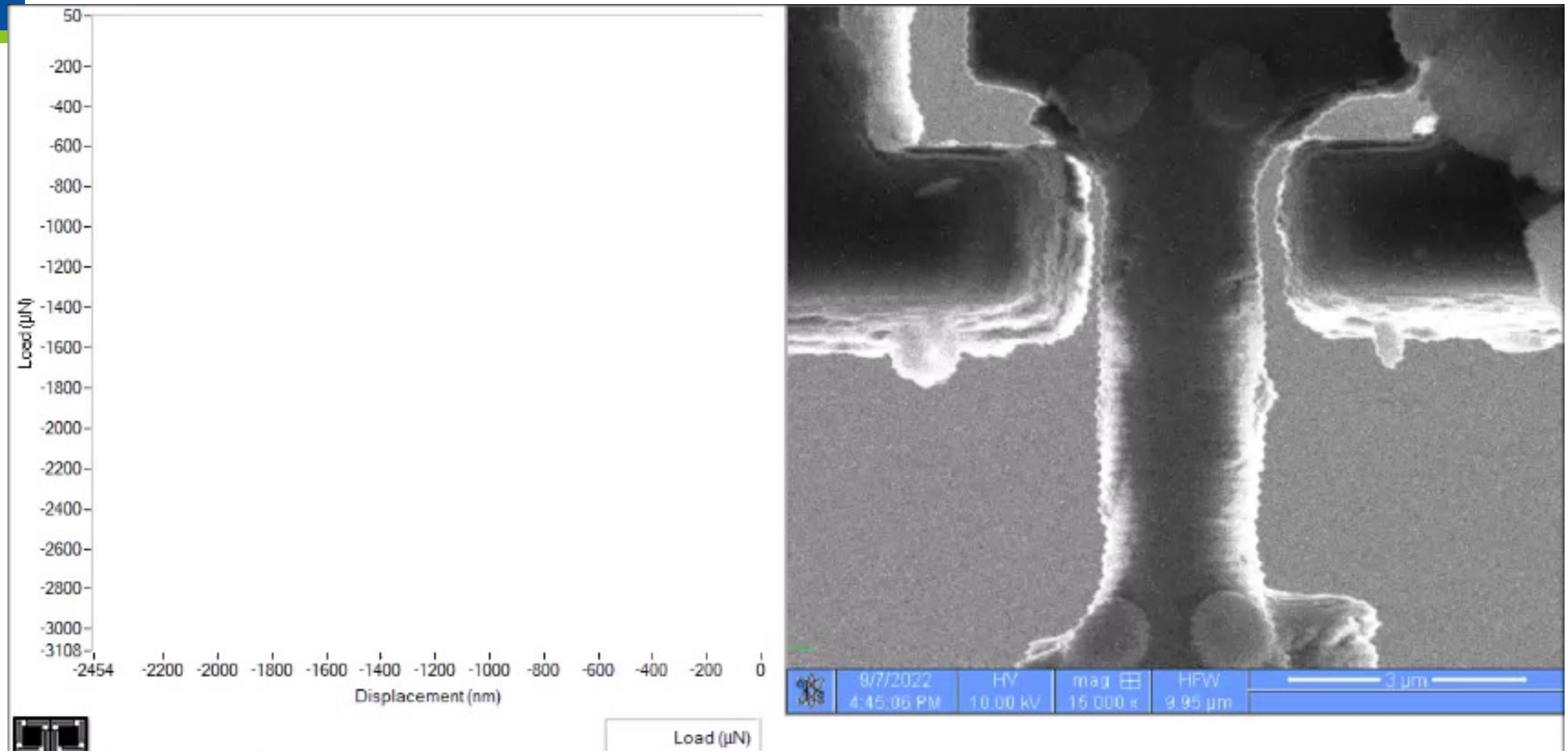

Tensile Specimen 4 Raw Engineering Stress-Strain

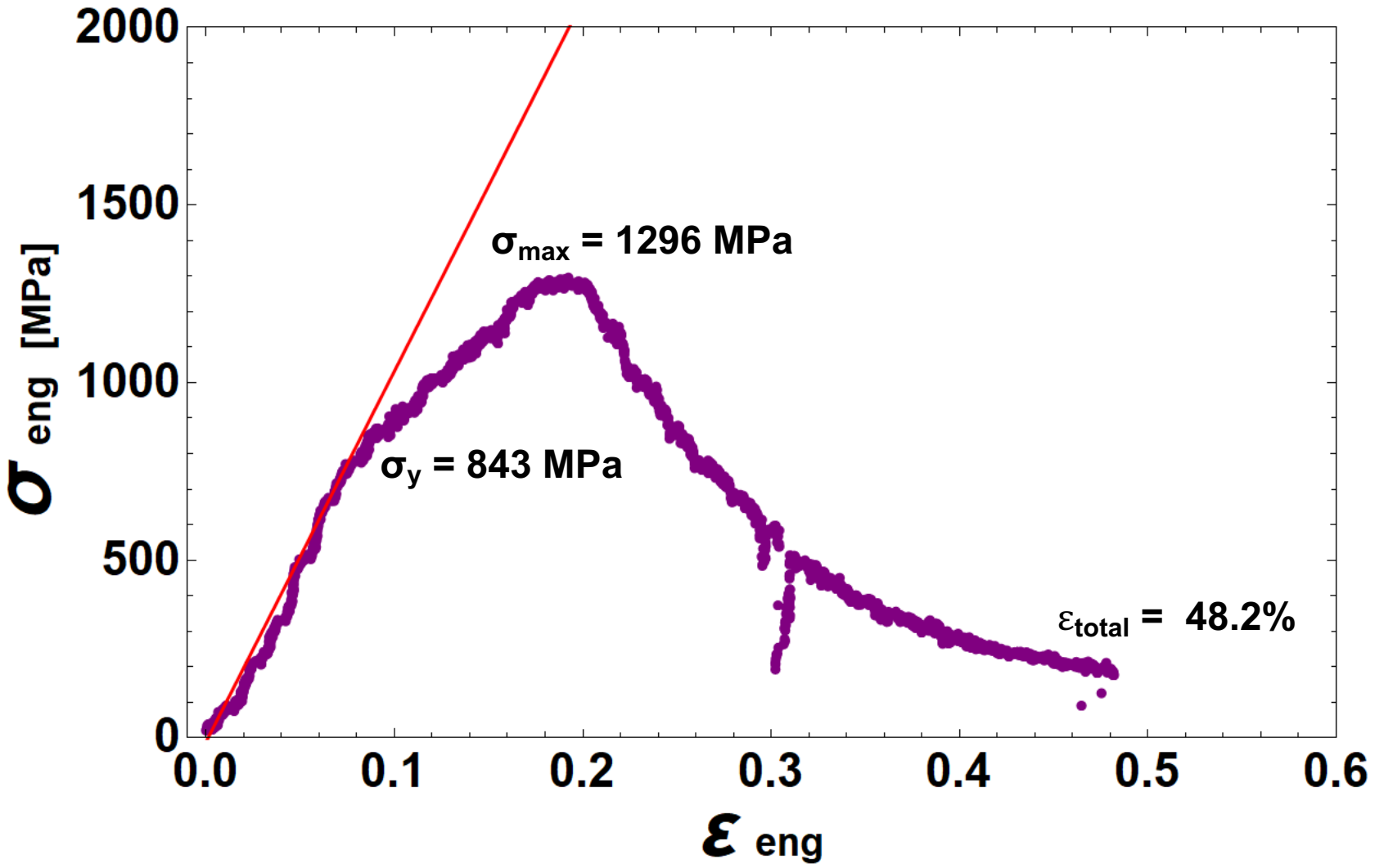

Tensile Specimen 4 DIC Corrected Engineering Stress-Strain

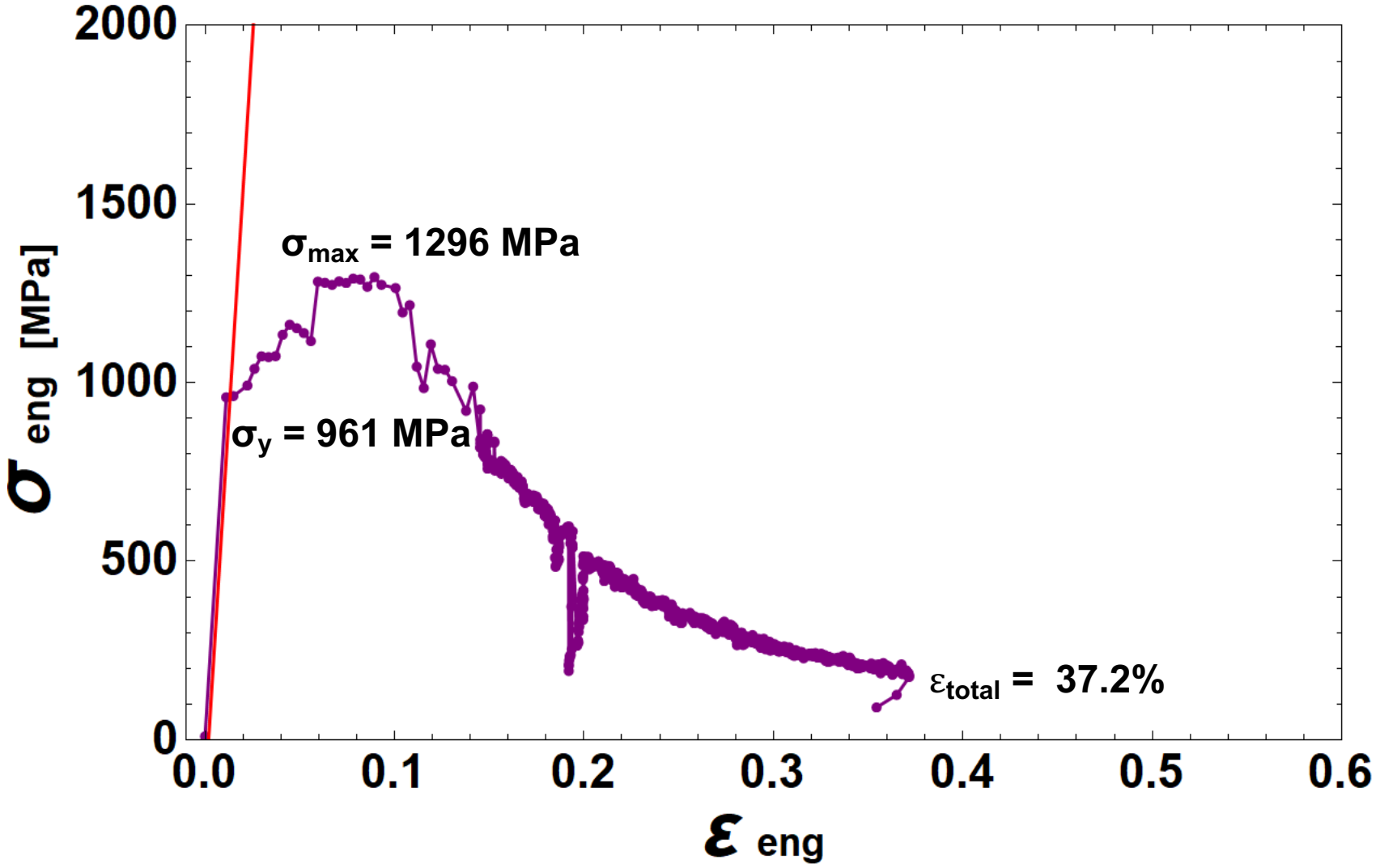

Tensile Specimen 4 Post Test Images

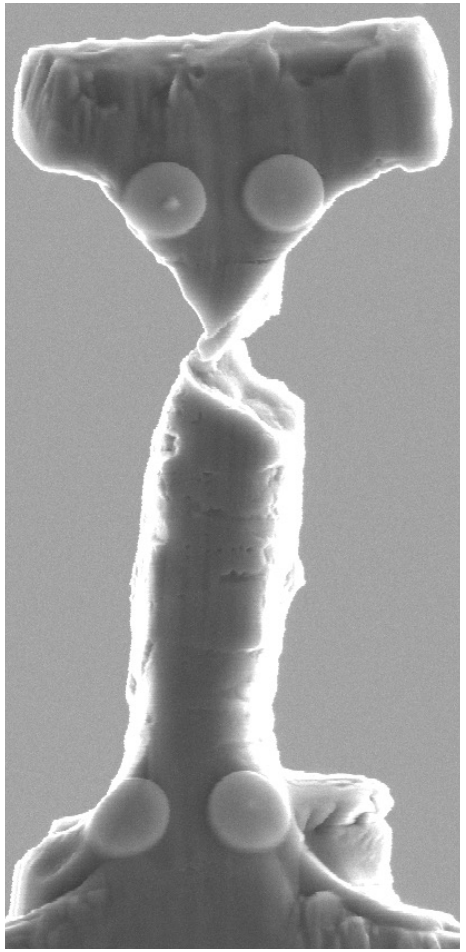

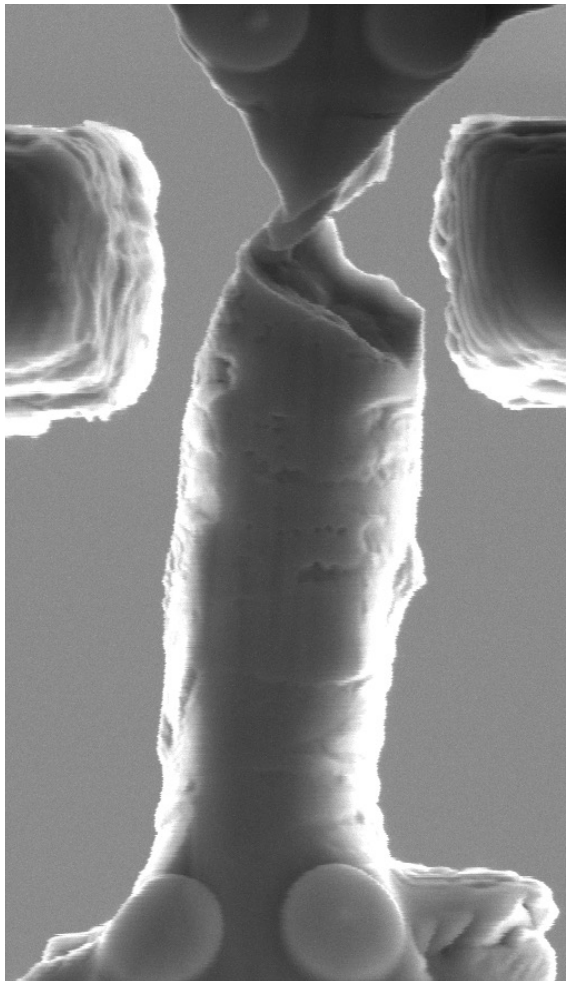

Tensile Specimen 5: HT9 Cladding

w_{min} = 1.969 µm
w_{avg} = 2.059 ± 0.046 µm

t = 1.427 ± 0.064 µm

ℓ = 4.949 ± 0.095 µm, $\dot{e} = 10^{-3}$ -> loading rate = 5 nm/s

Aspect Ratios $\ell : t$ = 3.47:1, $\ell : w_{avg}$ = 2.40:1, $\ell : w_{min}$ = 2.51:1

A_{min} = 2.810 ± 0.126 µm^2
A_{avg} = 2.938 ± 0.197 µm^2

Top

5 µm

Side

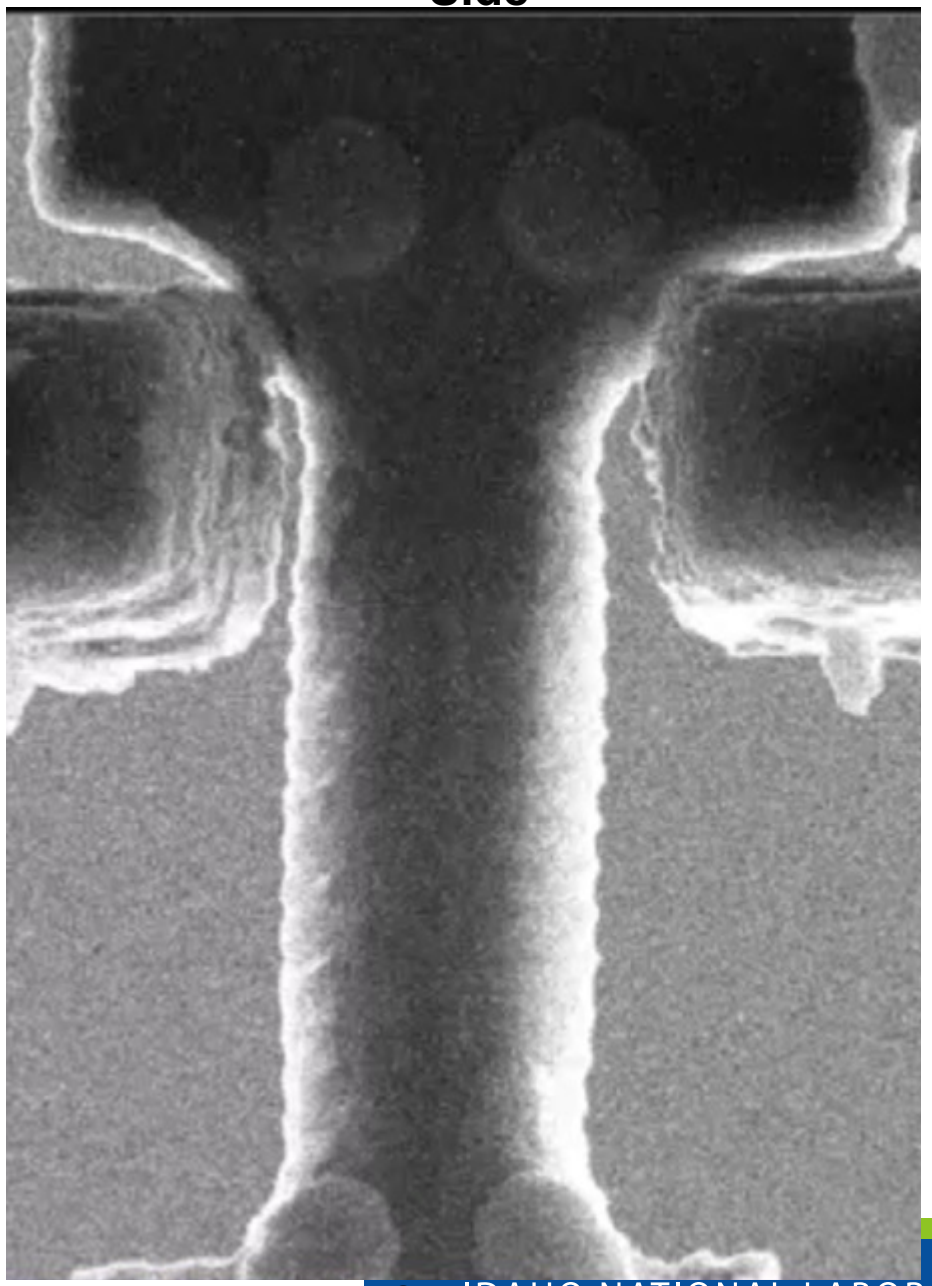

3 µm

Tensile Specimen 5 Test Video

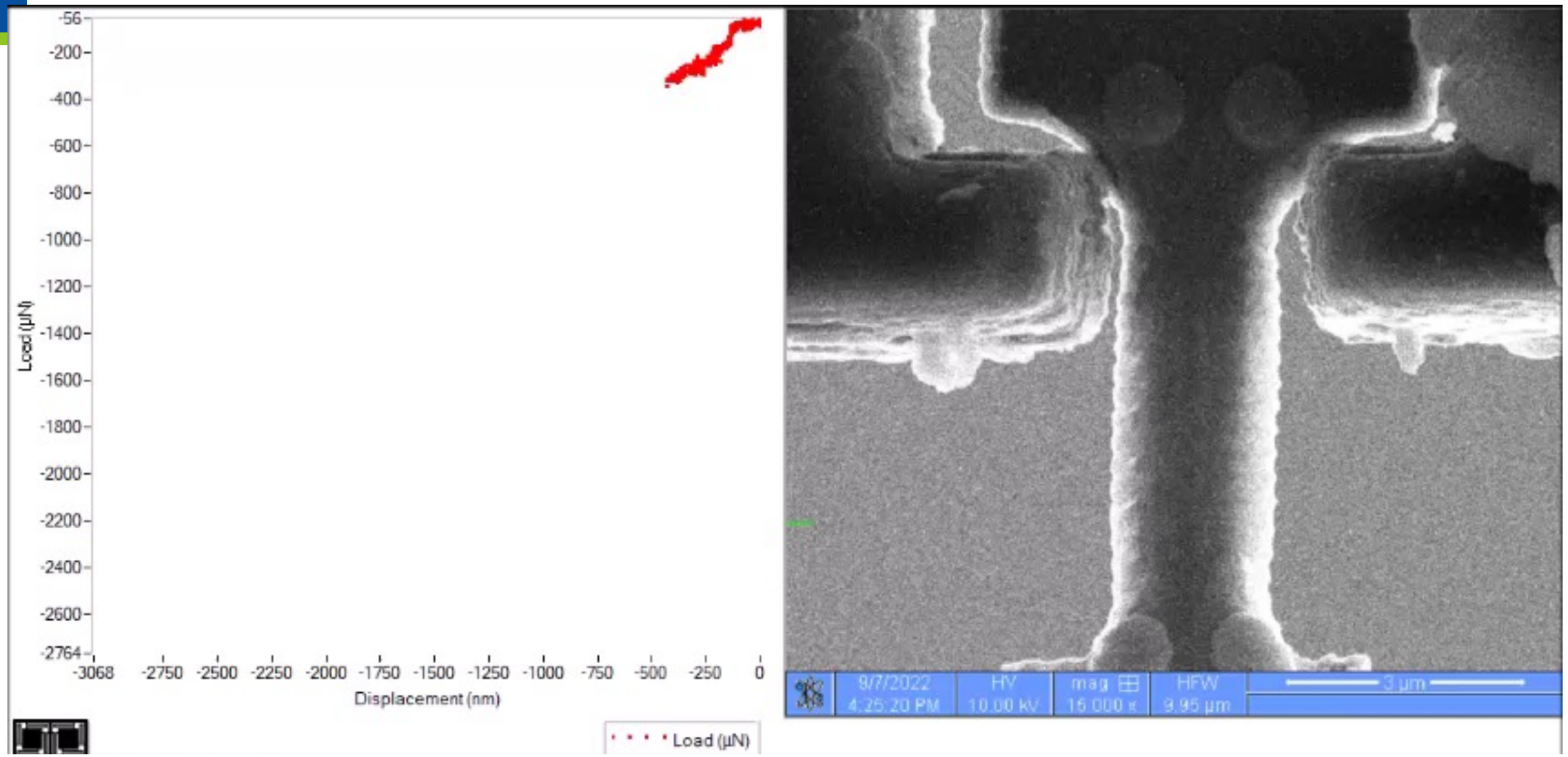

Tensile Specimen 5 Raw Engineering Stress-Strain

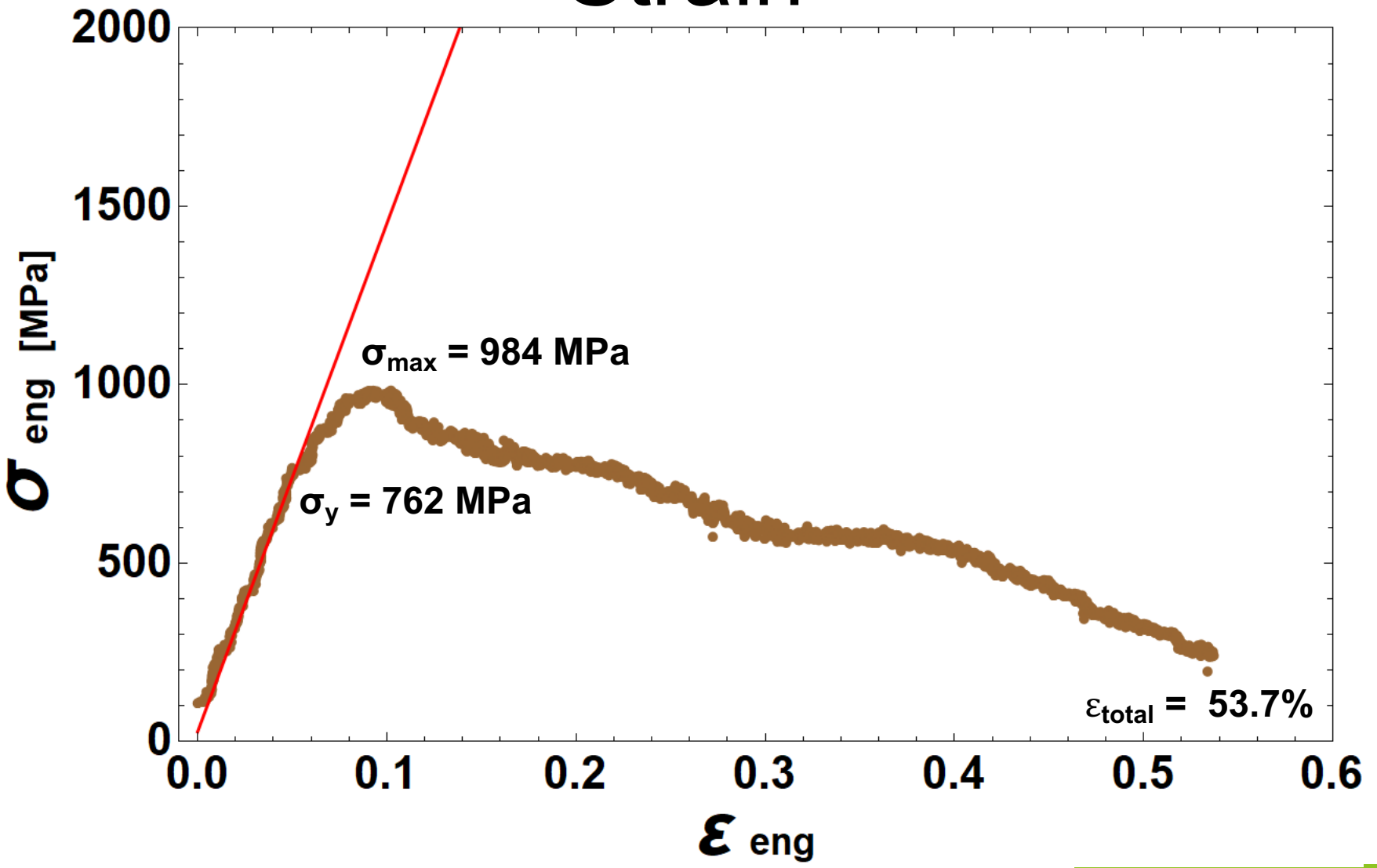

Tensile Specimen 5 DIC Corrected Engineering Stress-Strain

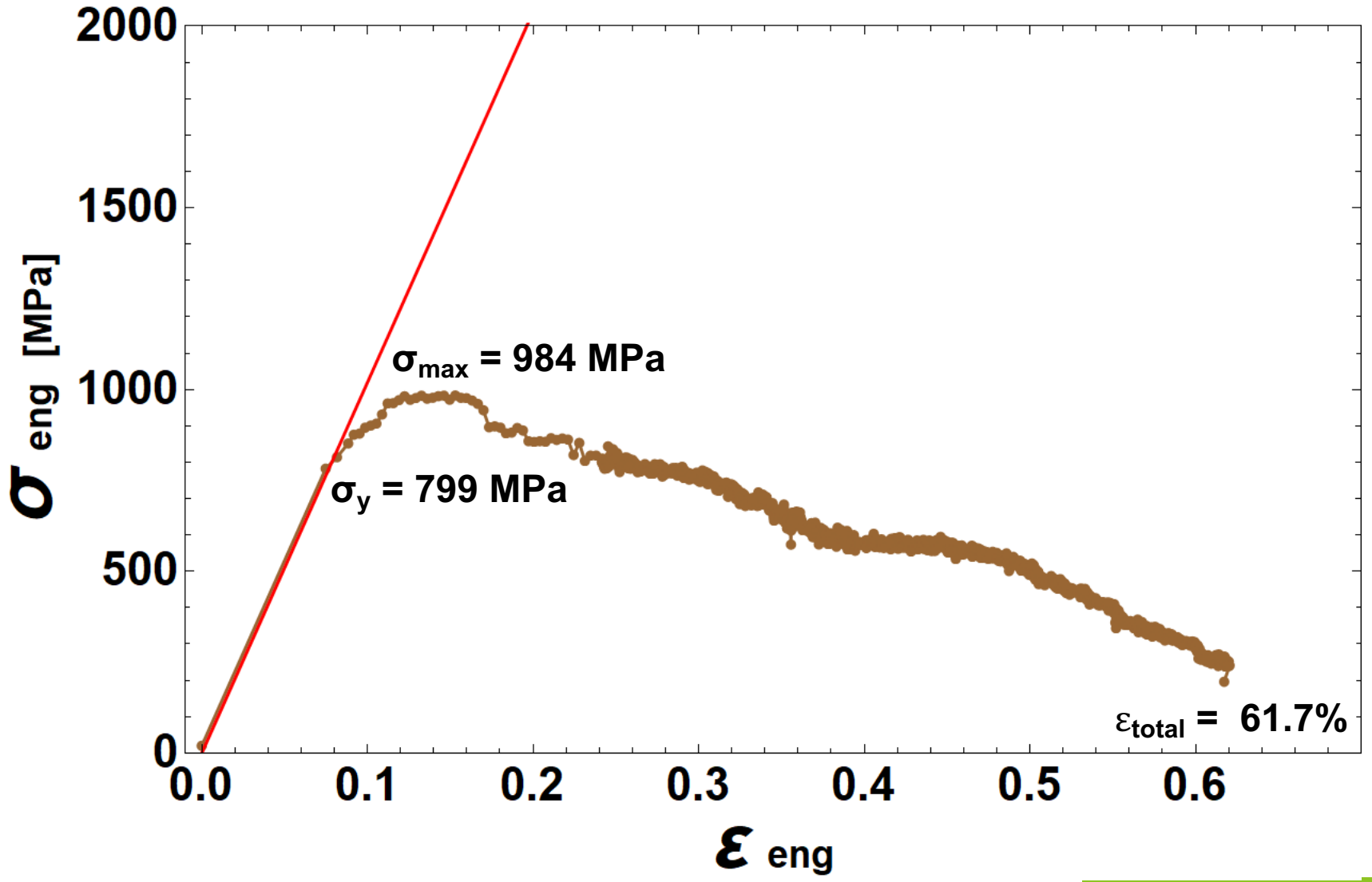

Tensile Specimen 5 Post Test Images

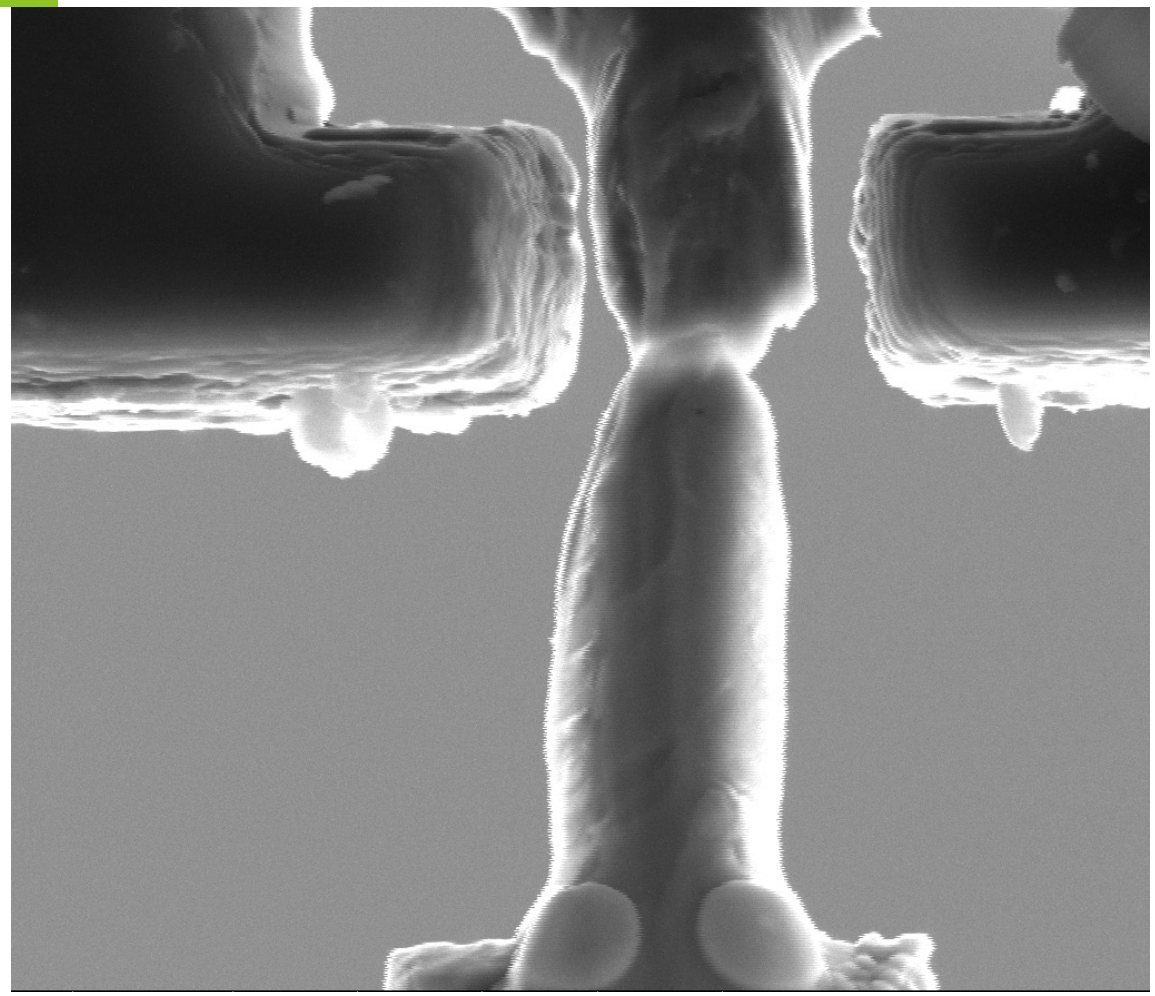

3 µm

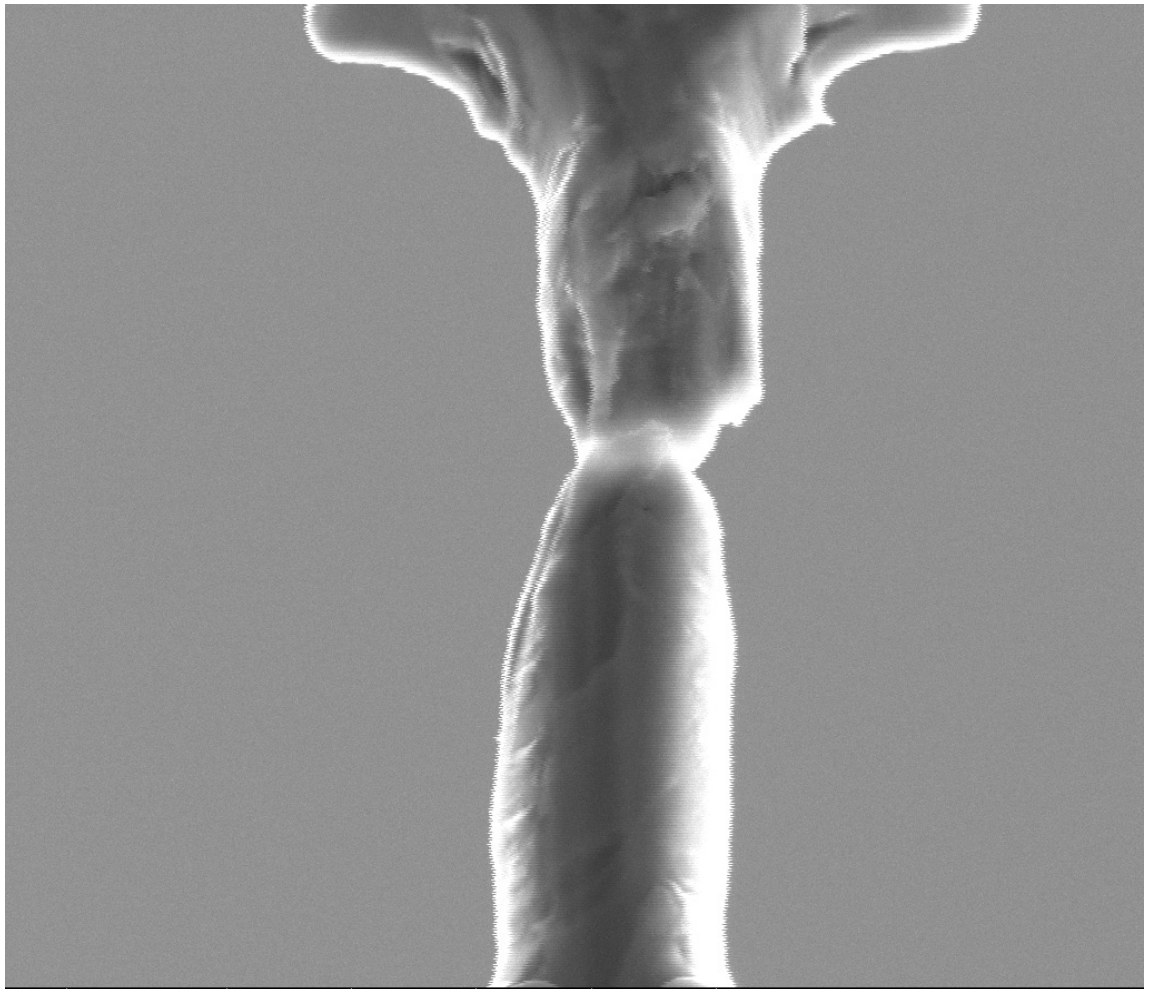

3 µm

Tensile Specimen 6: HT9 Cladding

w_{min} = 1.847 µm
w_{avg} = 1.991 ± 0.062 µm

t = 1.367 ± 0.041 µm

ℓ = 4.738 ± 0.287 µm, $\dot{e} = 10^{-3}$ -> loading rate = 5 nm/s

Aspect Ratios $\ell : t$ = 3.:1, $\ell : w_{avg}$ = 2.:1, $\ell : w_{min}$ = 2.:1

A_{min} = 2.525 ± 0.287 µm^2
A_{avg} = 2.722 ± 0.166 µm^2

Top

5 µm

Side

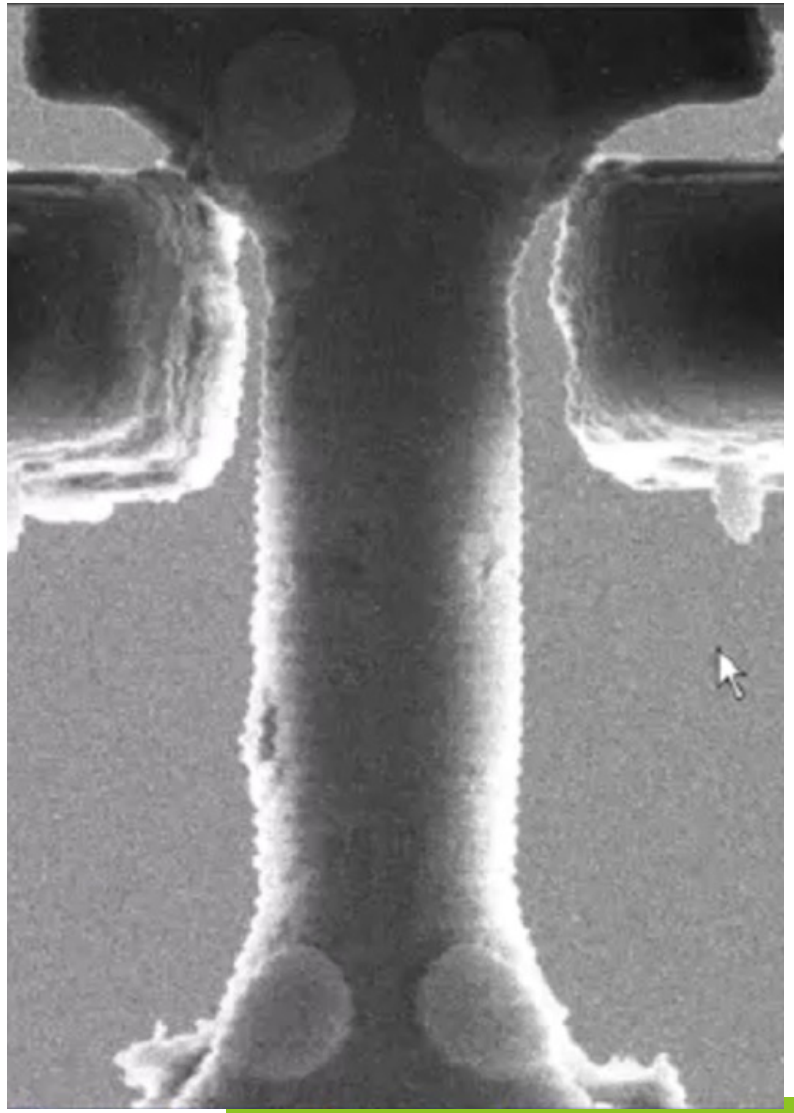

3 µm

Tensile Specimen 6 Test Video

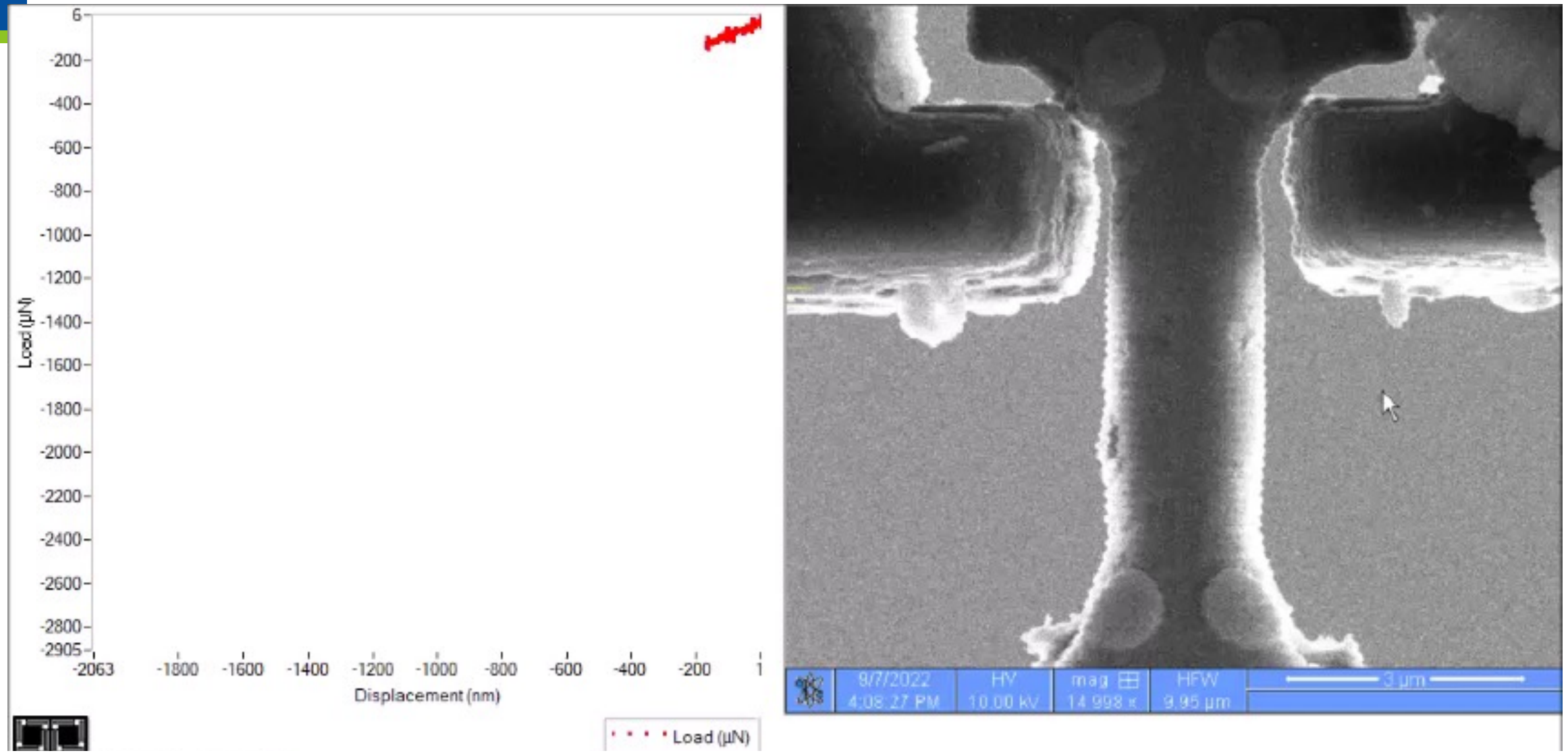

Tensile Specimen 6 Raw Engineering Stress-Strain

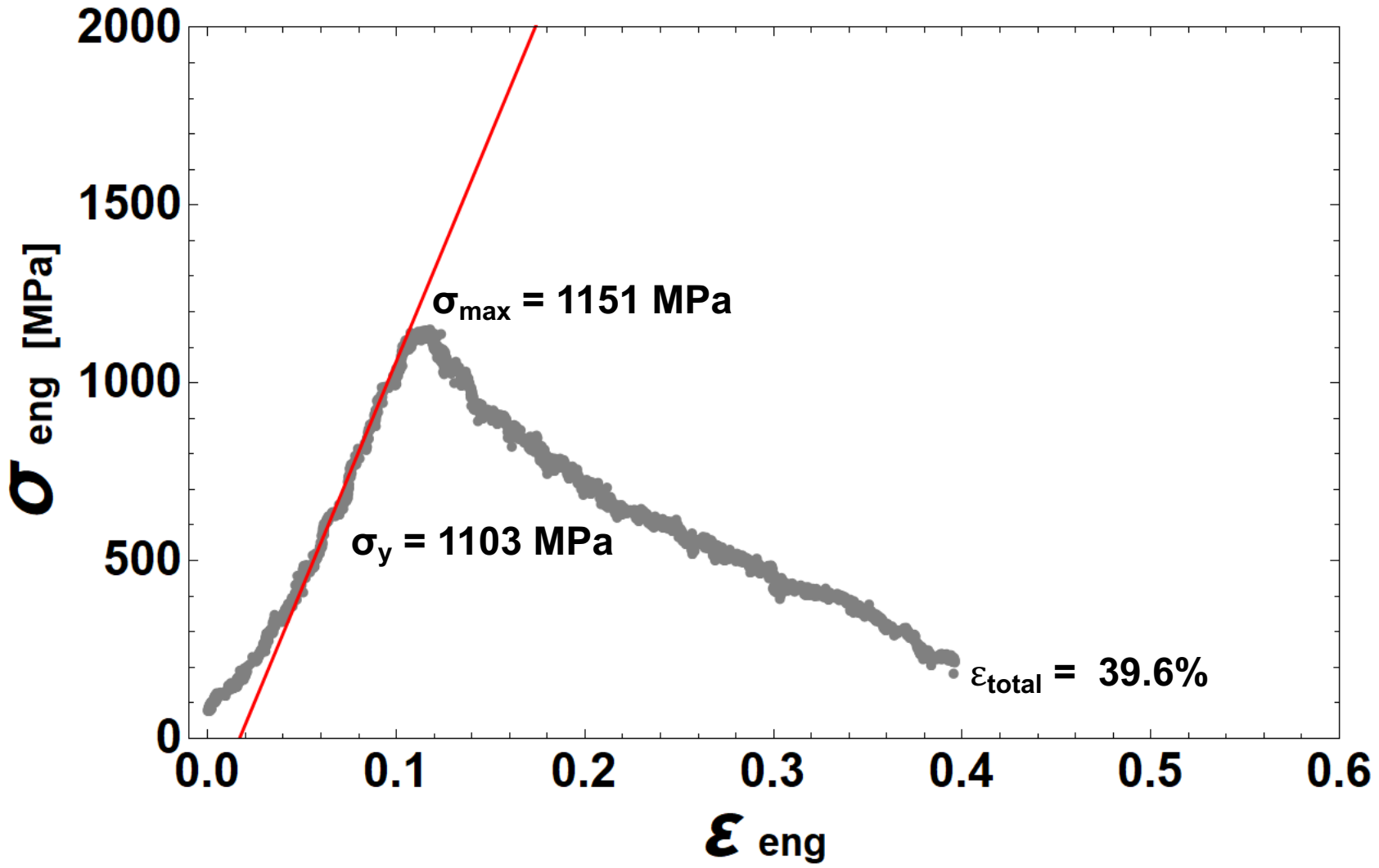

Tensile Specimen 6 DIC Corrected Engineering Stress-Strain

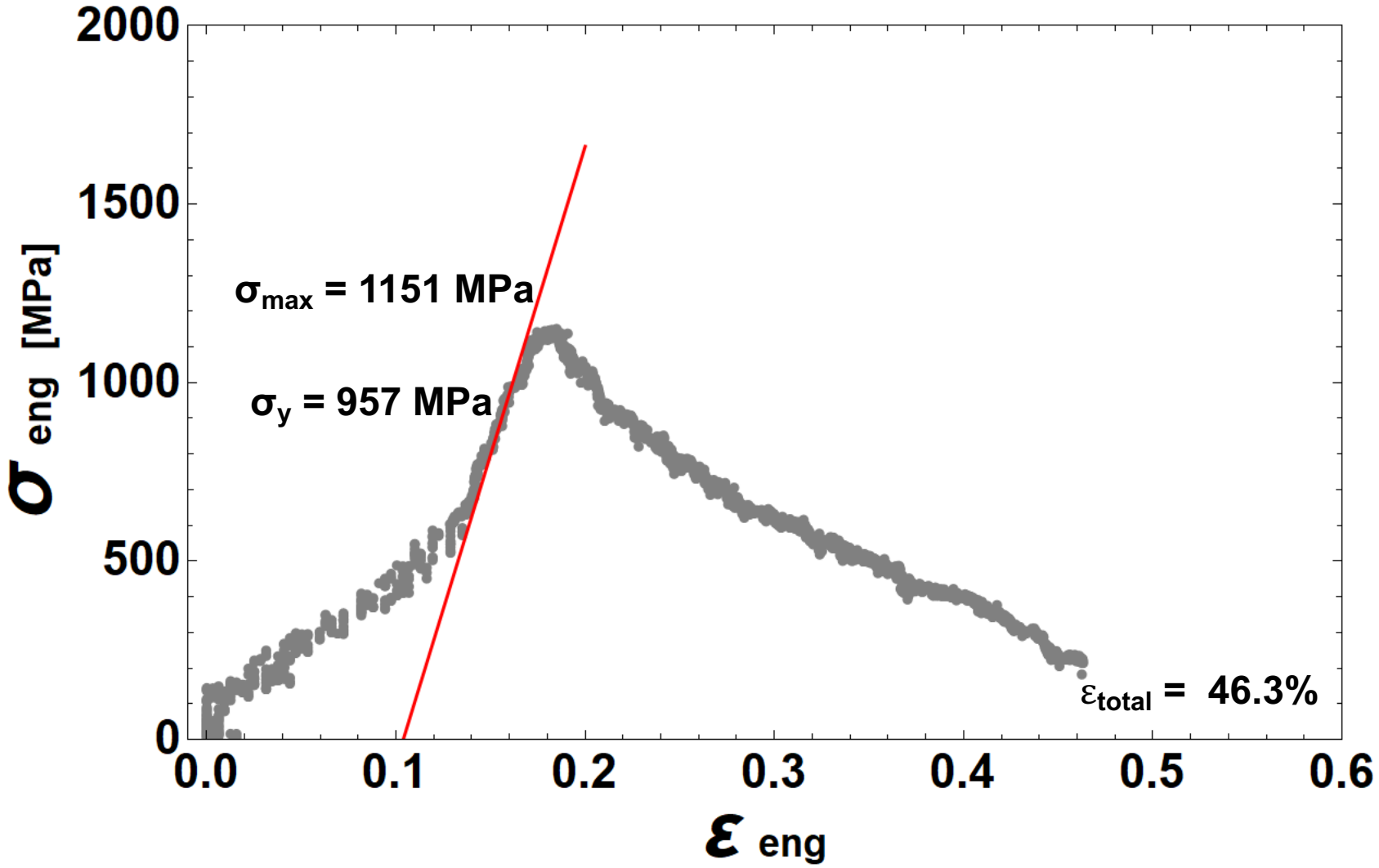

Tensile Specimen 6 Post Test Images

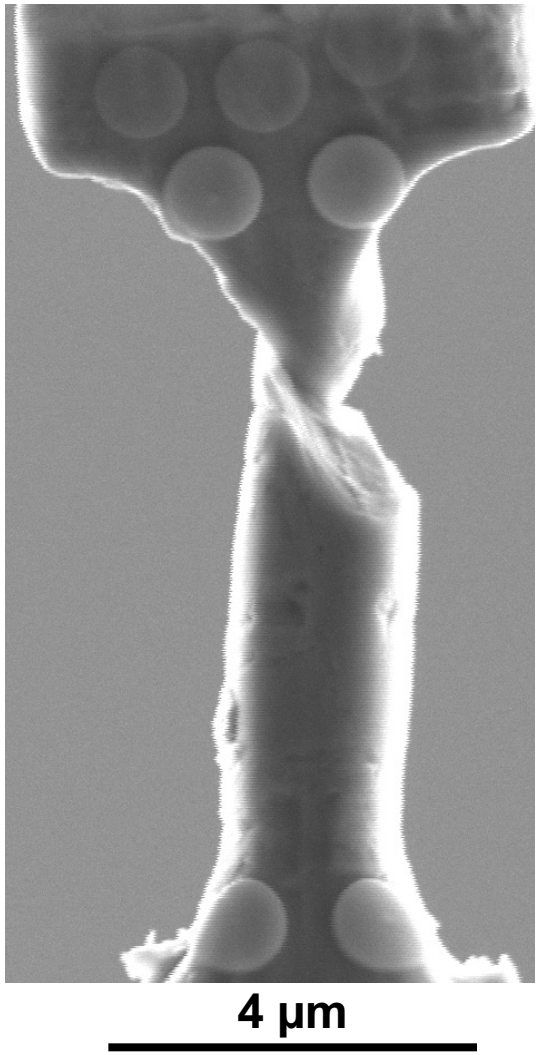

Backup Slides

Element	Atomic Percentage (%)	Atomic Error (%)	Mass Percentage (%)	Mass Error (%)
Cr (#1)	**46.4**	2.5	**22.2**	1.8
Cr (#2)	**53.1**	2.9	**31.4**	2.3
Cr (#3)	**44.7**	2.9	**25.6**	2.0
Zr (#1)	**27.2**	2.7	**22.8**	2.6
Zr (#2)	**34.8**	3.2	**36.0**	3.3
Zr(#3)	**43.3**	3.4	**43.5**	3.5
U (#1)	**23.1**	2.2	**50.6**	3.2
U (#2)	**12.1**	1.3	**32.6**	2.9
U (#3)	**11.4**	1.3	**29.9**	2.8
Ce (#1)	**0.7**	0.1	**0.9**	0.1
Ce (#2)	**0.0**	0.0	**0.0**	0.0
Ce (#3)	**0.0**	0.0	**0.0**	0.0
Nd (#1)	**2.6**	0.3	**3.4**	0.4

on (%)	Mass Error (%)	Fit Error (%)
	1.55	0.54
	2.78	0.63
	0.47	0.31
	0.50	0.42
	3.18	0.36

on (%)	Mass Error (%)	Fit Error (%)
	2.56	0.82
	3.48	0.30
	0.01	0.00
	0.03	0.00
	2.15	0.51

on (%)	Mass Error (%)	Fit Error (%)
	1.43	0.33
	2.75	0.24
	0.02	150.05
	0.10	1.64
	3.22	0.25

#2	Cr	50.5	31.3
	Zr	41.1	44.8
	U	8.4	23.9
	Ce	0.0	0.0
	Nd	0.0	0.0
#3	Cr	37.7	16.1
	Zr	31.1	23.3
	U	30.5	59.8
	Ce	0.0	0.0
	Nd	0.7	0.8
#4	Cr	9.5	3.8
	Zr	26.8	18.7
	U	10.9	19.9
	Ce	14.7	15.7
	Nd	38.1	41.9
#5	Cr	41.4	19.6
	Zr	30.8	25.5
	U	21.7	46.9

Study on Barrier between Fuel and Cladding

- ❑ Barrier to prevent interaction between fuel and cladding
  - Eutectic melting at high temperature
  - Degradation of cladding by rare earth fission products
- ❑ Investigation of barriers
  - Effective barrier material : Cr, V, Cr_2O_3 ..
  - Barrier fabrication methods : electroplating, oxidation, nitrification, metal liner..
  - Barrier on fuel slug : Surface oxidation of metal fuel slug

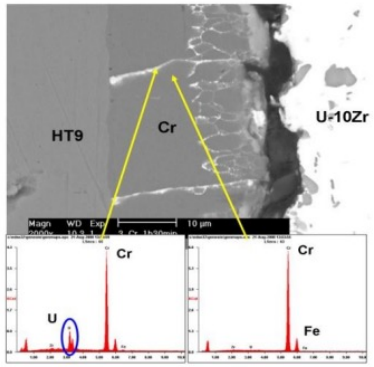

Cr Electroplating
(800°C/25 hr)

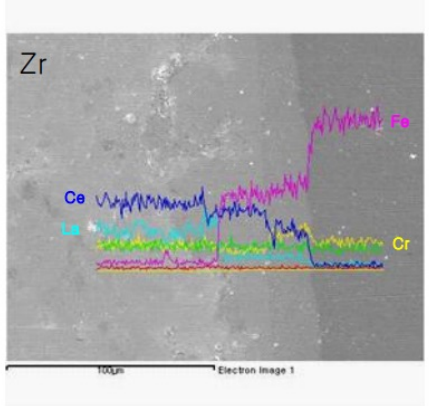

Zirconium
(660°C/25 hr)

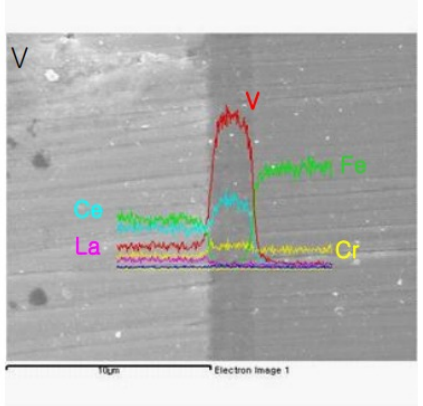

Vanadium
(660°C/25 hr)

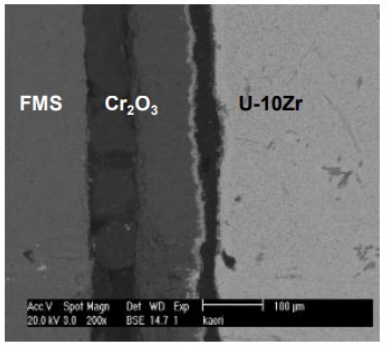

Cr_2O_3
(800°C/25 hr)

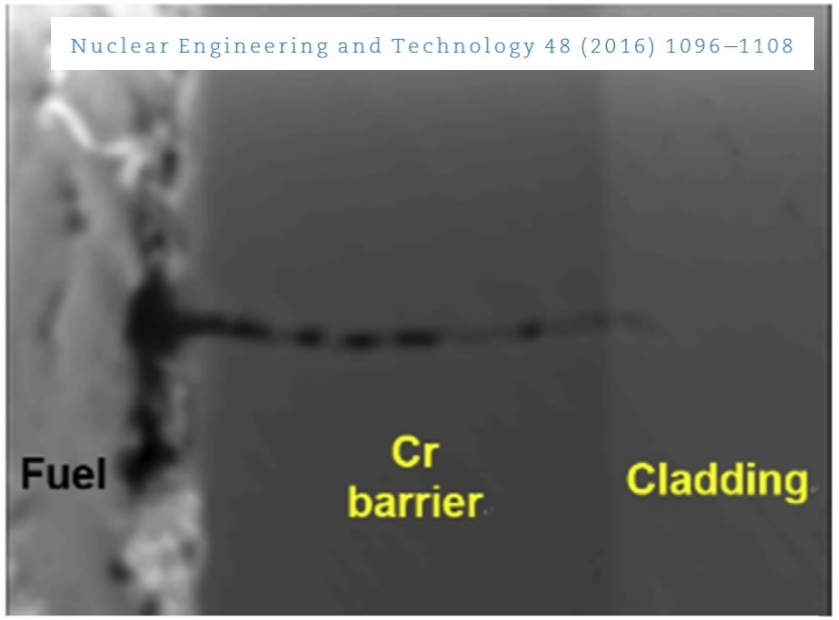

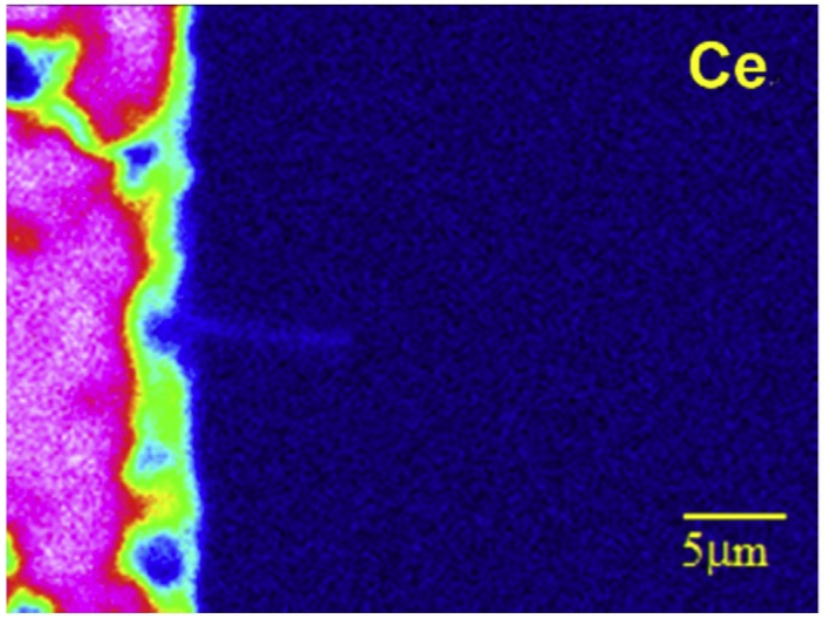

Fig. 17 – SEM image and EPMA map at fuel–cladding interface for U–Zr–5Ce. EPMA, electron probe micro-analysis; SEM, scanning electron microscope.

Fuel cladding of the ferriticemartensitic steel FC92, which has higher mechanicalstrength at a high temperature than conventional HT9 cladding, was developed andfabricated, and is being irradiated in the fast reacto

TEM characterization on post-tested specimens

1. High density of voids observed in Cr-liner. This is because of neutron irradiation effect
    - Then how voids affect on Cr integrity. Microcracks are not wanted to ensure To prevent Lns penetration,
    - Voids typically cause swelling
    - Swelling could lead to cracks formation, then coating failure
    - Swelling associated the formation and growth of cavities (among the most damaging of radiation-induced degradation mode)
    - (multilayer coating, differential swelling could lead to coating failure)
2. In-depth characterization of reacted Cr liner (understand what happened on the interface)
3. In-depth characterization on the HT9-Cr interface understand potential microstructure changes

Voids in Cr coating

In this paper, the interface region of Cr-coated Zircaloy-4 materials was studied before and after a specific ion irradiation experiment. In the as deposited Cr-coated sample, a C15 Laves phase-type is observed in the Zr–Cr interface region. This phase possesses the characteristics of the equilibrium $ZrCr_2$ Laves phase as it displays an f.c.c structure, but presents a deviation to both stoichiometry composition and reference lattice parameters. During ion-irradiation, in situ experiments showed significant dissolution of this interlayer phase. Further, Energy Dispersion Spectroscopy (EDS) revealed that the phase dissolution is accompanied by an increase of the concentration profile abruptness, which corresponds to a counterintuitive effect, i.e., radiation-induced sharpening phenomenon. However, under ex situ irradiation of "bulk" samples, a significant evolution of the Cr-coating internal stress state is observed and the Zr-Cr profile appears broad instead of sharp, which tends to prove that the sharpening effect should be transient and potentially related to the specific effects of irradiation of a thin (foil) sample. Then, further additional experimental and modeling efforts should be done to better support the observed Zr–Cr interface evolution under ion irradiation, and, finally, to extend such analysis to neutron irradiation.

10.3390/ma15062322

4. Conclusion

In summary, the effects of heavy ion irradiation on the microstructures of Cr, CrN, TiAlCrN coatings and Zircaloy-4 have been investigated by TEM analysis. The following conclusions have been obtained:

(1) The ATF coatings exhibited better irradiation resistance than that of Zircaloy-4, indicated by less irradiation defects. The number density of dislocation loops in Zircaloy-4, Cr, CrN, TiAlCrN were measured to be $6.754 \times 10^{23}/m^3$, $6.568 \times 10^{23}/m^3$, $3.29 \times 10^{23}/m^3$, $1.21 \times 10^{24}/m^3$, respectively.
(2) TEM results showed that the irradiation defects were significantly restricted by grain boundaries in the columnar grains compared to equiaxed grains and the high-density boundaries could obviously reduce the formation of voids. Fast Fourier Transformation results of HRTEM images showed that Cr and CrN coatings maintained better lattice integrity than those of TiAlCrN coating and Zircaloy-4.
(3) Cr coating exhibited better irradiation resistance than TiAlCrN coating in terms of irradiation dislocation loops. High density of grain boundaries in CrN and TiAlCrN coatings could significantly reduce the number of voids and voids were rarely observed in these two coatings. The number density of irradiation defects was slightly larger in TiAlCrN coating than that in CrN coating.
(4) CrN coating showed the best irradiation resistance among all samples, due to its compact crystal structure and higher density of grain boundary, which contributed to reduce dislocations and voids.

Annals of Nuclear Energy 156 (2021) 108206

Contents lists available at ScienceDirect

Annals of Nuclear Energy

Voids in Cr coating (Cont.)

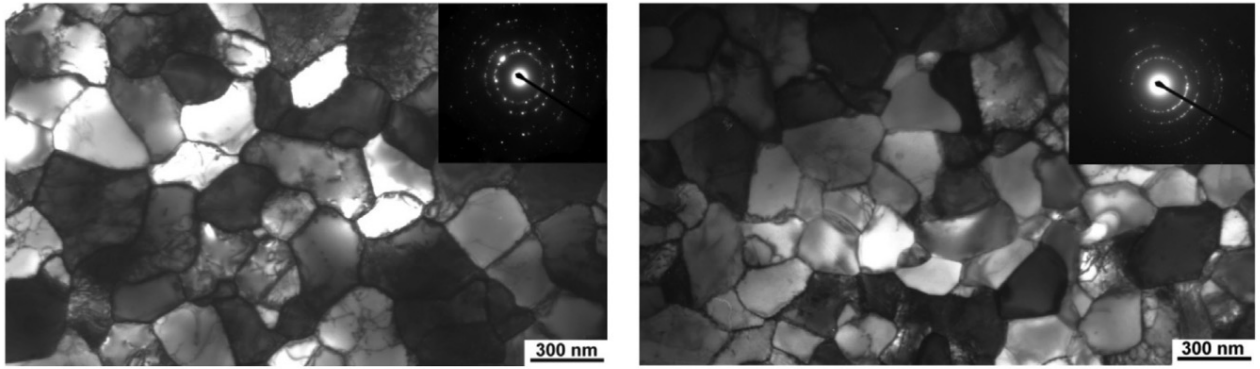

Fig. 4. TEM images and selected-area electron diffraction (as insets) of as-deposited Cr coating (a) and annealed in vacuum at 400 °C for 3 h (b).

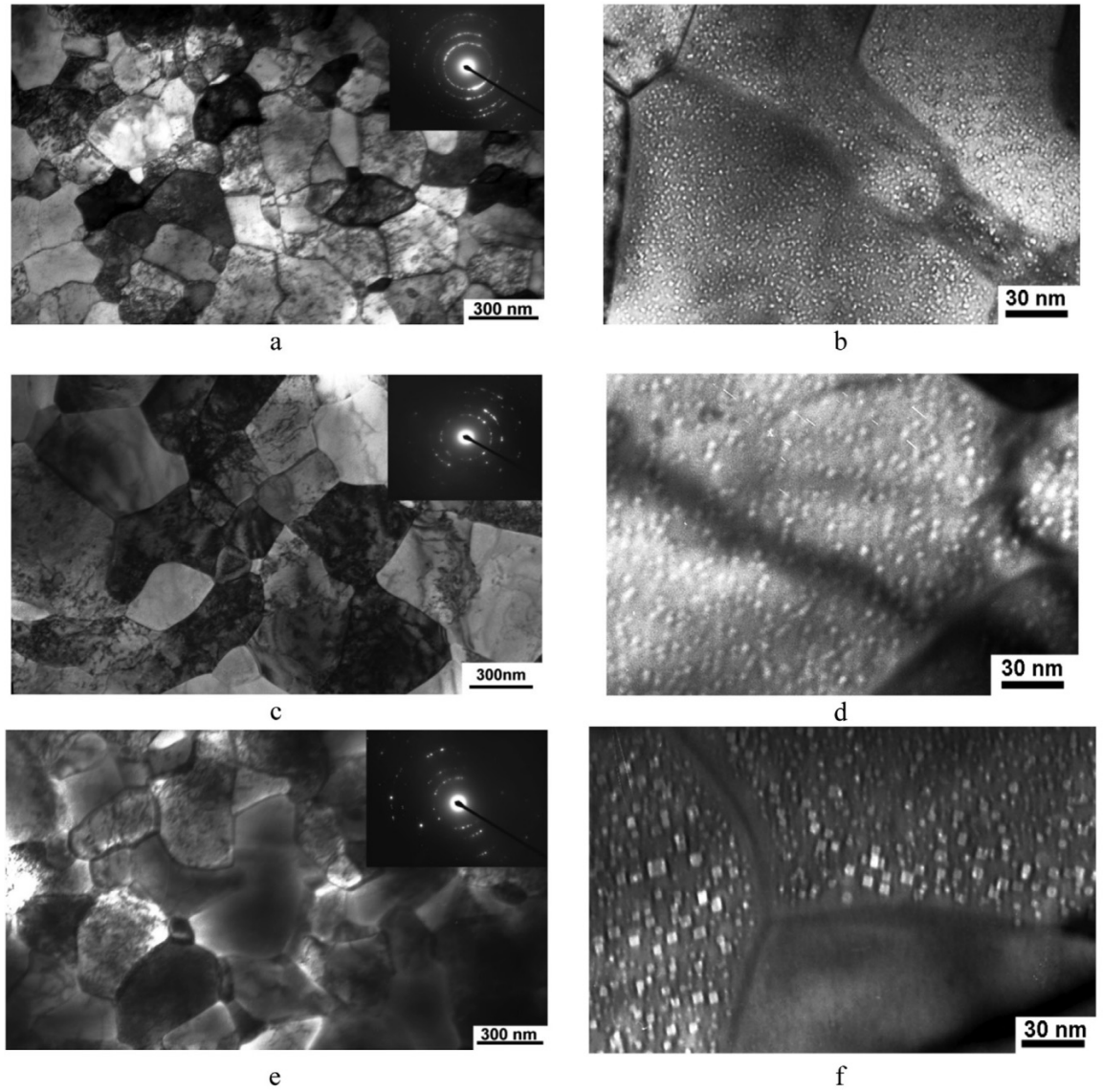

Fig. 5. TEM images and selected-area electron diffraction (as insets) of Cr coatings irradiated up to 5 (a,b), 15 (c,d) and 25 dpa (e,f).

Journal of Nuclear Materials 510 (2018) 163–167

Paper outline:

1st

- ❑ SEM examination: BSE + SEM-EDS
- ❑ Microtensile testing at RT
- ❑ TEM characterization of post-tested tensile specimen, HT9-Cr interface, Cr coating region

2nd paper: TEM characterization on fuel: periphery, intermediate, center region (TEM foils are ready, Reserve Time for TEM characterization)

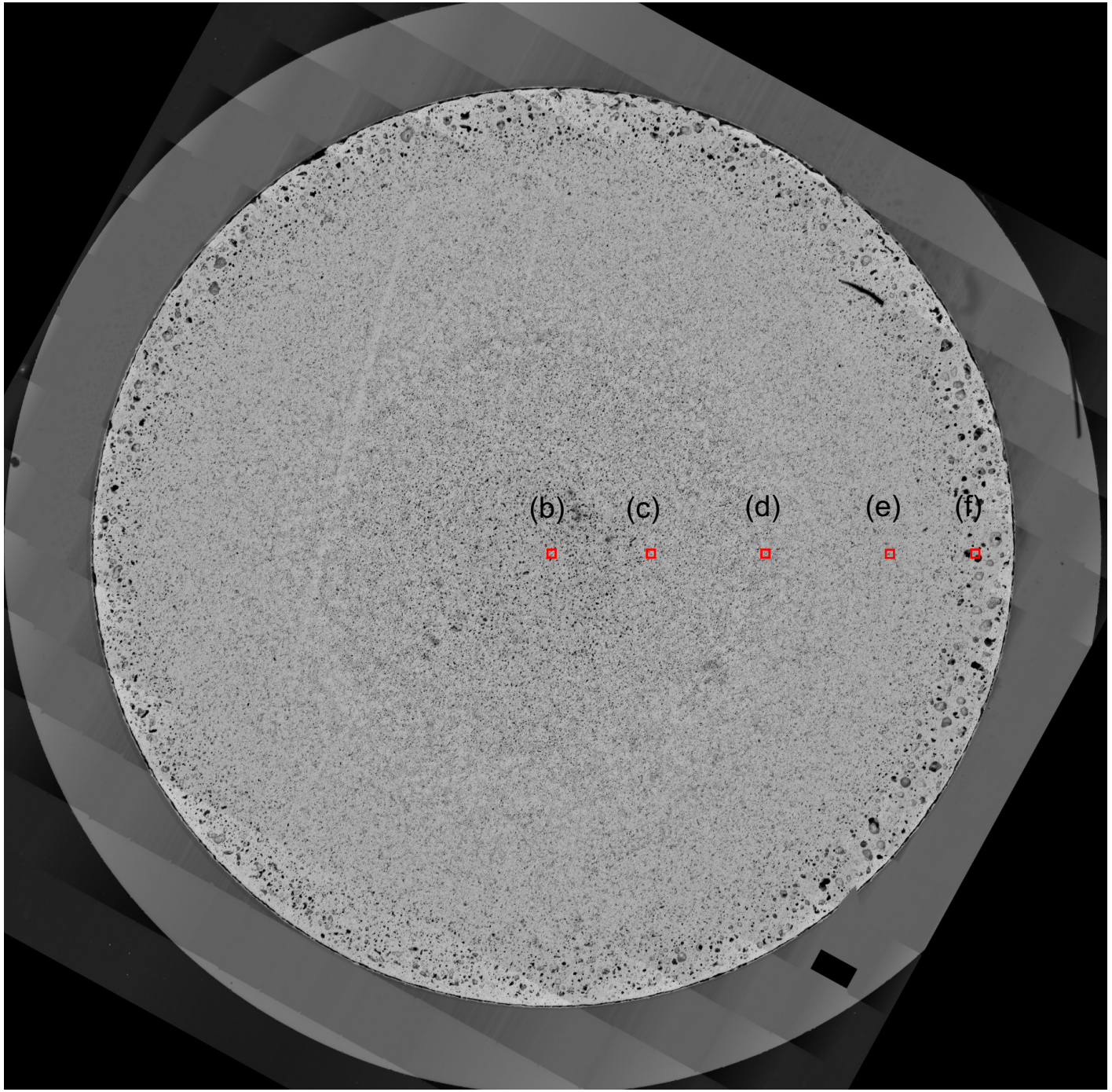

Radial locations for next slide high magnification SEM images

Center region

Intermediate (close to center)

Intermediate

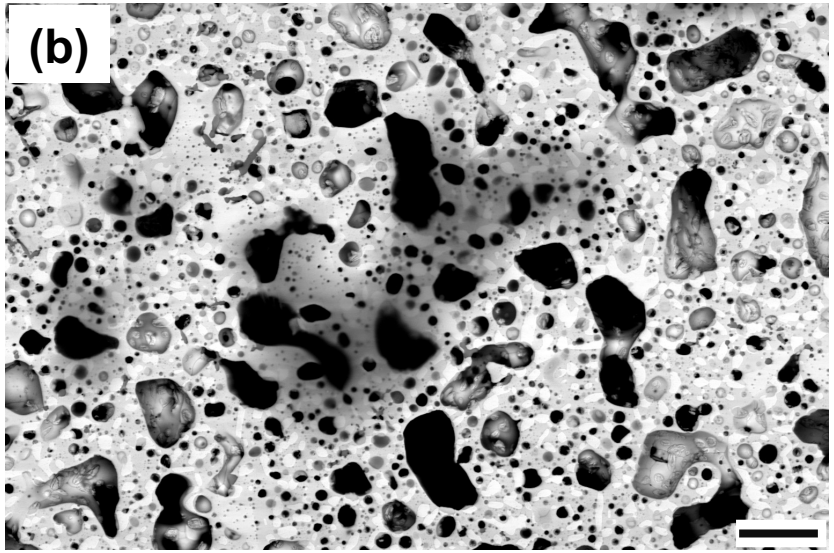

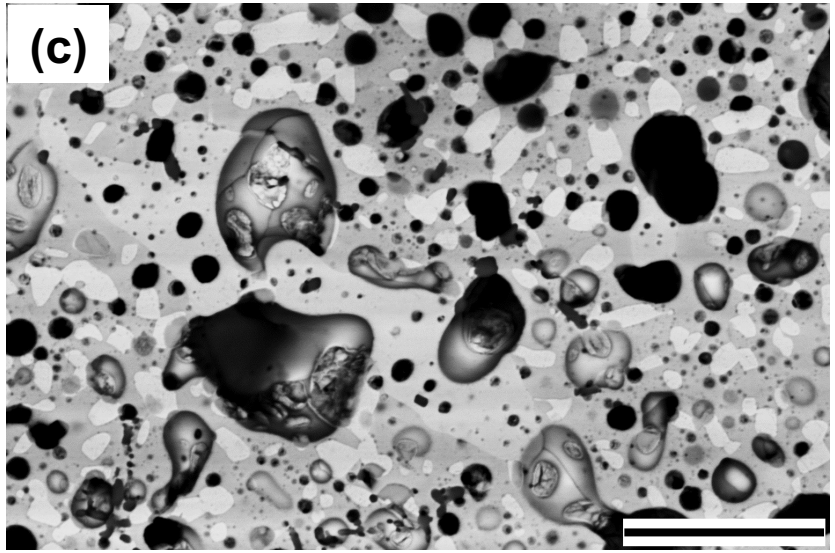

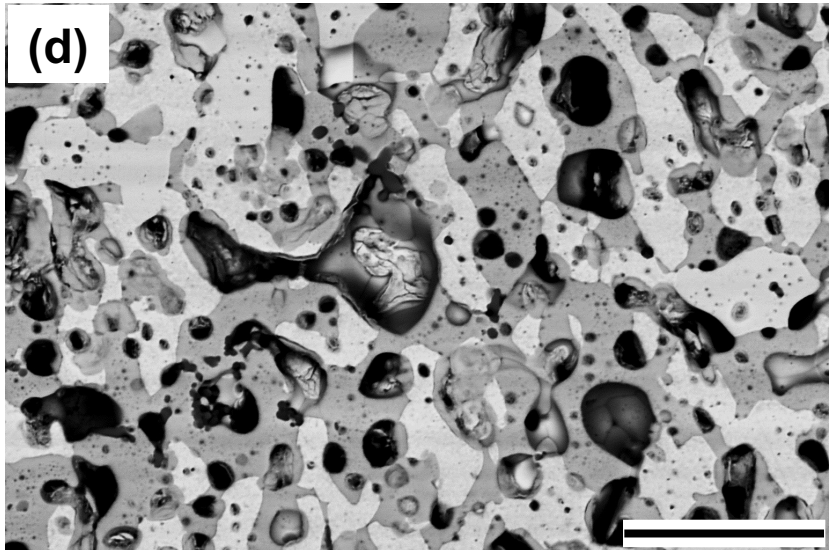

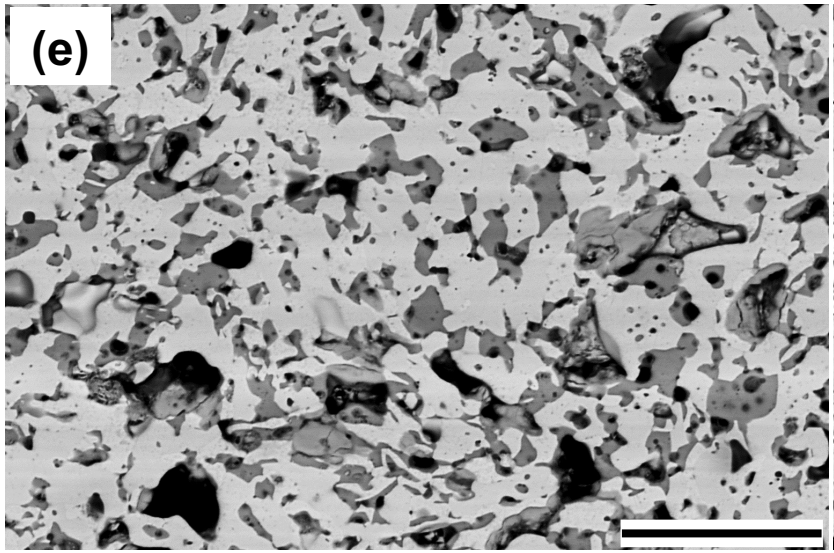

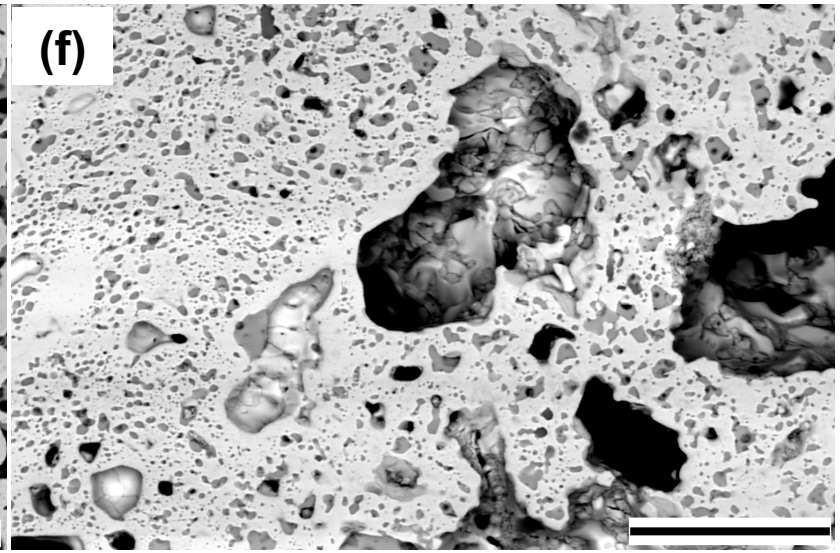

Scale bar is 20 μm

Two phases region

Porous Fuel periphery Region

SEM Characterizing Cr-linear (Monthly Highlight)

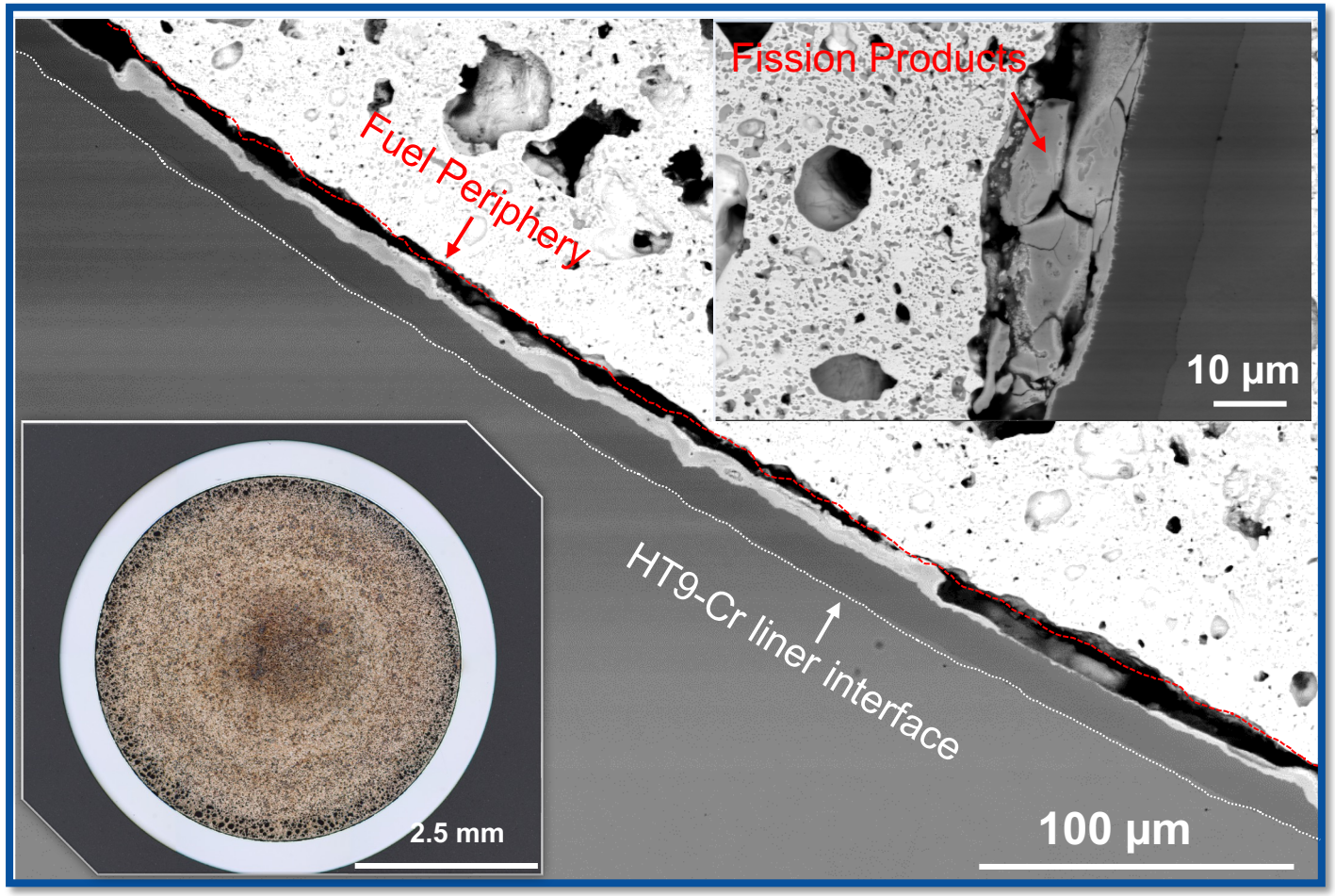

- Preliminary Scanning Elec Microscopy (SEM) characterization conducte examine possible irradiati induced damage on the C linear
- Cross-sectional backscatt electron imaging (BEI) examination revealed loca attack to Cr-liner possible to fission products accumulation
- More BEI image in followi slides

Backscattered electro image (BEI) showing the microstructure of Cr coating. Inserted: optical microscopy image of

Monthly Highlight

SEM-EDS Characterization on Cr-liner HT9 Cladding

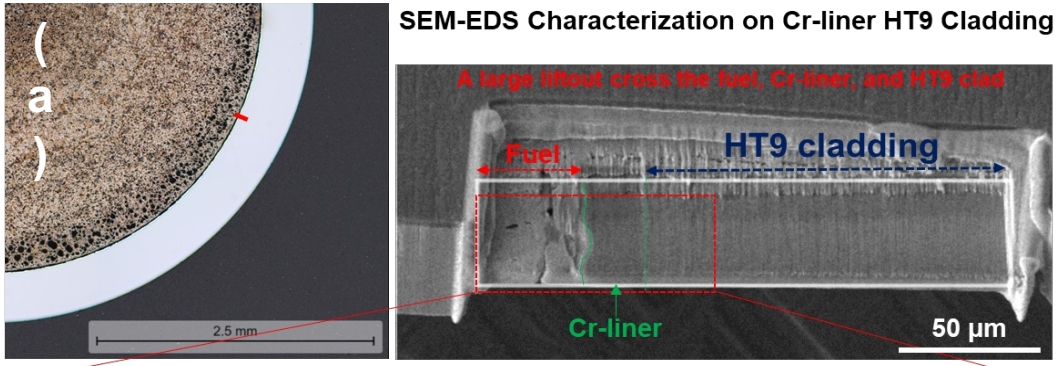

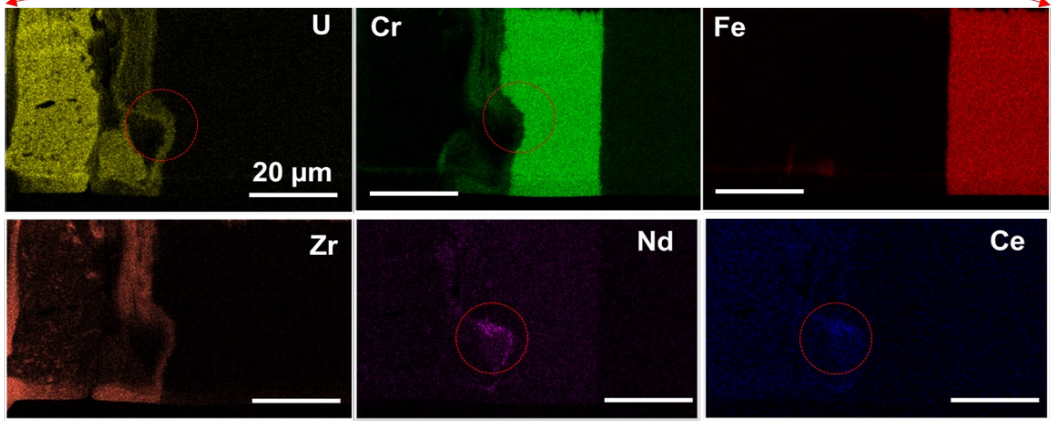

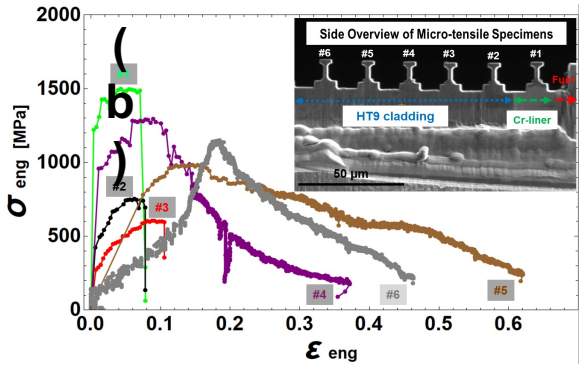

(c)

Micro-tensile specimens	Material	$\sigma_{y\text{-}DIC}$ [Mpa]	σ_{max} [Mpa]	$\varepsilon_{total\text{-}DIC}$ [%]
#1	Cr-liner	1231	1500	7.8*
#2	HT9	451	754	7.8*
#3	HT9	284	606	10.5*
#4	HT9	961	1296	37.2
#5	HT9	799	984	61.7
#6	HT9	957	1151	46.3

Note: *Stopped after yielding plus first observable deformation in tensile gauge

SEM-EDS Characterization on Cr-liner HT9 Cladding

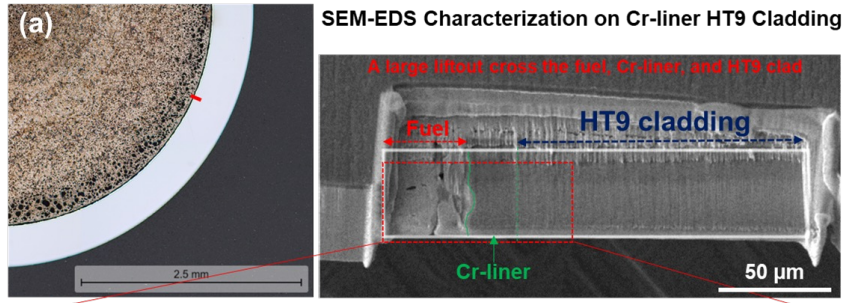

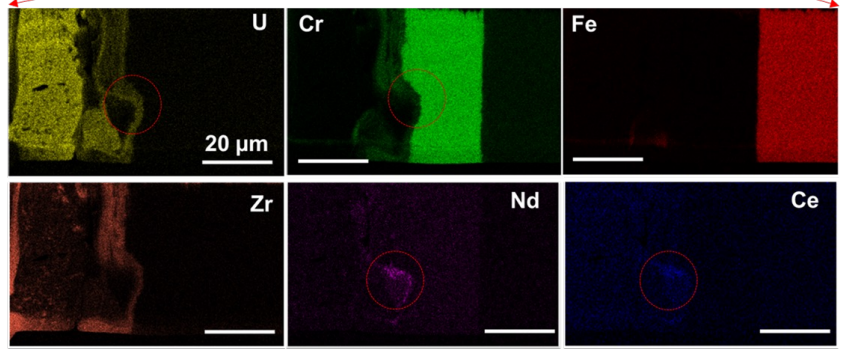

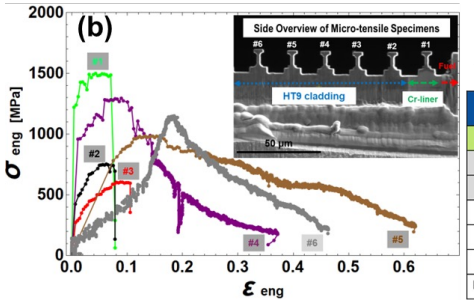

(c)

Micro-tensile specimens	Material	$\sigma_{y\text{-}DIC}$ [Mpa]	σ_{max} [Mpa]	$\varepsilon_{total\text{-}DIC}$ [%]
#1	Cr-liner	1231	1500	7.8*
#2	HT9	451	754	7.8*
#3	HT9	284	606	10.5*
#4	HT9	961	1296	37.2
#5	HT9	799	984	61.7
#6	HT9	957	1151	46.3

Note: *Stopped after yielding plus first observable deformation in tensile gauge

SEM-EDS Characterization on Cr-liner HT9 Cladding

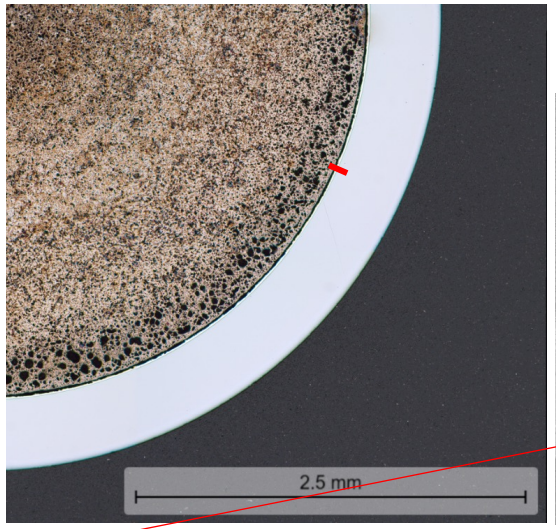

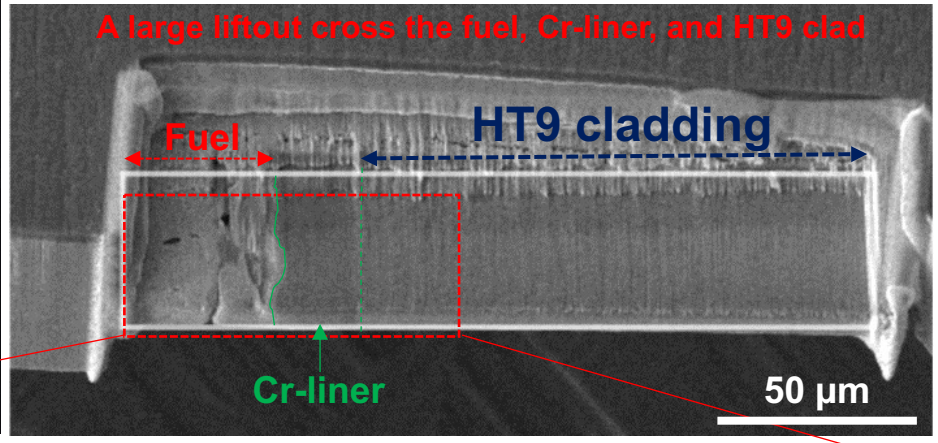

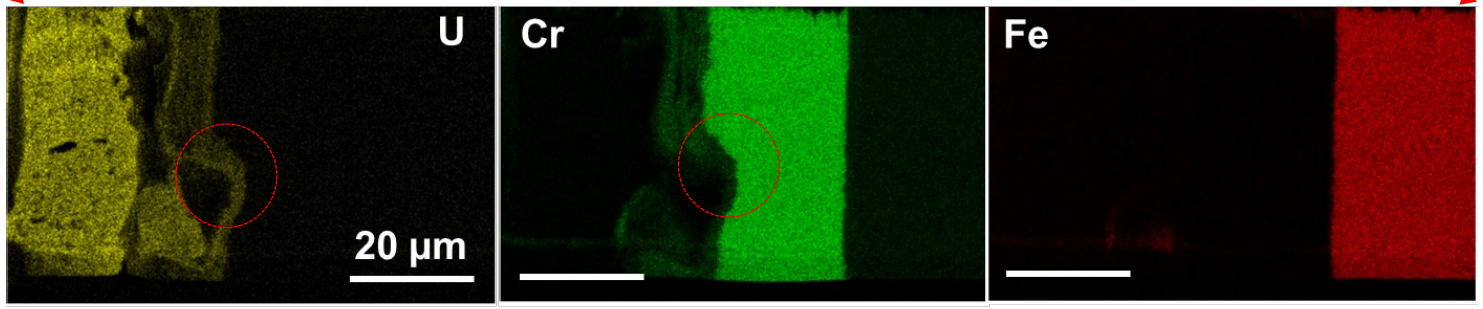

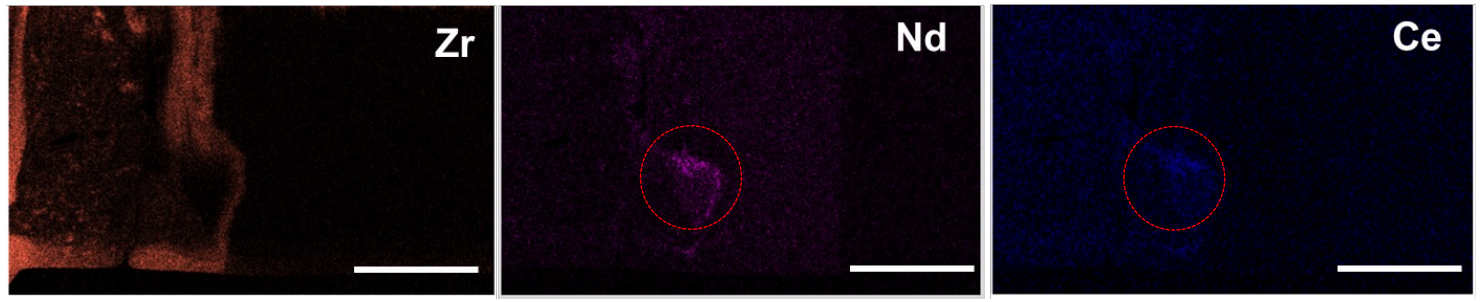

SEM-EDS characterization (cont.)

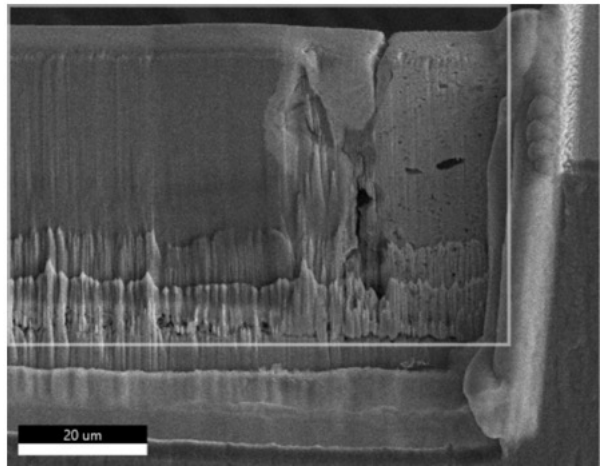

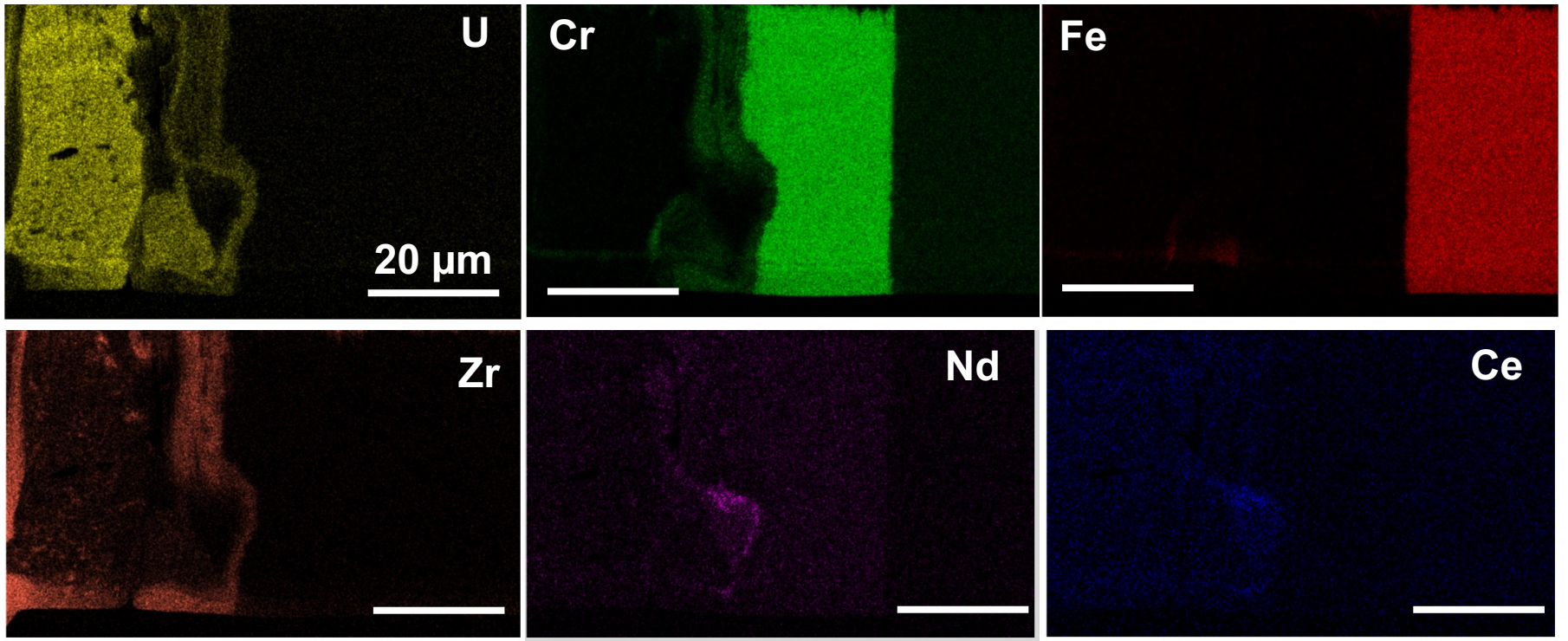

TEM Foils Extracted in Fuel Center

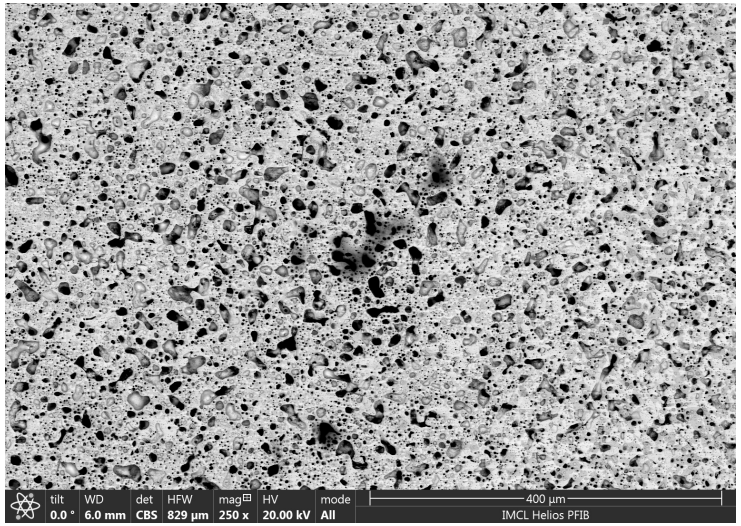

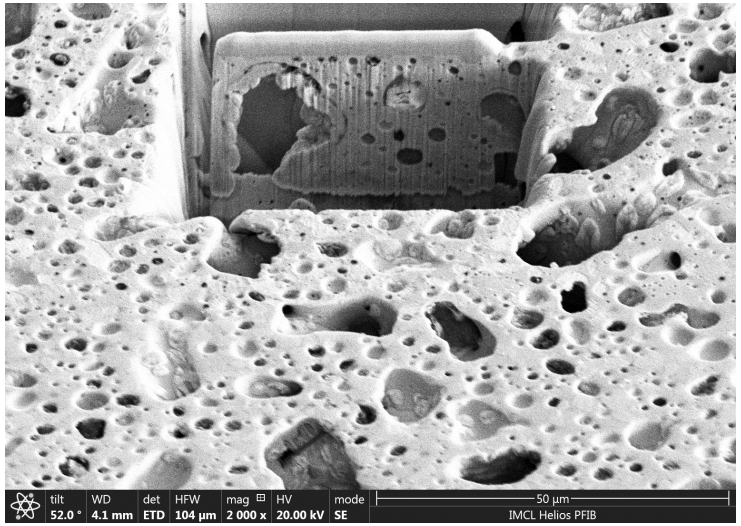

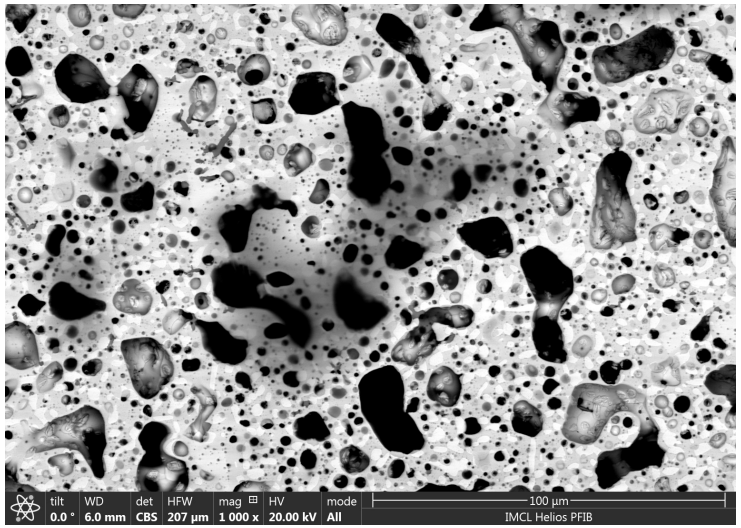

TEM Foils Extracted in Fuel Intermediate

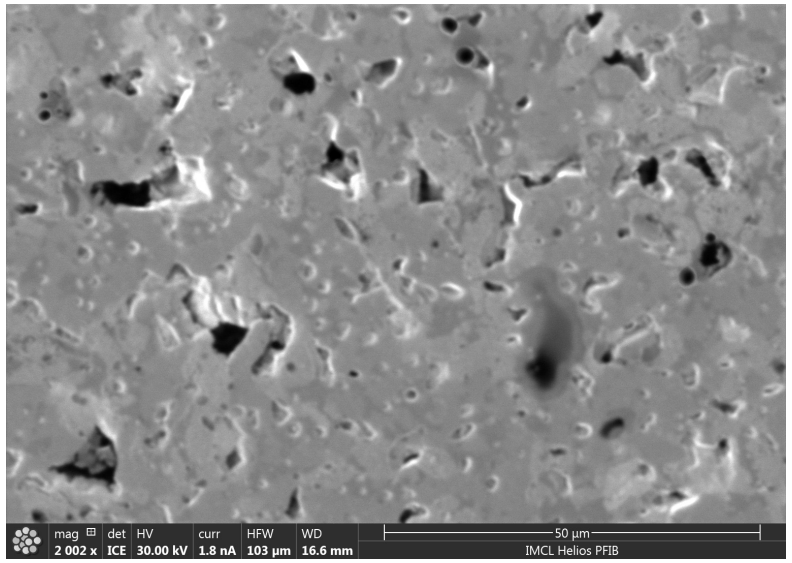

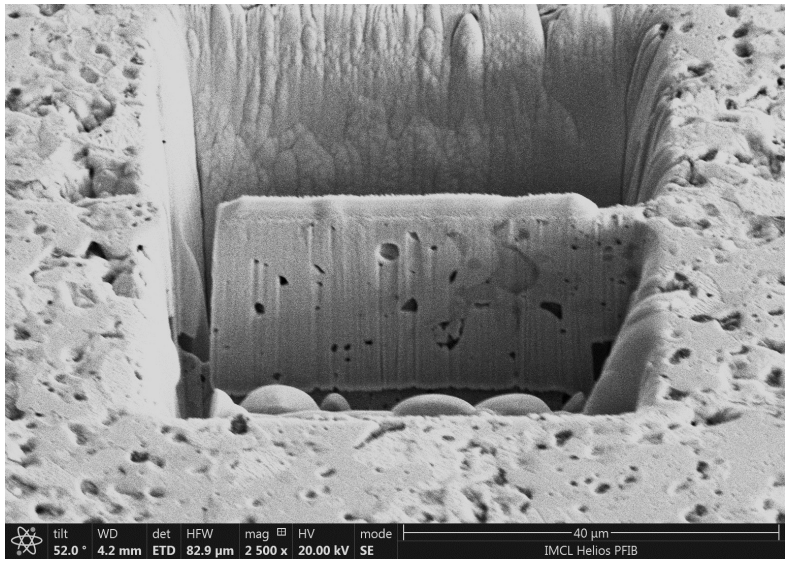

TEM foils are ready for TEM characterization